Numerical Analysis of Lightning by Finite Element Method

Salar Ismael Ahmed

Submitted to the
Institute of Graduate Studies and Research
in partial fulfilment of the requirements for the Degree of

Master of Science
in
Electrical and Electronic Engineering

Eastern Mediterranean University
September 2014
Gazimağusa, North Cyprus

Approval of the Institute of Graduate Studies and Research

Prof. Dr. Elvan Yılmaz
Director

I certify that this thesis satisfies the requirements as a thesis for the degree of Master of Science in Electrical and Electronic Engineering.

Assoc. Prof. Dr. Hasan Demirel
Chair, Department of
Electrical and Electronic Engineering

We certify that we have read this thesis and that in our opinion it is fully adequate in scope and quality as a thesis for the degree of Master of Science in Electrical and Electronic Engineering.

Asst. Prof. Dr. Suna Bolat
Supervisor

Examining Committee

1. Prof. Dr. Hasan Amca

2. Prof. Dr. Osman Kükrer

3. Asst. Prof. Dr. Suna Bolat

ABSTRACT

Lightning is a fractal phenomenon with its light (flash) and its sound (thunder), caused by ionization of electrical positive and negative charges by atmospheric processes. It is an electrical discharge that occurs in a big electrode separation with high current and high voltage.

Lightning discharges might have direct and indirect effects on electrical circuits as well as all living creatures. Since the lightning might be very destructive, it is very important to understand the phenomena.

In this study an electrostatic model is presented to determine the field distribution on transmission line tower during the preliminary breakdown phase of lightning. The model includes thundercloud (cumulonimbus), lightning leader and transmission line tower. Finite Element Method (FEM) is applied by software called COMSOL to calculate electric field and current density distribution simultaneously in several models. Lightning leader is first modelled with a fixed stepped leader that approaches to a transmission line tower vertically. By linking the COMSOL with MATLAB, the model is expanded to have a leader that approaches to the tower with a random path to create more realistic solution.

As the results of numerical analysis of this study, it is possible to get informative data about preliminary lightning breakdown. Therefore, the effects of lightning can be analysed; development pattern of lightning can be observed, striking position of lightning can be analyzed and transient electromagnetic behaviour can be

investigated. Numerical electrostatic lightning model is a good tool for risk assessment and protection.

Keywords: Lightning discharge, preliminary breakdown, finite element method.

ÖZ

Yıldırım ışığı (şimşek) ve sesi (gök gürültüsü) ile, atmosferik olaylar sonucu artı ve eksi elektriksel yüklerin iyonlaşmasıyla oluşan ayrımsal bir olaydır. Büyük elektrot açıklığında, yüksek akım ve yüksek gerilimli bir elektriksel boşalmadır.

Yıldırım boşalmalarının elektrik devreleri ve canlılar üzerinde dolaylı ve dolaysız etkileri vardır. Yıldırımın çok yıkıcı etkileri olabileceği için, yıldırım olayını anlamak çok önemlidir.

Bu çalışmada, yıldırım ön delinme aşamasında, iletim hattı direkleri üzerinde alan dağılımını belirlemek için elektrostatik bir model sunulmuştur. Bu çalışmada yıldırım bulutu (kümülonimbüs), öncü boşalma ve iletim hattı direği modellenmiştir. Farklı modeller için elektrik alan ve akım yoğunluğu dağılımı Sonlu Elemanlar Yöntemi (SEY) ile COMSOL yazılımı kullanılarak aynı anda çözülmüştür. Yıldırım öncü boşalması, önce sabit adımla direğe yaklaşacak şekilde modellenmiştir. Daha gerçekçi bir çözüm için COMSOL ve Matlab birleştirilerek model, yıldırım öncü boşalması direğe rastgele yaklaşacak şekilde genişletilmiştir.

Bu çalışmada, sayısal çözümleme sonucunda yıldırım ön delinmesi ile ilgili bilgi elde etmek mümkündür. Bu şekilde yıldırımın etkileri incelenebilir, yıldırımın oluşması ve gelişmesi sırasındaki gözlenebilir, yıldırım çarpma yerleri çözümlenebilir ve geçici elektromanyetik davranışlar incelenebilir. Sayısısal elektrostatik yıldırım modeli, risk değerlendirmesi ve koruma için iyi bir araçtır.

Anahtar Kelimeler: Yıldırım boşalması, ön delinme, sonlu elemanlar yöntemi

DEDICATION

I would like to dedicate my thesis to

My family

ACKNOWLEDGMENT

I would like to express my gratitude to my supervisor Assist. Prof. Dr. Suna Bolat, for her support and guidance, she was always motivating and showing me the required vision to complete this project. She was always ready to answer my questions. Also, she gave me all the help to understand my studies and my topic.

I would like to extend my appreciation to the lectures they tasked out to teach me during my master studies.

Moreover, I would like to extend my thanks and appreciation to my parents and my family whom where always supported and encouraged me to make this research.

Finally, I would like to thank everyone who wished me success to achieve this study.

TABLE OF CONTENTS

LIST OF FIGURES

LIST OF SYMBOLS / ABBREVIATIONS

A_{ext}	Known background field
A_{red}	Reduced vector potential
B_{ext}	Known external magnetic flux density
J_s	surface current density
J_e	externally generated current density
ρ_s	surface charge density
χ_e	Electric susceptibility
χ_m	Magnetic susceptibility
∇	Laplace's equation (Nabla)
μ_0	Permeability of vacuum
μ_r	relative permeability of the material
A	Magnetic vector potential
B	Magnetic flux density
B_r	remanent magnetic flux density
C	Capacitance
c_0	Velocity of an electromagnetic wave in a vacuum
Cc	Thundercloud capacitance
D	Electric displacement (or electric flux density)
D_r	remanent displacement
E	Electric Field Density
EM	Electromagnetic
FEM	Finite Element Method

FFT	Fast Fourier Transform
H	Magnetic flux density
IEC	International Electrotechnical Commission standard
Io	Source Current Parameters
i_o	Maximum current
J	Current density
M	Magnetization vector
P	Electric polarization vector
RL	Attacked structure Impedance
R(t)	Resistance of the channel changes in a complicated way
V	Electric scalar potential
Zo	Impedance of the line
Zs	Surge impedance
α, β	Time constant
ε_r	relative permittivity of the material
η	Correction Factor
τ	Strike Duration
τ_1	Lightning Surge Duration
Vpk	Peak pulse voltage
$i(t)$	Time Function of Current Source
ε_0	Permittivity of vacuum
ρ	Electric charge density
σ	Electrical conductivity

Chapter 1

INTRODUCTION

1.1 Background

Basically, lightning is an electrical discharge occurring naturally in the vicinity of positive and negative charges. It can be observed during thunderstorms, as shown in Figure 1.1, and sometimes by volcanic eruptions, Figure 1.2, or by dust storms, Figure 1.3. During a thunderstorm, via strong winds, the molecules with electrical charges in the water droplets and ice are separated. That leads particles to move over all the sky. When these separated electric charges accumulated in atmosphere, a force is created to neutralize the charges in the air. During this temporary neutralization through an electrical discharge, which is called lightning, the separate charges equalize themselves. Because of imbalanced condition of electrical charges, the static electricity is generated by the effect of the attraction between opposite charges.

Figure 1.1: Lightning in thunderstorms [1]

Figure 1.2: Lightning in volcanic eruptions [2]

Figure 1.3: Lightning in dust storm [3]

Lightning distinguished by its light, sound and electrical effects. This fast and massive electrostatic discharge can have voltages up to 100 MV, carry up to 200 kA current and MWs of power, however its energy is small, i.e. level of Js. Lightning when they strike by the current they carry, may cause damages to an object, induce electromagnetic field or effect living.

Lightning clouds which cause lightning strike are air masses having a diameter of approximately 5-10 km and a height of 10-15 km. 70-90% of lightning striking to ground have negative polarity. Most of the time clouds have positive charges at the top, negative charges at the bottom, which makes the part of ground facing the cloud, positively charged.

1.2 Motivation and Thesis Objective

Initiation of lightning discharges has been a great interest to researchers for a long time. Direct and indirect effects of lightning have a great impact on engineering systems. High current induced by lightning may cause thermal losses, heating, melting; thermodynamic, electromagnetic deformation which lead to mechanical damages and/or explosions. Moreover, electromagnetic coupling between lightning current and other electrical systems and electrical interference may lead to a malfunction or unsafe conditions in systems. Though it is not perfectly understood, it is very important to model lightning and predict the outcomes in case of a strike.

In this study, lightning is modelled considering cloud and earth to be a parallel plate electrode system. Change in the electric field with respect to stepped leader length and location are analysed by Finite Element Method (FEM).

1.3 Literature Review

The purpose of modelling is selecting suitable model for the work and to understanding its restrictions to obtain the best result. There are several models available according to different requirement of predictions [4].

Many models have been carried out for a lightning channel to investigate the phenomena. Most of the models are based on the Transmission Line Model, TLM in which the current distribution can be obtained from transmission line theory, and surrounding field can be expressed analytically using current [5].

In TLM, the current is assumed to travel without distortion and attenuation upwards the lightning channel at a constant velocity [6]. As a result of its simplicity,

transmission line model is used frequently in lightning models. Transmission line model has several models implemented.

In Modified Transmission Line Linear model (MTLL), current is represented by a linear decay current [7]. A current source is used at the channel base, which injects a specified current wave into the channel. Wave propagates upward without distortion but with specified linear attenuation.

Modified Transmission Line Exponential model (MTLE) can be viewed as incorporating a current source at the channel base [8], which injects a specified current wave into the channel, that wave propagates upward without distortion but with specified exponential attenuation.

Equivalent current source model represents the whole phenomenon of lightning, can be modelled in simple shape by a Norton equivalent circuit [4].

Three-dimensional model is a more realistic model to represent the lightning phenomenon. Generally, lightning channel is represented as a vertical conductor without branches and tortuosity, but this state is very different from the real phenomenon. Channel tortuosity has ability to significantly impact current propagation [15] [10].

Three-dimensional field models eliminate the limitations of other models if the whole interaction space is modelled in three dimensions [4]. In this model, buildings, communication towers, aircraft or other similar structures can be described in much more detail, including internal wiring and connected loads. The (3D) model consists

of the cloud-ground system and the conducting path represented by stepped leader, as shown in Figure 1.4.

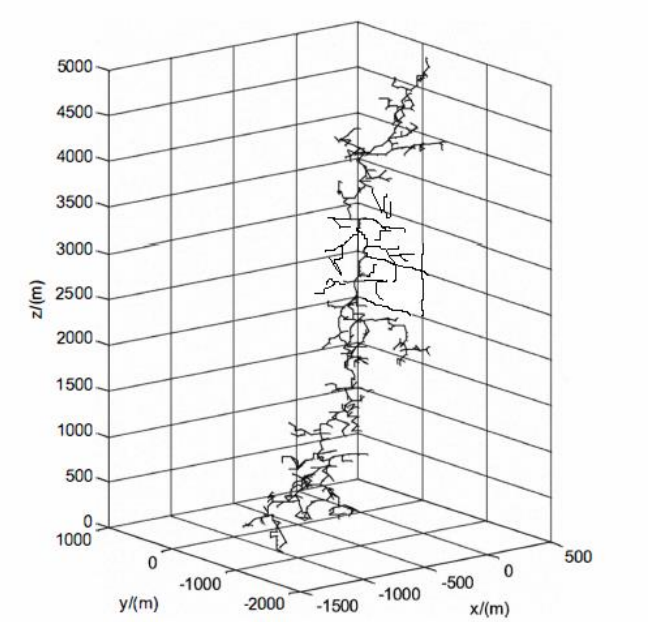

Figure 1.4: Three-dimensional model lightning discharge [11]

Channel-Base Current CBC model is one of the earliest applications of a numerical electromagnetic analysis to lightning study. The numerical analysis which used by time function of lightning can be described in the equation (1.1). Moreover; another name has been given to it which called Heidler's model. The current source wave form is shown in Figure 1.5 [12].

$$i(t) = \frac{Io}{\eta} \cdot \frac{(t/\tau_1)^n}{1 + (t/\tau_1)^n} \cdot e^{-t/\tau} \qquad \textbf{(1.1)}$$

where, peak value of the lightning current represented by Io and η is the correction factor of the peak value of lightning current, n is the factor influencing the rate of rise of the function, τ_1 is duration of the lightning surge front, τ is the strike duration also

called time to half value (interval between t = 0 and the point on the tail where the function amplitude has fallen to 50% of its peak value).

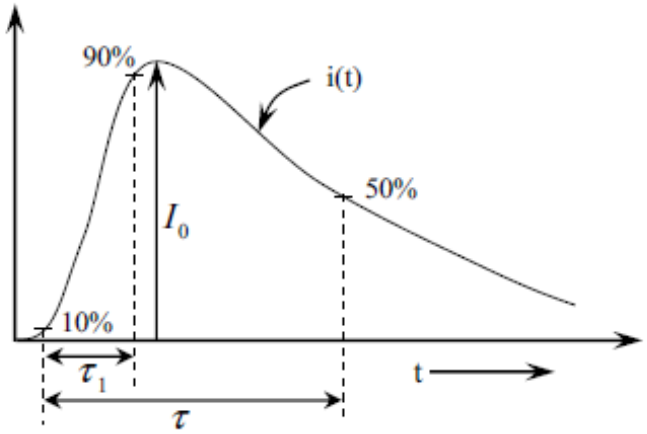

Figure 1.5: Wave form of Heidler's model current source [12]

This Heidler model dissimilar to double exponential model, it reproduces the observed concave rising portion of a typical channel base current waveform, it does not exhibit a discontinuity in its time derivative [13].

In this study, Finite Element Method is used to analyze the lightning channel. The system is modeled by using simple parallel plate electrode system. Considering lightning clouds are 1-3 km (approximately 2 km) above the ground, the electrical configuration can be represented by a plane-plane electrode system, having a 2 km electrode separation with a uniform field distribution where the cloud is the top electrode, ground is the bottom electrode. In this electrode configuration, discharge channels namely stepped leaders, move from the cloud towards the ground by 50-100 m long steps; they recombine with the points suitable with regard to potential and electric field and they eventually reach to the ground.

Chapter 2

LIGHTNING DISCHARGES

2.1 Basic Lightning Phenomenology

Lightning occurs as a result of a large charge separation inside a cloud. Clouds consist of huge amount of water droplets and ice particles. This particles acquires positive electrical charges when freezing in the shape of hail or ice crystals, also when ice and snow melt down to liquid water, and fragment into droplets and when steamed, condensed or any change from one case to another case of solid and fluid and the gas state, and the ambient air surrounding those particles acquires negative electric charges. Therefore, the positive charges accumulate at the top and bottom of the cloud where temperature is between -10 °C to -40 °C, whilst the negative charges are concentrated in the middle of the cloud where the temperature reaches to zero percentiles. When there is an electrical discharge between two opposite charge regions within the same cloud or between two adjacent clouds, the electric potential increases and reaches to certain level, if the electrical strength is enough to break air; lightning occurs [14].

The British scientist William Wall in 1708 [15], noticed that when an electrical discharge occurs quickly from a charged body to a close conductor without touching, then, the spark jumps between two objects, which he related it to a flash of lightning in the sky like a spark, but on a larger scale [14].

After almost fifty years (1752) [15] [4], the American scientist Benjamin Franklin performed his first experience in which he tried to prove that the discharge is produced by electricity. In this experiment, during a thunderstorm he threw a kite hanging by a metal wire connected to a floss silk at its lower end and grabbed it, and connected a metal key with floss silk at a distance along an arm. When the kite passes across the cloud thunderstorm, Franklin approached his finger from the metal key a spark jumped across the gap between them, where he re-experienced this several times and the result was same. He made sure that during the thunderstorm the clouds charged with electricity and that some of this electricity passes through the wet floss silk to the metal key and collect the charges on the key causes jumped spark across the gap to his finger. Indeed this was a great experience, undoubtedly it was venture risk, fortunately Franklin survived that experiment [16] [17]. Through this experience, he concluded that lightning is an electrical discharge then he designed a device now known as Franklin rod to protect high-rise buildings from lightning risk using a simple logical conclusion from the kite experiment. He had proved a metal bar at the top of the building connected to the ground with a wire, in case of lightning strike, charges was safely can take the charges safely from the building to the ground across the wire. The arresters reduced much of the lightning dangers and the destruction that was caused [4].

When the weather is balanced, an electrical field intensity of 100 V/m exists near the ground surface. This field is vertical an increase with approaching to the ground surface. At a height of nearly 50 km above the ground surface, air is adequately ionized, and that imagine a huge spherical capacity with the earth as its inner polarity and the outer polarity at 50 km radius. Usually the amount of total current flowing in this lossy capacitor is 1500 A [4]. Then the ground balance charge would gradually

change if this current flow allowed continuing. The lightning discharge supply an opposite current, which keeps, overall charge balance. In the atmospheric electrical discharge, the speed traveling of a stepped leader of thunderbolt at 60,000 m/s, 220 km/h, and the temperature reaches approximately 30,000 ºC [16].

2.2 Classification of Lightning Discharges

Lightning discharges can be classified in three main types according to the location of positive and negative charges.

2.2.1 Cloud – ground (CG) lightning

Cloud – ground lightning is the most common type lightning, which is a result of accumulation of two opposite charges on the cloud and the ground. It is also the most investigated lightning type because it affects human life more than the other types. Often the clouds are charged negatively at the bottom, the surface of the earth, which faces the cloud, in this case is charged positively. If the cloud is charged positively, then the earth becomes negatively charged. Cloud-Ground (CG) lightning discharges can be classified as negative upward, positive upward, bipolar upward, negative downward, positive downward, and bipolar downward, as shown in Figure 2.1 depending on how the charges are distributed.

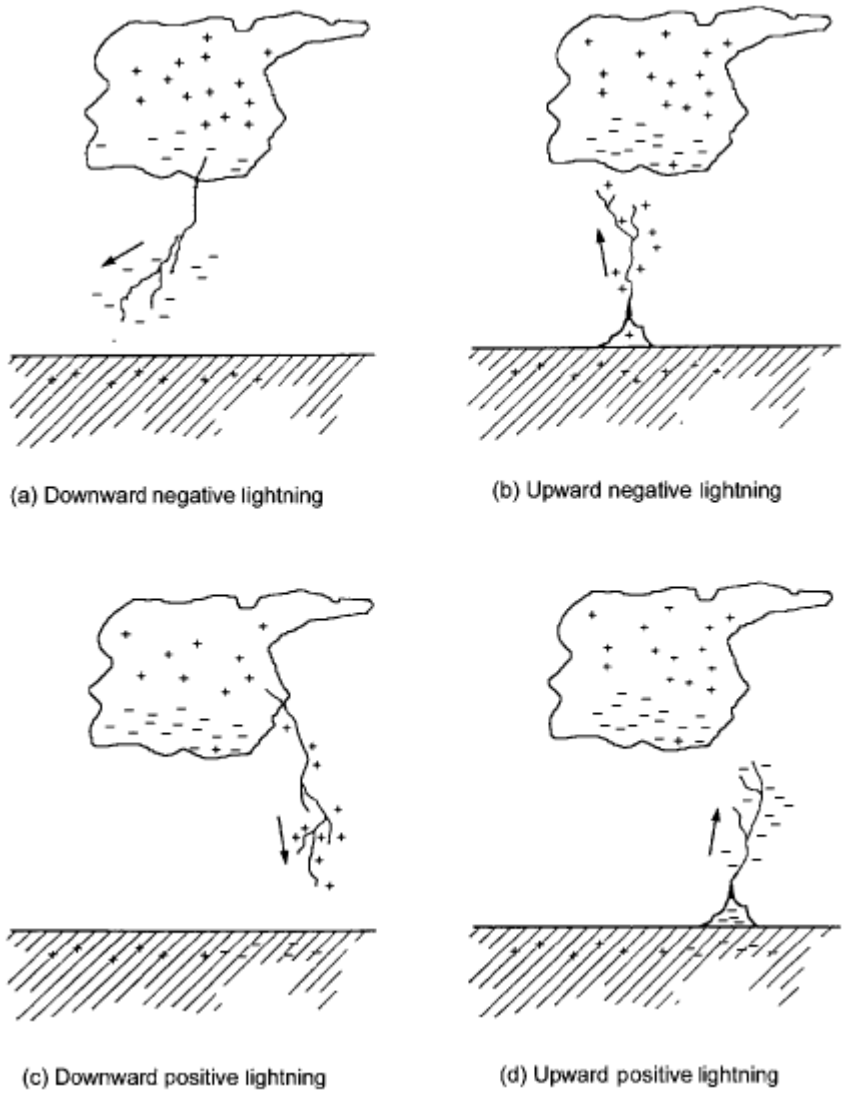

Figure 2.1: Different types of lightning discharge [18].

2.2.2 Cloud – cloud (CC) or inner cloud lightning

This type of lightning occurs between two clouds (important for aircraft in flight). The medium in which the clouds have electrical field, the likelihood of opposite charges is big. Therefore, possibility for cloud-cloud lightning to occur is high i.e. three-quarters of the flashes of lightning.

Similar process might happen inside one cloud since the cloud carries both negative and positive charges.

2.2.3 Cloud – air (CA) lightning

When a cloud is charged, surrounding air molecules will be charged with opposite charges. If the amount of electrical charges in the cloud and air is enough to increase electric field to a critical value, stems beam of lightning appears. This type of lightning is rare.

2.2.4 Cloud – space lightning

There is another kind of lightning between a cloud and the upper atmosphere. This phenomenon occurs between the upper layers of clouds and the ionosphere, which contains electric field permanently. It is possible to see this type of lightning by imaging devices is installed at the satellites.

2.3 Development of Lightning Discharge

Lightning begins with the launch of the beam, created at the base of the cloud, which is called stepped leader, Figure 2.2 show the steps of lightning development. And the beam does not arrive all at once, but passes through in the form of steps it travels discretely toward the ground, 50-100 m at the time then stops for about 50 μs, then travels another 50-100 m [19]. The stepped leader invisible to the eye and has a very narrow diameter (less than a millimeter), but a wide corona sheath in the form of an inverted cone is established around it [4].

As the stepped leader approaching the surface of the ground, often charge of this beam is negative, a positively charged is initiated on some tall objects on the ground which is called traveling spark, it moves upward and eventually connects with the stepped leader.

Once the stepped leader and the return stroke have connected, then electrons from the cloud can flow to the ground, and positive charges can flow from the ground to the cloud. This flow of electrons called return stroke, it is visible and in several cm in diameter.

After the first discharge, it is possible for another leader to propagate down the channel that created by the first leader, this new leader is called dart leader. This can happens three to four times in quick succession.

Lightning strike repeats itself a number of times and appear like one flash. However it seems that the lightning is moving from the cloud to the ground, in reality the beam is moving from the ground towards the cloud, but the speed of the process makes it seem like the opposite to human eye.

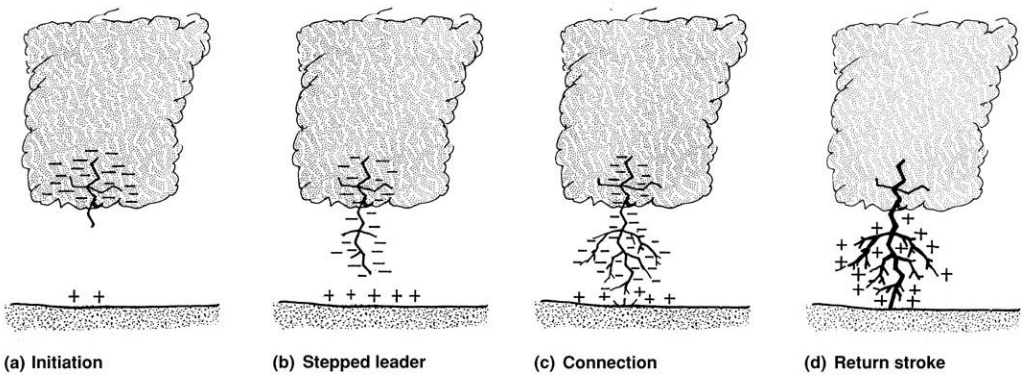

Figure 2.2: Steps of lightning development [19]

2.4 Lightning Models

There are different lightning models available in the literature depending on the purpose of the modelling.

2.4.1 Transmission line

Transmission line model (TLM) is one of the most simple and widely used lightning return stroke models. In this model, the current pulse taking the benefit from the lightning return stroke to get originated at the ground level and this process can be done with no dispersion and attenuation by a fixed speed [20].

The construction of transmission line model can be done by putting some conductors in parallel inside the system. The conductor cross section between the point of dielectric in a uniform transmission line and the cross sections differ in space in a non-uniform transmission lines.

In this process the images are perfectly conducted and the return strokes are the leader channel. In the ground there are two plane conductors of the transmission line [21].

The non-uniform lossy transmission line is a more realistic model uses to describing and obtain lightning return stroke. The thundercloud capacitance (Cc) and the impedance (RL) represents the attack structure are then connected at the ends of this line as shown in Figure 2.3.

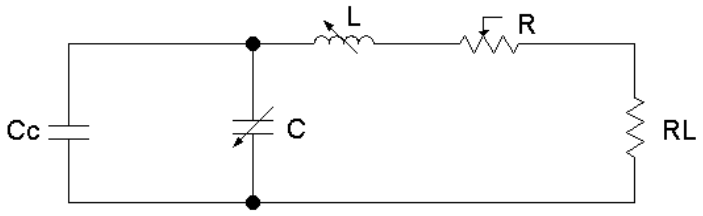

Figure 2.3: Transmission line model of a lightning discharge [4]

The model can be improved to contain corona effects and losses, and based on equation (2.1).

$$R(t) = \frac{1}{\pi\sigma a^2(t)} \ \Omega/_{e} \qquad \textbf{(2.1)}$$

Where $a(t) = 0.93\rho_o i^{-1/3} t^{1/2}$, ρ_o is the air density at atmospheric pressure, i is the current, t is the time and electrical conductivity $\sigma = 10^4$ S/m. The model shown in Figure 2.4.

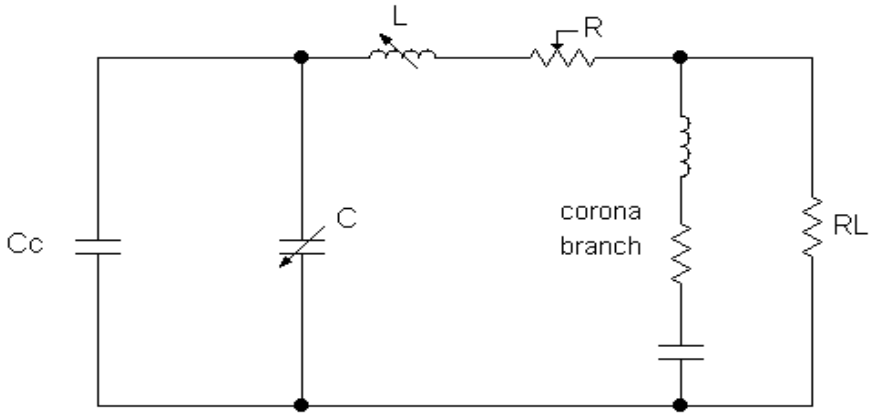

Figure 2.4: Transmission line model of a lightning discharge with corona branch [4]

This model combines information on loss variation with current and time and on the effect of the corona charge on the development of the return stroke.

The ideal transmission line considered to be the leader channel, in the end of the leader channel the current pulse is getting attached in the ground and the propose for that is to propagate at all the length of transmission line with the speed of light by eliminating attenuation or distortion. The current pulse produces the electromagnetic fields as it is attached along the ideal transmission line.

The relation between the return stroke current at the channel base and the electromagnetic fields are identical to those of the TLM with a return stroke speed equal to the speed of light.

In fact, both the leader and the return stroke channel are not perfect conductors; therefore, the channel resistance in the transmission line equations has to be taken into account. Because the return stroke current is propagating along the leader channel, the resistance experienced by the front of the return stroke is equal to the resistance of the leader channel. As the reverse relation, whenever the return stroke current increases, the channel resistance decreases. Thus, channel resistance treats as a time depending parameter.

2.4.2 Equivalent current source

The current source parameters (*I*o) represent a statistical average case or the worst case of typical return strokes and the impedance (*Z*o) represents the surge impedance of the discharge channel and, usually it is around 1500 Ω, as shown in Figure 2.5.

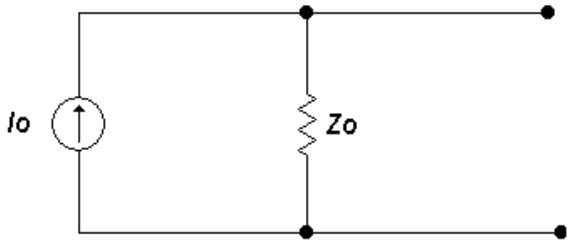

Figure 2.5: Norton equivalent circuit of the return stroke [4]

The interaction of lightning with structures can be simulated even with this simple model. A lightning striking on a power line at mid-span between two towers can be an application of this model. Voltage pulse amplitude traveling toward the towers will be established on the line. Assuming that a strike of moderate intensity with 10

kA peak amplitude and surge impedance of the line is Z=300 Ω, then by Norton equivalent circuit that shown in Figure 2.6, the induce peak pulse voltage is equal to:

$$Vpk = I.(Zo//\frac{Z}{2}) \approx 1.36 \text{ MV}$$

where Zo is the surge impedance of the discharge channel, and Z is the impedance of the line.

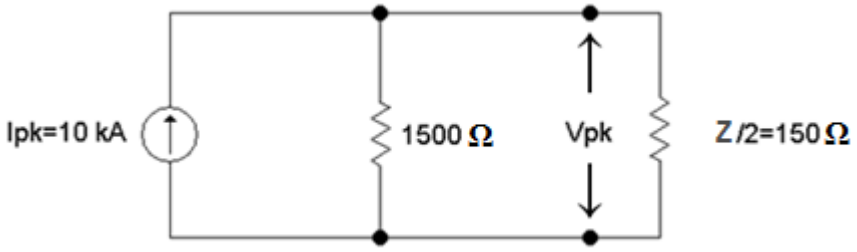

Figure 2.6: Equivalent circuit of a lightning strike on a line at mid-span between two towers [4]

From the result of the calculation above, since the lightning strike on a line is located at mid-span between two towers, two pulses to the right side and left side will propagate away from the strike point, it was recognized that the effective surge impedance of the line at the strike point is 300/2 Ω.

For a more complex problem, that of a strike on the top of the ground structure of a tower, as shown schematically in Figure 2.7. Lightning attached to point S at the top of the tower.

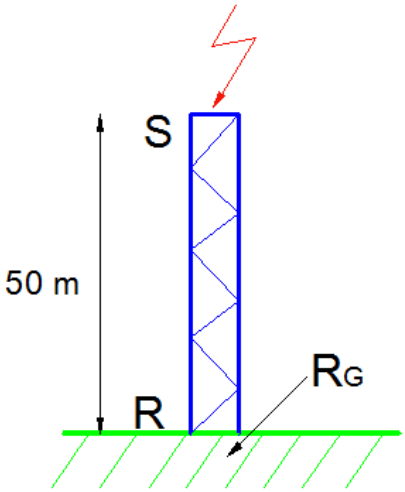

Figure 2.7: Lightning strike on a tower (schematic diagram of configuration) [4]

The Propagation down the tower represented approximately by propagation along a transmission line of characteristic impedance $ZT \approx 130\,\Omega$ and propagation velocity $v \approx 240\,m\,/\,\mu s$. The load resistance at the end R of this line is the tower footing resistance $RG \approx 10\,\Omega$ representing the effectiveness of the tower grounding. The complete model is shown in Fig 2.8.

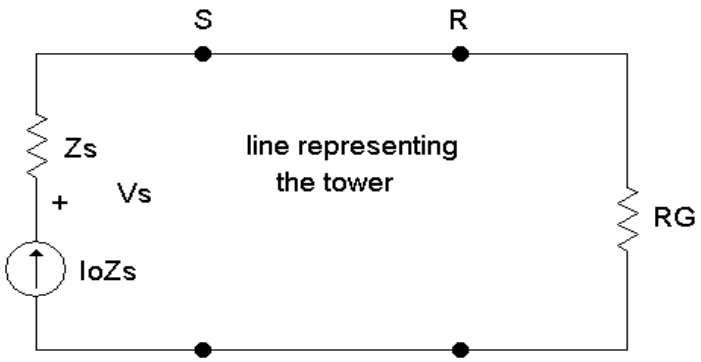

Figure 2.8: Lightning strike on a tower (transmission line equivalent) [4]

2.4.3 Three dimensional field

This model consists of the cloud-ground system and stepped leader as a conducting path. A computational grid used for calculating electromagnetic (EM) fields in space.

There is several numerical simulation methods used to describe electromagnetic field propagation, transmission-line model is one of the methods that developed at Nottingham. This method the computational grid is a network of transmission line segments, on the transmission lines, the voltage and current pulses represent electric and magnetic fields in this part of space. The introduction of a conducting surface or path terminating the appropriate transmission line segments has a low resistance, if conducted perfectly is zero resistance. The thunder cloud and earth surfaces to a first approximation may be assumed perfectly conducting, as can the walls of the victim structure. According to equation (2.1) the resistance of the return stroke path varying. The current distribution on the surface of the victim structure and the electromagnetic field in and around it are obtained from the TLM model [4].

There are several types of three dimensional field models. The Thin-Wire Time Domain Lightning model it is obtained by combining the basic four models of positive, negative, upwards, and downwards lightning models into one return stroke model. To form a new 3-D Thin Wire Time Domain Lightning Code (TWTDL), the Thin-Wire Time Domain (TWTD) Code and the Waterloo Analysis and Design (WATAND) Code are combined. The new TWTDL Code permits calculation of the currents of thin-wire structures using a moment method solution of the electric field Maxwell's integral equations [22].

The 3-D fractal simulation of lightning discharge is derived from the macroscopic phenomenon of lightning discharges and do not deal with the microscopic processes of breakdown. Based on Laplace's equation (or Poisson's equation) and the boundary conditions, the potential distribution in the interested region is fixed. Then the 3-D

simulation of lightning discharge is realized according to fractal theory and bidirectional leaders independent develop mechanism [11].

Digital Simulation of Thunder from Three-Dimensional Lightning is constructed by using MATLAB software, and used N-waves. In addition Fast Fourier Transforms FFT taken of the thunder signature. MATLAB software used to attempt to recreate lightning. Starting from the strike location on the ground, the lightning channel was built upwards in segments of average length 3 meters, with a normalized random distribution around the average. N-waves are the solution to creating thunder out of the digital thunder. N-wave is the summation of two parabolic pressure waves, one positive and one negative, emitted from a short spark. The overall shape of the N-wave is dependent on the observed angle from the normal of the segment. Both the peak and horizon angles generated randomly. The peak angle was restricted to a cone of 30^0, and biased towards the last 4 values of this angle, while the horizon angle was allowed to be any value. In creating digital thunder, each segment from the digital lightning bolt emits N-waves. Each of those waves is then summed at each point in time to obtain the final thunder signature. The digital thunder signature is determined by the relation of adjacent segments of the digital lightning. If two segments are parallel, then the N-waves from them completely cancel in the middle, leaving two parabolic pressure waves with a large gap in between them. If two segments have an angle between them, then there will be incomplete cancellation, and there will be a larger pressure wave, and two smaller parabolas of the opposite orientation [23].

2.4.4 Channel-Base Current model CBC

Basically, by Bruce and Golde the double exponential model of channel-base current was presented in 1941; it is widely used, it is determining the maximum of the

current time decay, current rise and current steep. Different Mathematical calculations in integration and differentiation can be made directly in this model. Equation (2.2) show the expression of parameters in this model [24].

$$i = i_o[e^{(-\alpha t)} - e^{(-\beta t)}] \quad \textbf{(2.2)}$$

where i_o is maximum current, α, β is the time constant.

By Dennis and Pierce suggested basis on experimental measurements the value of $\alpha = 2 \times 10^4 \ / \ s, \beta = 2 \times 10^5 \ / \ s$, $I = 30$ kA for ideal first strokes, and $\alpha = 1.4 \times 10^4 \ / \ s$, $\beta = 6 \times 10^6 \ / \ s$, $I = 10$ kA for ideal after first strokes for equation (2.2).

The original form is changed by Uman and McLain. Equation (2.3) show the new function of the current peak;

$$i_o(t) = \left(I_o/\eta\right)[e^{(-\alpha t)} - e^{(-\beta t)}] \quad \textbf{(2.3)}$$

Another channel-base current function presented, by Heidler. The functional form of the current is shown in equation (2.4);

$$i_o(t) = I_o \, x(t) y(t) \quad \textbf{(2.4)}$$

where I_o is the peak current, y (t) represent current decay-time while x (t) represent the current rise-time. During the rise-time of the current pulse the value of current decay-function is approximately equal to one. Similar, the value of the current rise-function is equal to one during the decay-time of the current pulse. Furthermore, at the time onset the current rise-function contains the first derivative without discontinuities. In order to represent exponential function and power respectively for the current decay- and the current rise-function, equation (2.5) show that;

$$x(t) = K_s^n \ / \ (1 + K_s^n) \ , \ y(t) = e^{(-t/\tau_2)} \quad \textbf{(2.5)}$$

Where $K_s = t/\tau_1$, τ_1 and τ_2 are the time constants determining current rise- and current decay-time, respectively. n is a current steepness factor. Because of $t > 0$,

$x(t) < 1$, the maximum of the current becomes less than 10. From the equation (2.6), the correction factor of the maximum current η can be calculated;

$$i_o(t = t') = I_o \tag{2.6}$$

where the instantaneous time represented by t', when the current reaches the peak value.

Equation (2.7) shows the last expression of the channel-base current model;

$$i_{o(t)} = (Io/\eta)[K_s^n/(1 + K_s^n)]e^{(-t/\tau_2)} \tag{2.7}$$

We can prove that the continuity of the first current derivative at the time onset is satisfied for the minimum value of the current steepness factor n>1. At the all, let $n = 2$, the function becomes:

$$i(0,t) = \frac{Io}{\eta}\frac{(t/\tau_1)^2}{[(t/\tau_1)^2 + 1]} \cdot e^{-t/\tau_2} \tag{2.8}$$

A new function presented by, Heilder, in 1987, it is improved from combining the function in equation (2.8) and the double exponential function. Equation (2.9) show the new function;

$$i(0,t) = \frac{I_{01}}{\eta}\frac{(t/\tau_1)^2}{[(t/\tau_1)^2 + 1]} \cdot e^{-t/\tau_2} + I_2(e^{-t/\tau_3} - e^{-t/\tau_4}) \tag{2.9}$$

The function as shown in equation (2.9) that proposed by Heidler, it is more suitable than the double exponential function to describe the lightning as a channel-base current model. By changing the parameters, I_0, τ_1, τ_2; the function (2.9), suitable to do several mathematical procedures; transferred charge, changing the maximum value of current with derivative operations. In addition the derivative of current function of double exponential reaches to the peak value but that of Heidler presented function at the time onset is zero. The Disadvantages of Heidler function, it is cannot integrated directly. Therefore, it is not easy to calculate the lightning electromagnetic pulse by this model.

Lightning electromagnetic pulse LEMP is a new function and more predominant than the other two functions. It is high efficient to calculate lightning electromagnetic pulse fields. The pulse model is expressed by the function as shown in (2.10);

$$i(0,t) = \frac{\mathrm{I}_0}{\eta}\,(1 + \mathrm{e}^{-\mathrm{t}/\tau_1})^2 \cdot\ \mathrm{e}^{-\mathrm{t}/\tau_2} \qquad \textbf{(2.10)}$$

2.5 Numerical Analysis of Lightning Discharge

Lightning is an electrical discharge occurring in a big electrode separation with high voltage and high current and is a typical damaging source in the nature. Analytical solution of this phenomenon is very difficult. Therefore, to analyse the effect of lightning, a numerical model is chosen in this study.

There are several numerical methods that can be applied to analyse lightning effects, as a result of numerical analysis it is possible to get informative data about lightning phenomena and it's electrostatic, electromagnetic and/or heat distribution on different structures on the ground and to find ways to prevent the risks by analyzing striking position of lightning.

In this study, electrostatic analysis of lightning discharge is carried out by COMSOL, software of Finite Element Method. The details of the method are explained in the next chapter.

Chapter 3

FINITE ELEMENT METHOD

3.1 Finite Element Method

Finite element method (FEM) is a numerical method to find approximate solutions of partial differential equations. It is usable to solve several physical problems in engineering and mathematics. The method is started being used in electrical engineering industry around late sixties, and continued developing since then [25].

Basically, finite element method is composed of considering the piecewise (hybrid) continuous function for the solution and obtaining the variables of the functions to decrease the error in the solution. The solution depends on either the cancellation of partial differential equations utterly (in the case of static) or approximation of partial differential equations to systematic differential equations. The process of finite element method analysis is summarized in Figure 3.1 [26].

The finite element method is able to handle more complex geometries by choosing appropriate elements. It can solve a wide variety of engineering problems with complex restraints and complex loading. FEM is particularly suitable for structural mechanical engineering, product development manufacturing processes, improving the efficiency of existing design, and failure analysis investigations.

On the other hand, finite element method has a general closed-form solution; it only obtains approximate solutions. Moreover there is a possibility for inherent errors, and it heavily depends on the designer [27].

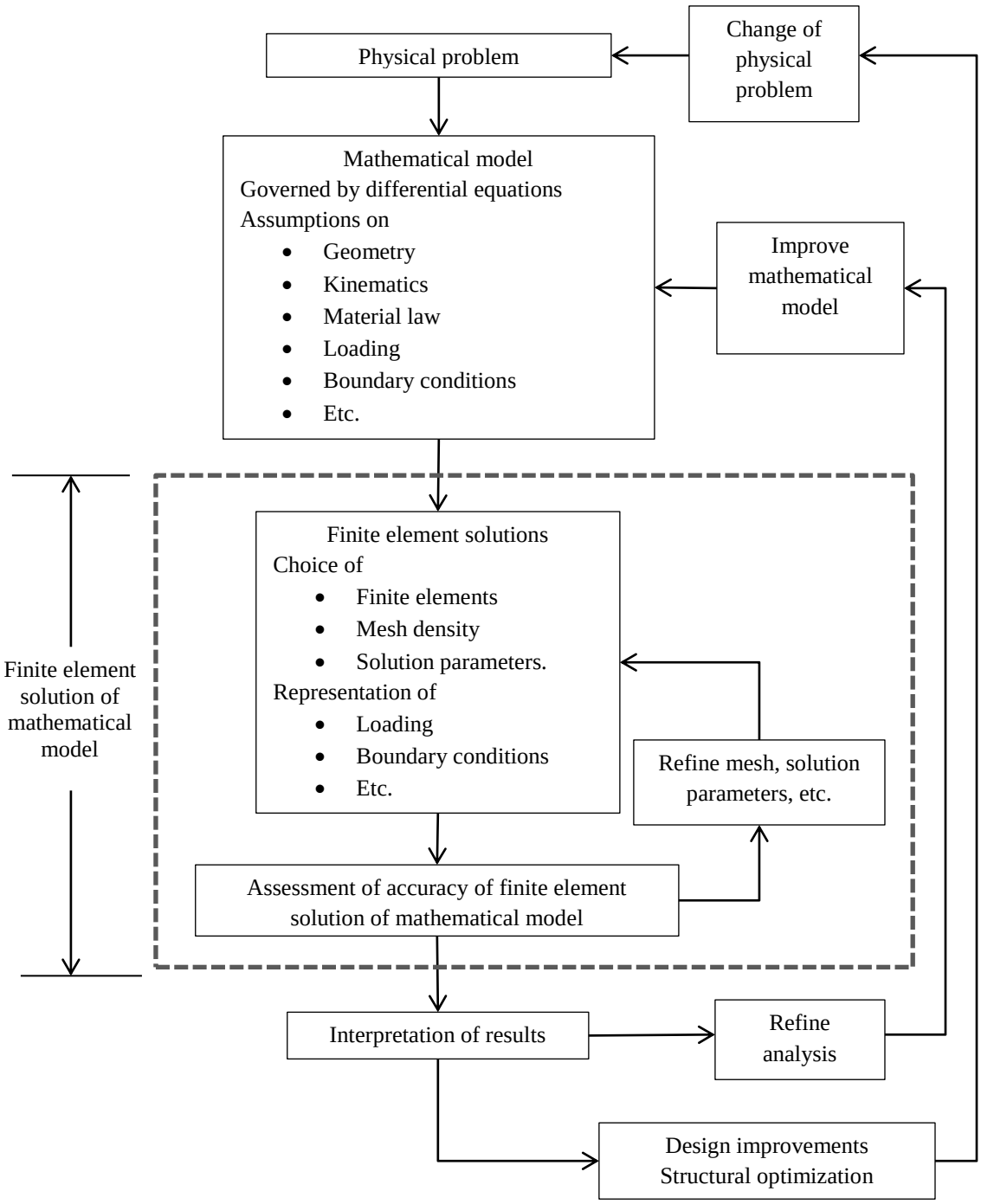

Figure 3.1: The process of Finite Element Method Analysis [26]

The idea of finite element method is to break the problem down into large number of regions, each with a simple geometry. This process is called discretization. In general, triangular elements are used through the discretization process. The actual solution for the desired potential is approximated by very simple function using boundary conditions, known potentials and material properties, after breaking the insulating region down into triangles. In the form of a sparse matrix, the approximation functions are written for each triangle to constitute a linear equation system. This linear system is solved by a numerical method iteratively and potentials at the nodes of each triangle are calculated. After that, potential approximation functions are formed. In this way, it is possible to determine electric potential and electric field strength of any point with respect to potential magnitudes at the triangle's corners [28]

The approximate solution closely matches the exact solution, if the problem is broken down into small enough region. By discretization, the problem is transformed from a small but difficult to solve problem into a big but relatively easy to solve problem.

Mesh generation is a procedure of generating the geometric data of the elements and their nodes, and involves computing the coordinates of nodes, defining their connectivity and thus constructing the elements. In this study, the electric field data is determined by FEM as shown in Figure 3.2.

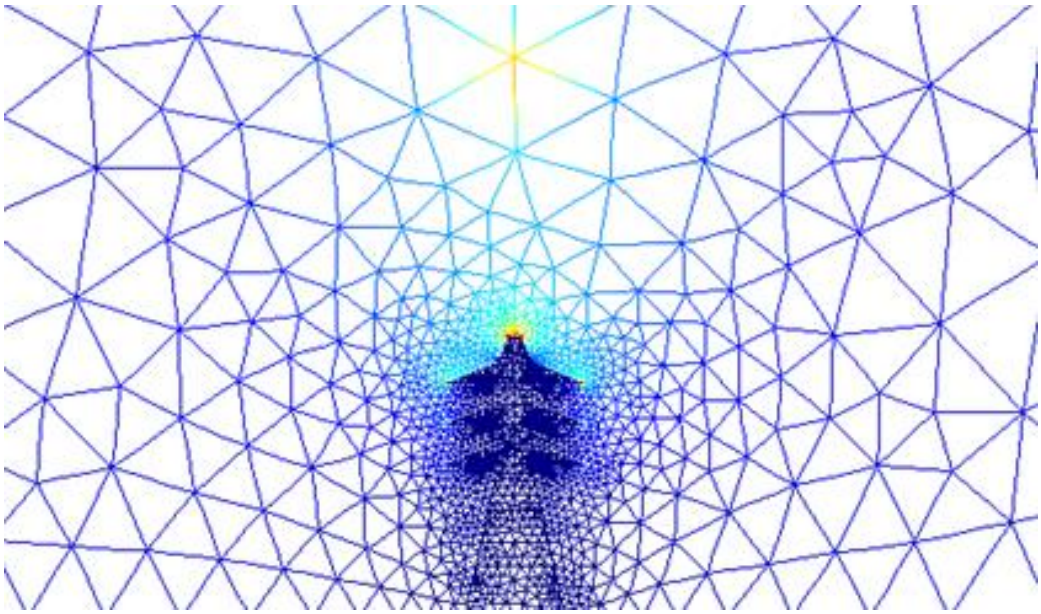

Figure 3.2: Finite elements mesh method used in this study.

3.2 Finite Element Solution

Maxwell's equations subject needs to be solved [29], in order to solve the problem of electromagnetic analysis to certain boundary conditions.

3.2.1 Maxwell's equations

Maxwell's equations for general-varying time fields are formulated as in differential or integral form as follows;

$$\nabla \times \mathbf{H} = \mathbf{J} + \frac{\partial \mathbf{D}}{\partial t} \tag{3.1}$$

$$\nabla \times \mathbf{E} = -\frac{\partial \mathbf{B}}{\partial t} \tag{3.2}$$

$$\nabla \cdot \mathbf{D} = \rho \tag{3.3}$$

$$\nabla \cdot \mathbf{B} = 0 \tag{3.4}$$

$$\nabla \cdot \mathbf{J} = -\frac{\partial \rho}{\partial t} \tag{3.5}$$

where, **E** is electric field density, **D** is electric displacement or electric flux density, **H** is magnetic field intensity, **B** magnetic flux density, **J** is current density, and ρ is electric charge density.

Equation 3.1 is called Maxwell-Ampere's law and equation 3.2 is called Faraday's law. Equation 3.3 is Gauss' law of electrostatic; 3.4 is Gauss' law of magnetostatic. Equation 3.5 is referred to as the equation of continuity.

The macroscopic properties of the medium that described in equations 3.5 include constitutive relations, to obtain a closed system, they are given as:

$$\mathbf{D} = \varepsilon_0 \mathbf{E} + \mathbf{P} \tag{3.6}$$

$$\mathbf{B} = \mu_0(\mathbf{H} + \mathbf{M}) \tag{3.7}$$

$$\mathbf{J} = \sigma \mathbf{E} \tag{3.8}$$

where, ε_0 is the permittivity of vacuum, μ_0 is permeability of vacuum, and σ the electrical conductivity. In the SI system, $\mu_0 = 4\pi \cdot 10^{-7}$ H/m. The velocity of an electromagnetic wave in a vacuum is given as c_0 and the permittivity of a vacuum ε_0 is derived from the relation:

$$\varepsilon_0 = \frac{1}{C_0^2 \mu_0} = 8.854 \cdot 10^{-12} \text{ F/m} \approx \frac{1}{36\pi} \cdot 10^{-9} \text{ F/m}$$

P is the electric polarization vector, which describes polarization of the material in the vicinity of an electric field. It also defines the volume density of electric dipole moments. **P** is generally a function of **E**. Some materials might have an electric polarization even if there is no electric field in the medium.

M is the magnetization vector similar to **P** that describes magnetization of the material when there is a magnetic field **H**. As well as it defines the density's size of magnetic dipole moments. **M** is a function of **H**. Permanent magnets have a magnetization even the magnetic field does not exist.

The polarization is directly proportional to the electric field for linear materials, $\mathbf{P} = \varepsilon_0 \chi_e \mathbf{E}$, where χ_e is the electric susceptibility. Also the magnetization is directly proportional to the magnetic field for linear materials, $\mathbf{M} = \chi_m \mathbf{H}$, where χ_m is the magnetic susceptibility. For linear materials, the relations can be expressed as follows:

$$\mathbf{D} = \varepsilon_o(1 + \chi_e)\mathbf{E} = \varepsilon_o\varepsilon_r\mathbf{E} = \varepsilon\mathbf{E} \quad \textbf{(3.9)}$$

$$\mathbf{B} = \mu_o(1 + \chi_m)\mathbf{H} = \mu_o\mu_r\mathbf{H} = \mu\mathbf{H} \quad \textbf{(3.10)}$$

where, ε_r symbolize the relative permittivity (dielectric constant) and μ_r symbolize the relative permeability of the material.

For nonlinear materials, the relationship used for electric fields is:

$$\mathbf{D} = \varepsilon_o\varepsilon_r\mathbf{E} + \mathbf{D}_r \quad \textbf{(3.11)}$$

where $\mathbf{D}_r$ represent the remanent displacement, which is the displacement when no electric field is present.

Also, for the magnetic field:

$$\mathbf{B} = \mu_o\mu_r\mathbf{H} + \mathbf{B}_r \quad \textbf{(3.12)}$$

where $\mathbf{B}_r$ represent the remanent magnetic flux density, which is the magnetic flux density when no magnetic field is present.

There is a nonlinear relationship between **B** and **H** for some materials:

$$\mathbf{B} = f(|\mathbf{H}|) \quad \textbf{(3.13)}$$

By introducing an externally generated current, the current density is generalized $\mathbf{J}_o$.

$$\mathbf{J} = \sigma\mathbf{E} + \mathbf{J}_o \quad \textbf{(3.14)}$$

Equations 3.15 and 3.16 show the problems formulate in terms of the electric scalar potential V and the magnetic vector potential A:

$$\mathbf{B} = \nabla \times \mathbf{A} \quad \textbf{(3.15)}$$

$$\mathbf{E} = -\nabla \mathrm{V} - \frac{\partial \mathbf{A}}{\partial t} \tag{3.16}$$

The magnetic vector potential is a consequence directly of the magnetic Gauss' law. The electric potential, however, is a result of Faraday's law. In the magnetostatic case where there are no currents present, Maxwell-Ampère's law reduces to $\nabla \times \mathbf{H} = 0$. When this holds, it is also possible to define a magnetic scalar potential ($\mathrm{V_m}$) by the relation:

$$\mathbf{H} = -\nabla \mathrm{V_m} \tag{3.17}$$

The reduced potential option is useful for models involving a uniform or known external background field, usually originating from distant sources that may be expensive or inconvenient to include in the model geometry. In static formulations, the induced current is zero. Maxwell-Ampère's law reduces to:

$$\nabla \times \left(\mu^{-1} \nabla \times (\mathbf{A}_{\mathrm{red}} + \mathbf{A}_{ext})\right) = \mathbf{J}_e \tag{3.18}$$

where $\mathbf{A}_{red}$ is reduced vector potential and $\mathbf{A}_{\mathrm{ext}}$ is the known background field.

Also, in this case possible to express the external field through a known external magnetic flux density. The domain equation in reduced form then reads:

$$\nabla \times \left(\mu^{-1} \nabla \times (\mathbf{A}_{\mathrm{red}} + \mathbf{B}_{ext})\right) = \mathbf{J}_e \tag{3.19}$$

where $\mathbf{B}_{ext}$ is known external magnetic flux density.

The electric and magnetic energies are defined as in two equations 3.20, 3.21, below respectively:

$$W_e = \int_V \left(\int_0^D \mathbf{E} \cdot d\mathrm{D} \right) dV = \int_V \left(\int_0^T \mathbf{E} \cdot \frac{\partial \mathbf{D}}{\partial t} dt \right) dV \tag{3.20}$$

$$W_m = \int_V \left(\int_0^B \mathbf{H} \cdot d\mathbf{B} \right) dV = \int_V \left(\int_0^T \mathbf{H} \cdot \frac{\partial \mathbf{B}}{\partial t} dt \right) dV \tag{3.21}$$

Under the assumption that the material is linear and isotropic,

$$\mathbf{E} \cdot \frac{\partial \mathbf{D}}{\partial t} = \varepsilon \mathbf{E} \cdot \frac{\partial \mathbf{E}}{\partial t} = \frac{\partial}{\partial t}\left(\frac{1}{2}\varepsilon \mathbf{E} \cdot \mathbf{E}\right) \quad \textbf{(3.22)}$$

$$\mathbf{H} \cdot \frac{\partial \mathbf{B}}{\partial t} = \frac{1}{\mu}\mathbf{B} \cdot \frac{\partial \mathbf{B}}{\partial t} = \frac{\partial}{\partial t}\left(\frac{1}{2\mu}\mathbf{B} \cdot \mathbf{B}\right) \quad \textbf{(3.23)}$$

By interchanging the order of differentiation and integration, the result is:

$$-\frac{\partial}{\partial t}\int_V \left(\frac{1}{2}\varepsilon \mathbf{E} \cdot \mathbf{E} + \frac{1}{2\mu}\mathbf{B} \cdot \mathbf{B}\right) \mathrm{dV} = \int_V \mathbf{J} \cdot \mathbf{E} \mathrm{dV} + \oint_S (\mathbf{E} \times \mathbf{H}) \cdot \mathrm{nds} \quad \textbf{(3.24)}$$

The integrand of the left-hand side is the total electromagnetic energy density:

$$w = w_e + w_m = \frac{1}{2}\varepsilon \mathbf{E} \cdot \mathbf{E} + \frac{1}{2\mu}\mathbf{B} \cdot \mathbf{B} \quad \textbf{(3.25)}$$

The quasi-static approximation is a system to obtain the electromagnetic fields by considering stationary currents at every instant. The quasi-static approximation implies that the equation of continuity can be written as $\nabla \cdot \mathbf{J} = 0$ and that the time derivative of the electric displacement $\partial \mathbf{D} / \partial \mathrm{t}$ can be disregarded in Maxwell-Ampere's law.

There are also effects of the motion of the geometries. Consider a geometry moving with velocity v relative to the reference system. The force per unit charge, **F**/q, is then given by the Lorentz force equation:

$$\frac{\mathbf{F}}{q} = \mathbf{E} + \mathrm{v} \times \mathbf{B} \quad \textbf{(3.26)}$$

To an observer traveling with the geometry, the force on a charged particle can be interpreted as caused by an electric field $\mathbf{E}' = \mathbf{E} + \mathrm{v} \times \mathbf{B}$. In a conductive medium, the observer accordingly sees the current density:

$$\mathbf{J} = \sigma(\mathbf{E} + \mathrm{v} \times \mathbf{B}) + \mathbf{J}_e \quad \textbf{(3.27)}$$

where $\mathbf{J}_e$ is an externally generated current density.

Faraday's law remains unchanged, while Maxwell-Ampère's law for quasi-static systems is consequently extended to:

$$\nabla \times \mathbf{H} = \sigma(\mathbf{E} + \mathrm{v} \times \mathbf{B}) + \mathbf{J}_e \quad \textbf{(3.28)}$$

3.2.2 Boundary conditions

Boundary conditions should be defined at material interfaces and physical boundaries, in order to describe an electromagnetics problem. The boundary conditions are expressed mathematically at interfaces between two media as:

$$\mathbf{n_2} \times (\mathbf{E_1} - \mathbf{E_2}) = 0 \quad \textbf{(3.29)}$$

$$\mathbf{n_2} \cdot (\mathbf{D_1} - \mathbf{D_2}) = \rho_s \quad \textbf{(3.30)}$$

$$\mathbf{n_2} \times (\mathbf{H}_1 - \mathbf{H}_2) = \mathbf{J}_s \quad \textbf{(3.31)}$$

$$\mathbf{n_2} \cdot (\mathbf{B}_1 - \mathbf{B}_2) = 0 \quad \textbf{(3.32)}$$

where $\mathbf{J}_s$ show surface current density, and ρ_s show surface charge density, and $n_2$is the outward normal from media two.

These relationships for current density from interface condition can be described in equation (3.33)

$$\mathbf{n_2} \cdot (\mathbf{J}_1 - \mathbf{J}_2) = -\frac{\partial \rho_s}{\partial t} \quad \textbf{(3.33)}$$

One of the specifications of the perfect conductor, it has no internal electric field with infinite conductivity. In the other hand, the relation of the third fundamental constitutive would produce an infinite current density.

The boundary conditions for the **E** and **D** fields are simplified by any interface between perfect conductor and a dielectric. For example subscript 1 bellowed to perfect conductor; in this case $\mathbf{D}_1 = 0$ and $\mathbf{E}_1 = 0$. If, it is a time-varying case, then $\mathbf{B}_1 = 0$ and $\mathbf{H}_1 = 0$, as well, as a consequence of Maxwell's equations. Equations 3.34, 3.35, 3.36, 3.37, show the result of boundary conditions for the fields in the dielectric medium for the time-varying case:

$$-\mathbf{n_2} \times \mathbf{E}_2 = 0 \quad \textbf{(3.34)}$$

$$-\mathbf{n_2} \times \mathbf{H}_2 = \mathbf{J}_S \quad \textbf{(3.35)}$$

$$-\mathbf{n_2} \times \mathbf{D}_2 = \rho_S \quad \textbf{(3.36)}$$

$$-\mathbf{n_2} \times \mathbf{B}_2 = 0 \quad \textbf{(3.37)}$$

3.2.3 Finite element formulation

In finite element method, the domains are generally discretized into triangular mesh elements. These elements represent an approximation of the original geometry, if the boundary is curved. The bases of the triangles are called mesh sides, and the corners of the triangles are called mesh vertices. A mesh side does not contain mesh vertices in its interior.

The boundaries defined in the geometry are discretized into mesh sides, referred to as side elements or boundary elements, which must conform to the mesh elements of the adjacent domains.

Using equations 3.11 and 3.16, Poisson equation can be formed:

$$\nabla \cdot \nabla \mathrm{V} = -\frac{\rho_v}{\varepsilon_o \varepsilon_r} \quad \textbf{(3.38)}$$

Equation (3.38) applies to a homogeneous medium. If free charge density ρ_v is zero, the equation transforms to Laplace's equation for homogeneous media.

$$\frac{\partial^2 \mathrm{V}}{\partial x^2} + \frac{\partial^2 \mathrm{V}}{\partial y^2} + \frac{\partial^2 \mathrm{V}}{\partial z^2} = 0 \quad \textbf{(3.39)}$$

Equation (3.39) is the voltage potential distribution in high voltage state where $\rho_v = 0$ and the medium is homogeneous.

Using equation (3.39) in order to transform energy function which is related to electrical energy an equation is needed to finite element formulation. There are many

possibilities to derive the function equation. In this study, Galerkin Method has been used.

The Galerkin method assumes that there is a trial solution potential at each node. Interpolation of this set of potentials into the ruling equation will lead to a residual at each node. Obviously the trial values will not be correct. It is however possible to achieve an approximate solution by adjusting the potentials to minimize the sum of the remains at all the nodes. If weighting functions are introduced at each node to try to minimize the sum of the local residual errors over the whole domain, this solution reaches to better results.

The total electrical energy in a system of volume Ω is:

$$W_e = \int_{\Omega} \frac{1}{2} \varepsilon_0 \varepsilon_r \mathbf{E}^2 \, d\Omega \tag{3.40}$$

If the permittivity is constant within the region, then equation (3.40) can be written as:

$$W_e = \int_{\Omega} \frac{\varepsilon_0 \varepsilon_r}{2} \left[\left(\frac{\partial V}{\partial x}\right)^2 i_x + \left(\frac{\partial V}{\partial y}\right)^2 i_y + \left(\frac{\partial V}{\partial z}\right)^2 i_z \right] \mathrm{dx\ dy\ dz} \tag{3.41}$$

In order to get the minimum energy function, as in any function, the derivative of the function should be zero. The variable in this case is the potential. Physically, this process can be considered as minimizing the supplied electrical energy of the system for the imposed boundary conditions.

Equation (3.41) can be written for one element by integrating over the element.

$$W_e^{(e)} = \frac{\varepsilon_0 \varepsilon_r}{2} \int_{(e)} \left[\left(\frac{\partial V}{\partial x}\right)^2 + \left(\frac{\partial V}{\partial y}\right)^2 \right] \mathrm{dx\ dy} \tag{3.42}$$

Hence, the contribution to the rate of changes of energy with respect to potential from the variation of potential of node i in element (e) is only:

$$X^{(e)} = \frac{\partial W_e^{(e)}}{\partial \mathrm{V_i}} = \frac{\varepsilon_0 \varepsilon_\mathrm{r}}{2} \int_{(e)} \left[\left(\frac{\partial V}{\partial x} \right)^2 + \left(\frac{\partial V}{\partial y} \right)^2 \right] \mathrm{dx\ dy} \tag{3.43}$$

$$X^{(e)} = \frac{\varepsilon_0 \varepsilon_\mathrm{r}}{2} \int_{(e)} \left[2 \frac{\partial V}{\partial x} \frac{\partial}{\partial \mathrm{V_i}} \left(\frac{\partial V}{\partial x} \right) + 2 \frac{\partial V}{\partial y} \frac{\partial}{\partial \mathrm{V_i}} \left(\frac{\partial V}{\partial y} \right) \right] \mathrm{dx\ dy} \tag{3.44}$$

To represent a problem numerically, the problem region is separated into elements and (3.44) is applied at the nodes forming the element vertices. The variation of the potential over the element is approximated by a polynomial distribution. The order of the chosen polynomial defines the type of element. For example or a triangular element a linear distribution would suffice. For higher order shape functions, the number of nodes describing the element should be equal to order of the function [31]. The contributions are appeared when the rate of regional change functional χ with respect to the potential $\mathrm{V_i}$ at node i from all the elements connected to i. As it is shown in Figure 3.3, the elements from 1 to 6 are making contribution. As a result, the contribution to $\partial W_e^{(e)} / \partial \mathrm{V}$ from a change in $\mathrm{V_i}$ is shown in equation (3.45).

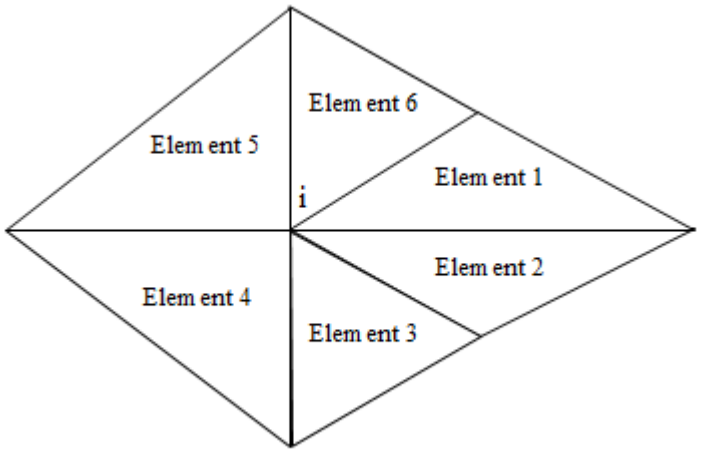

Figure 3.3: Finite elements [25]

$$\frac{\partial W_e}{\partial V_{\mathrm{i}}} = \sum_{(\mathrm{e})} \frac{\partial W_e{}^{(e)}}{\partial V_{\mathrm{i}}} \tag{3.45}$$

The summation of contributions from all related elements are shown by $\sum_{(\mathrm{e})}$, node i is linked with the all elements.

There are four basic steps in Finite Element Method.

1. Discretization: In discretization step, all vertices are numbered; a coordinate is assigned to each vertice; elements are numbered; and environmental properties and boundary conditions are determined.
2. Element basic equations:

For a two dimensional, first-degree polynomial approximation function can be written as follows:

$$V(x, y) = a + bx + cy = a_1 + a_2 x + a_3 y \tag{3.46}$$

The properties for the approximation function are; potential V changes linearly within the finite element and electric field **E** is constant inside the finite element.

$$\mathbf{E} = \mathbf{E}_x \cdot i_x + \mathbf{E}_y \cdot i_y \tag{3.47}$$

$$\mathbf{E}_x = -\frac{dV(x,y)}{dx} = -b \quad , \quad \mathbf{E}_y = -\frac{dV(x,y)}{dy} = -c \tag{3.48}$$

$$|E| = \sqrt{E_x{}^2 + E_y{}^2} = \sqrt{(-b)^2 + (-c)^2} = \sqrt{b^2 + c^2} = \text{constant} \tag{3.49}$$

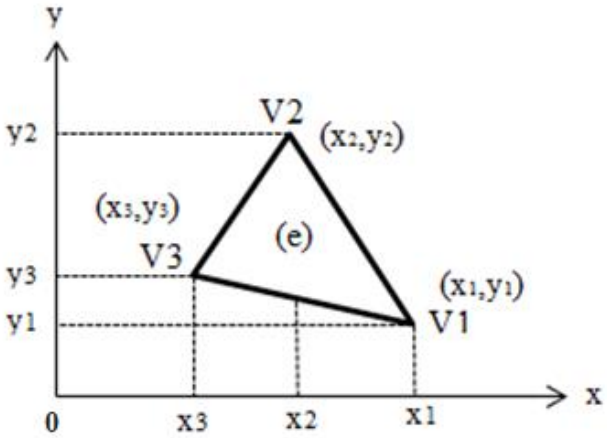

Figure 3.4: Triangular finite element

For each vertice , it is possible to write down potential functions by using approximation function

$$V_1 = a + bx_1 + cy_1 \tag{3.50}$$

$$V_2 = a + bx_2 + cy_2 \tag{3.51}$$

$$V_3 = a + bx_3 + cy_3 \tag{3.52}$$

The equation system can be written also in a matrix form:

$$\begin{bmatrix} 1 & x_1 & y_1 \\ 1 & x_2 & y_2 \\ 1 & x_3 & y_3 \end{bmatrix} \begin{bmatrix} a \\ b \\ c \end{bmatrix} = \begin{bmatrix} V_1 \\ V_2 \\ V_3 \end{bmatrix} \tag{3.53}$$

By using (3.53), a, b, c coefficients can be solved by using Cramer method. The determinant of the matrix in equation 3.53 is also equal to twice of the triangle's area, which is denoted by A. Therefore, the determinant is 2A.

$$a = \frac{1}{2A}[a_1V_1 + a_2V_2 + a_3V_3] \tag{3.54}$$

where a_1, a_2 and a_3 are represented as follows.

$$a_1 = x_2y_3 - x_3y_2 \tag{3.55}$$

$$a_2 = x_3y_1 - x_1y_3 \tag{3.56}$$

$$a_3 = x_1y_2 - x_2y_1 \tag{3.57}$$

In general the term a_i can be calculated as;

$$a_i = x_jy_k - x_ky_j \tag{3.58}$$

where $i \neq j \neq k$ and $i, j, k = 1,2,3$.

Similarly, coefficients b and c can be solved from the equation (3.53).

$$b = \frac{1}{2A}[b_1V_1 + b_2V_2 + b_3V_3] \tag{3.59}$$

$$b_1 = y_2 - y_3 \tag{3.60}$$

$$b_2 = y_3 - y_1 \tag{3.61}$$

$$b_3 = y_1 - y_2 \tag{3.62}$$

The term b_i can be written in a general form

$$b_i = y_j - y_k \tag{3.63}$$

where $i \neq j \neq k$ and $i, j, k = 1,2,3$.

$$c = \frac{1}{2A}[c_1V_1 + c_2V_2 + c_3V_3] \tag{3.64}$$

$$c_1 = x_3 - x_2 \tag{3.65}$$

$$c_2 = x_1 - x_3 \tag{3.66}$$

$$c_3 = x_2 - x_1 \tag{3.67}$$

$$c_i = x_k - x_j \tag{3.68}$$

where $i \neq j \neq k$ and $i, j, k = 1,2,3$.

The term A in the equations 3.54-68 is the area of the triangle as mentioned before and can be calculated as follows.

$$A = \frac{1}{2}\begin{bmatrix}1 & x_1 & y_1\\ 1 & x_2 & y_2\\ 1 & x_3 & y_3\end{bmatrix} = \frac{1}{2}[(y_2 - y_3)(x_1 - x_3) - (y_3 - y_1)(x_3 - x_2)] \tag{3.69}$$

$$= \frac{1}{2}(b_1 \cdot c_2 - b_2 \cdot c_1)$$

$$= \frac{1}{2}[(y_3 - y_1)(x_2 - x_1) - (y_1 - y_2)(x_1 - x_3)]$$

$$= \frac{1}{2}[b_2 \cdot c_3 - b_3 \cdot c_2]$$

$$= \frac{1}{2}[(x_2y_3 - x_3y_2) + (x_3y_2 - x_1y_3) + (x_1y_2 - x_2y_1)]$$

$$= \frac{1}{2}[a_1 + a_2 + a_3]$$

All the a, b, c coefficients are substituted in the approximation function along with the vertices' coordinates and equation 3.70 is obtained.

$$V(x,y) = [1\ x\ y]\frac{1}{2A}\begin{bmatrix}(x_2y_3 - x_3y_2) & (x_3y_1 - xy_3) & (x_1y_2 - x_2y_1)\\ (y_2 - y_3) & (y_3 - y_1) & (y_1 - y_2)\\ (x_3 - x_2) & (x_1 - x_3) & (x_2 - x_1)\end{bmatrix}\begin{bmatrix}V_1\\V_2\\V_3\end{bmatrix} \quad \textbf{(3.70)}$$

$$= [1\ x\ y]\frac{1}{2A}\begin{bmatrix}a_1 & a_2 & a_3\\ b_1 & b_2 & b_3\\ c_1 & c_2 & c_3\end{bmatrix}\begin{bmatrix}V_1\\V_2\\V_3\end{bmatrix}$$

$$= \alpha_1V_1 + \alpha_2V_2 + \alpha_3V_3 = \sum_{i=1}^{3}\alpha_i \cdot V_i$$

$$= V(x,y) = [\alpha_1\ \alpha_2\ \alpha_3]\begin{bmatrix}V_1\\V_2\\V_3\end{bmatrix}$$

where $\alpha_1,\ \alpha_2,\ \alpha_3$are the shape functions and can be determined as follows:

$$\alpha_1 = \frac{1}{2A}\left[\left(x_2y_3 - x_3y_2\right) + \left(y_2 - y_3\right)x + (x_3 - x_2)y\right] \quad \textbf{(3.71)}$$

$$= \frac{1}{2A}(a_1 + b_1x + c_1y) = \alpha_1(x,y)$$

$$\alpha_2 = \frac{1}{2A}\left[\left(x_3y_1 - x_1y_3\right) + \left(y_3 - y_1\right)x + (x_1 - x_3)y\right] \quad \textbf{(3.72)}$$

$$= \frac{1}{2A}(a_2 + b_2x + c_2y) = \alpha_2(x,y)$$

$$\alpha_3 = \frac{1}{2A}\left[\left(x_1y_2 - x_2y_1\right) + \left(y_1 - y_2\right)x + (x_2 - x_1)y\right] \quad \textbf{(3.73)}$$

$$= \frac{1}{2A}(a_3 + b_3x + c_3y) = \alpha_3(x,y)$$

In a triangular finite element, the approximation function for the potential, which is, satisfied within the element then, can be written as:

$$V(x,y) = \sum_{i=1}^{3}\alpha_i(x,y)V_i \quad \textbf{(3.74)}$$

The electrical energy in the element is:

$$W^{(e)} = \frac{1}{2}\int \varepsilon\,.\,|E|^2 ds = \frac{1}{2}\int \varepsilon\left|\nabla V^{(e)}\right|^2 ds. \quad \textbf{(3.75)}$$

$$\nabla V^{(e)} = \sum_{i=1}^{3} V_i \cdot \nabla \alpha_i \tag{3.76}$$

$$\left|\nabla V^{(e)}\right|^2 = \sum_{i=1}^{3}\sum_{j=1}^{3} V_i \cdot V_j \cdot \nabla \alpha_i \cdot \nabla \alpha_j \tag{3.77}$$

3. Recombination of finite elements:

All the finite elements in the region are considered together to form the energy function. Energy function can be rewritten by using shape functions.

$$W^{(e)} = \frac{1}{2}\varepsilon \sum_{i=1}^{3}\sum_{j=1}^{3} V_i \left| \int \nabla \alpha_i \, \nabla \alpha_j \, ds \right| \cdot V_j \tag{3.78}$$

The integrand $\int \nabla \alpha_i \, \nabla \alpha_j \, ds$ is the general term for the element coefficient matrix S.

$$W^{(e)} = \frac{1}{2}\varepsilon \left[V^{(e)}\right]^T \cdot \left[S^{(e)}\right]\left[V^{(e)}\right] \tag{3.79}$$

Element vertice potentials are:

$$\left[V^{(e)}\right] = \begin{bmatrix} V_1 \\ V_2 \\ V_3 \end{bmatrix} \tag{3.80}$$

$$\left[V^{(e)}\right]^T = [V_1 \; V_2 \; V_3] \tag{3.81}$$

The matrix S is also called stiffness matrix.

$$\left[S^{(e)}\right] = \begin{bmatrix} {S_{11}}^{(e)} & {S_{12}}^{(e)} & {S_{13}}^{(e)} \\ {S_{21}}^{(e)} & {S_{22}}^{(e)} & {S_{23}}^{(e)} \\ {S_{31}}^{(e)} & {S_{32}}^{(e)} & {S_{33}}^{(e)} \end{bmatrix} \tag{3.82}$$

By using equations 3.71-73, the stiffness matrix can be written in a general form

$${S_{ij}}^{(e)} = \int \nabla \alpha_i \cdot \nabla \alpha_j \, ds \, , \quad \vec{\imath} \; \vec{\imath} = \vec{\jmath} \; \vec{\jmath} = 1 \, , \; \vec{\imath} \; \vec{\jmath} = 0 \tag{3.83}$$

$$S_{ij} = \frac{\varepsilon}{4A}\left(b_i \cdot b_j + c_i \cdot c_j\right) \tag{3.84}$$

where $i = 1,2,3$ and $j = 1,2,3$

$$\left[S^{(e)}\right] = \frac{\varepsilon}{4A}\begin{bmatrix} {b_1}^2 + {c_1}^2 & b_1b_2 + c_1c_2 & b_1b_3 + c_1c_3 \\ b_1b_2 + c_1c_2 & b_2 + c_2 & b_2b_3 + c_2c_3 \\ b_1b_3 + c_1c_3 & b_2b_3 + c_2c_3 & {b_3}^2 + {c_3}^2 \end{bmatrix} \tag{3.85}$$

4. Solution of equation system:

If the energy equation (3.79) within the element is written for the entire solution region the total energy can be obtained.

$$W = \sum_{e=1}^{n_e} W^{(e)} \tag{3.86}$$

where n_e is the total number of elements. Since the basic principle of the FEM is minimization of the energy,

$$\frac{\partial W}{\partial [V]} = 0 \tag{3.87}$$

is solved for the entire region. Known potentials are written, for the unknown potentials the equation system is solved. In general, the potentials can be written as follows:

$$V_j = \frac{1}{S_{jj}} \sum_{\substack{i=1 \\ i \neq j}}^{n_d} S_{ij} \cdot V_i \tag{3.88}$$

Chapter 4

NUMERICAL ANALYSIS OF LIGHTNING DISCHARGE

4.1 Electrostatic Model

In this study, lightning strike phenomena is investigated using electric field and potential calculations. The thundercloud is considered to be a plane electrode considering they are 1-3 km (approximately 2 km) above the ground.

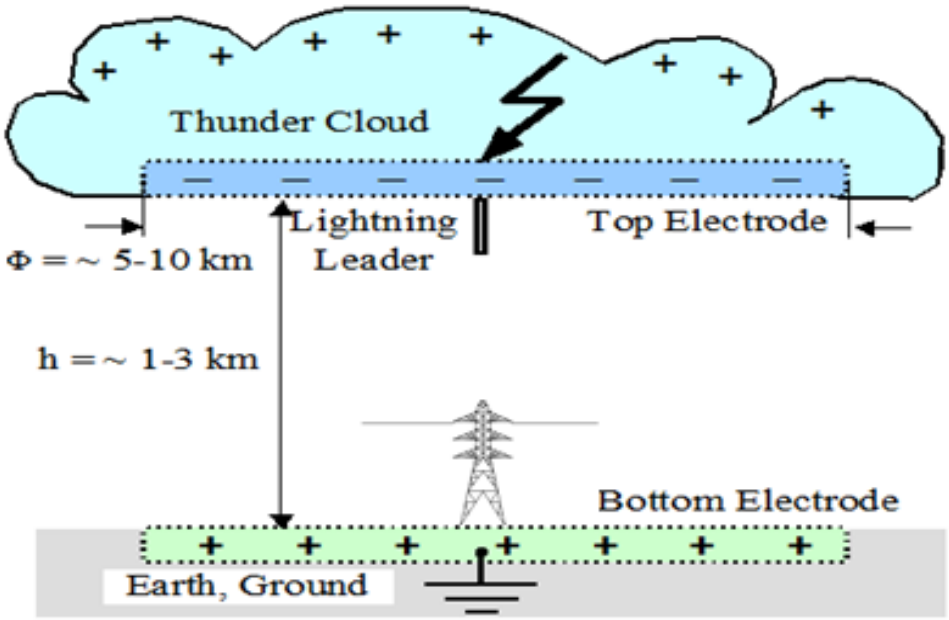

Figure 4.1: The electrostatic model

The electrical configuration can be represented by a parallel plate electrode system, having a 2km electrode separation with a uniform field distribution. In this model, the cloud is the top electrode; ground is the bottom electrode. In this electrode configuration, discharge channels namely stepped leaders, move from the cloud

towards the ground by 50-100 m long steps; they recombine with the points suitable with regard to potential and electric field and they eventually reach to the ground.

The power line tower is considered to be chargeless conductor object and maximum electric field points; magnitudes and change with outer field have been calculated. All these calculations have been carried out for the cases lightning leader approaching the tower step by step vertically at a constant speed, and leader approaching to the tower with a random path. Therefore, it is possible to evaluate case regarding a lightning approaching to power line tower, and striking to it by determining maximum field change on and around the tower in time and space domains. COMSOL Multiphysics software as a Finite Element Method used to analyse electric field distribution and current density distribution.

4.2 Finite Element Analysis

The thundercloud is simulated as an infinitely large plate with a given potential of 100 MV. This arrangement gives a uniform field between the ground and the cloud. Since there is no need for mesh generation for conductors, the leader is represented by a chargeless line, which is compatible with the real diameter (less than a millemeter) of a lightning channel. The leader stretches downward to the surface of the earth step by step. The location of the tower is usually in the ground level. The stepped leader is situated directly upon the tower and stretched toward the ground in discrete steps. At each step 100 m, the electric field, potential and current density are calculated using finite element method in various locations around the tower to investigate the conditions.

In finite element method, the problem should be in a closed geometry in order to generate mesh. If the physical problem does not have boundaries as in this case, the

problem is closed by using artificial boundaries. For that reason, 8000 m wide 2000 m high rectangle is created to represent the thundercloud 2000 m above the ground as shown in the Figure 4.2. A single line of 100 m at the location of (0, 2000) represents the leader. A tower with a height of 50 m is placed at ground 0. Electric potential of 100 MV applied to thunder cloud and the lightning leader. The insulation medium is air with a permittivity of 1.

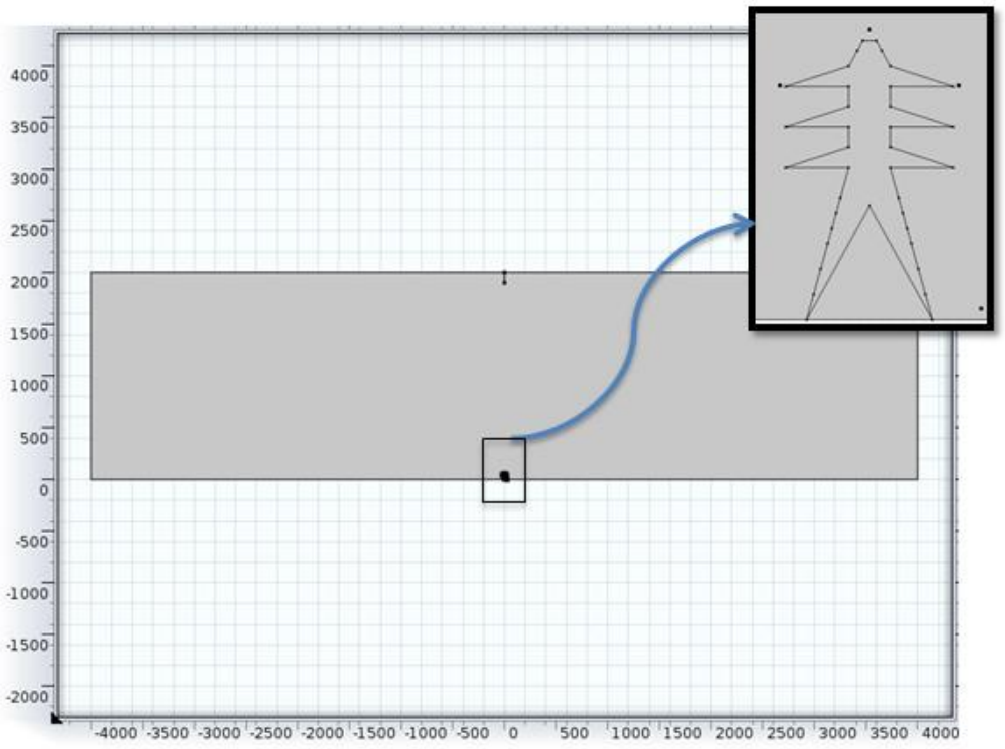

Figure 4.2: Problem structure for FEM

4.2.1 Vertical steps to the tower

In this case, lightning leader is assumed to be approaching to a tower with 100 m steps vertically. The model has 3 domains, 45 boundaries and 47 vertices, all of which are evaluated for electrical field and current density. The complete mesh consist of 2288 to 2388 domain elements for each case while changing the starting location of the leader, and FEM solves the problem with 299 boundary elements.

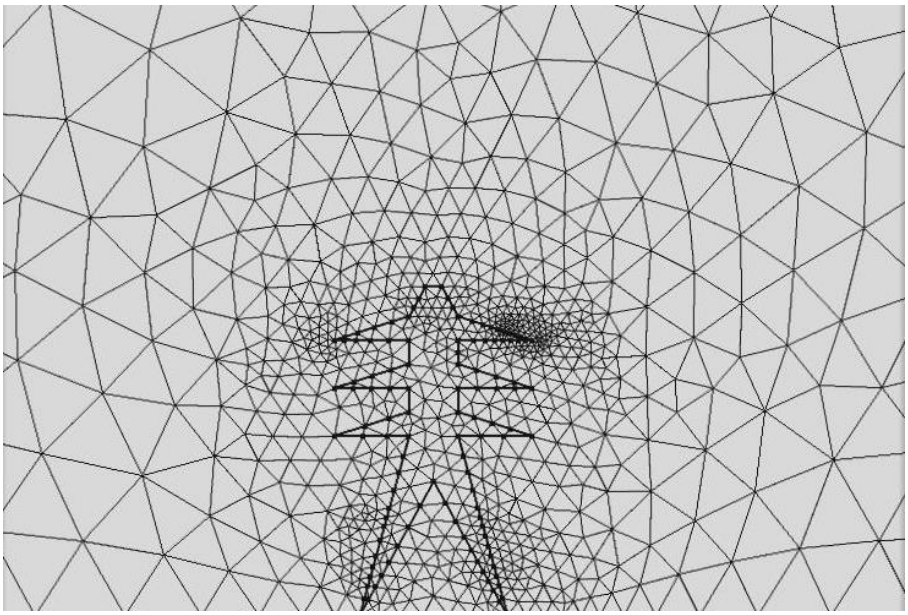

Figure 4.3: Finite element mesh used in this study.

The electric field and current density are higher at the top of the tower compared to the left and right sides of the tower, and electric field intensity gradually decreases inversely with the y coordinate as shown in Figure 4.4. In other words, the electric field and current density increases when the leader reaches to the ground.

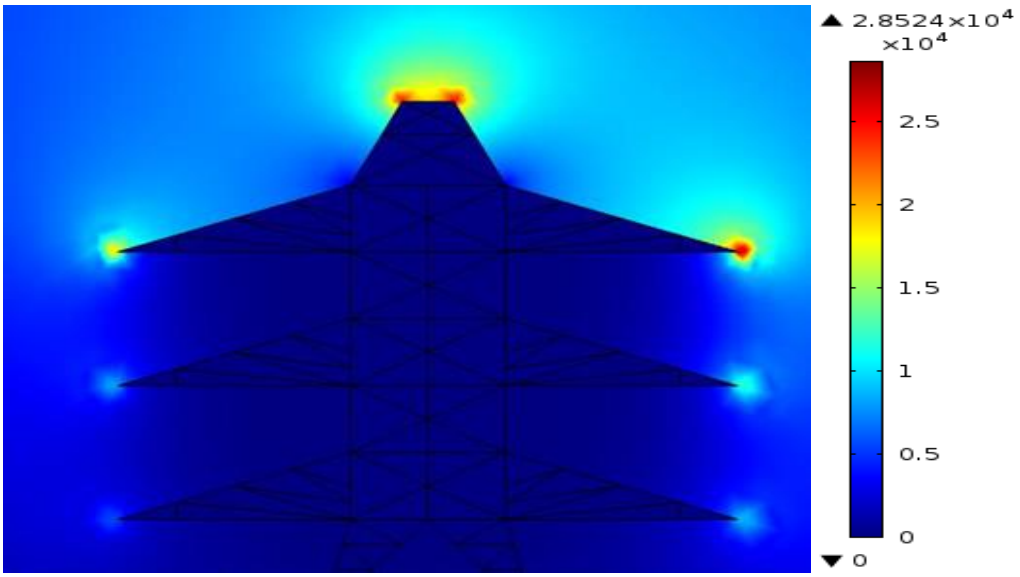

Figure 4.4: Electric field distribution on the tower.

When the leader is initiated, which is simulated by a single line 100 m far from the thunder cloud, the value of electric field intensity at the top of tower is 15497.46143 [V/m] and current density is 0.31929 [A/m^2], after 19 steps, the leader reaches to the length of 1900 m (100 m above the tower) the level of the electric field intensity is increased to 245654 [V/m], and current density is increased to 259.86713 [A/m^2]. Similar trends are observed for other locations as well.

Figures 4.5 and 4.6 show the electric field and current density distribution at the top (green), left side (blue) and right side (red) of the tower, for a leader which is initiated directly on top of the tower (0,2000).

Foreseeably, when the lightning leader approaches to the tower, both electric field intensity and current density increase. The calculations from the right side and the left side of the tower are very close to each other because of the symmetry of the model. The slight change in the magnitudes is as a result of approximate solution in

the FEM. Since a lightning channel takes a step of 10 to 100 m every 300 ns, the change in electric field and current density in time have the same trends.

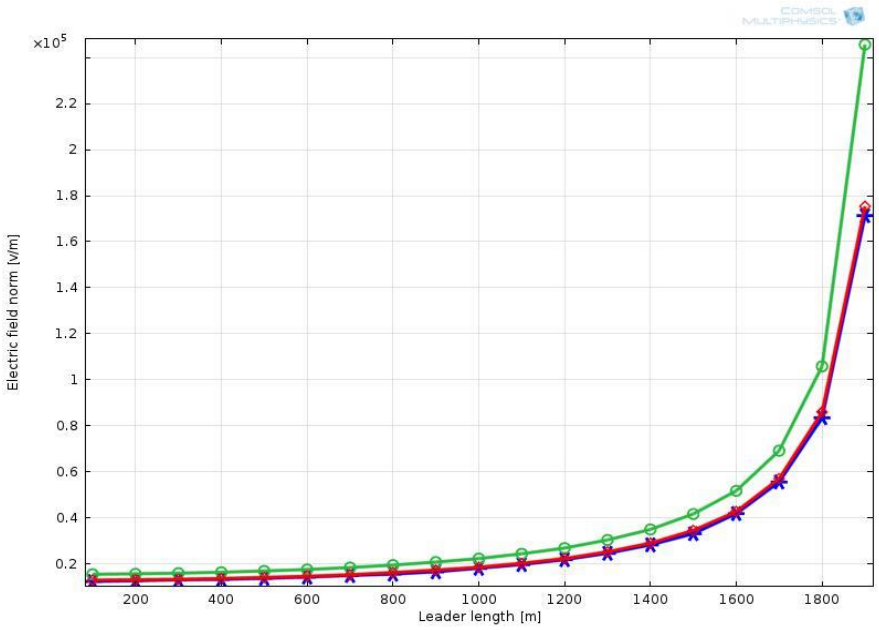

Figure 4.5: Electric field distribution with respect to leader length.

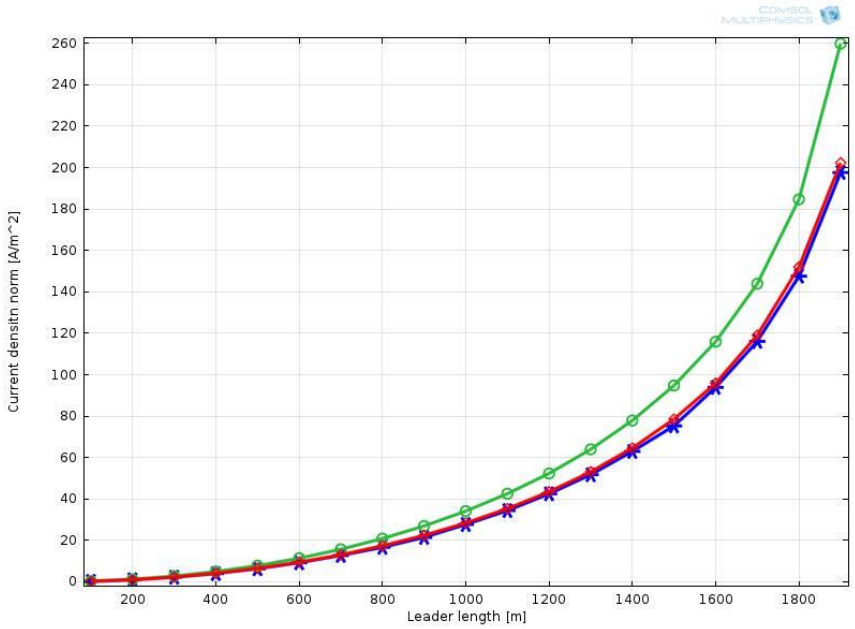

Figure 4.6: Current density with respect to leader length.

In order to investigate the possible harmful effects on living, similar studies have been carried out at 2 m above the ground, which is denoted as the human level. The field intensity and current density are both very small at the human level compared to those on the tower; therefore, the analysis is done separately. The results are shown in the Figure 4.7 and 4.8.

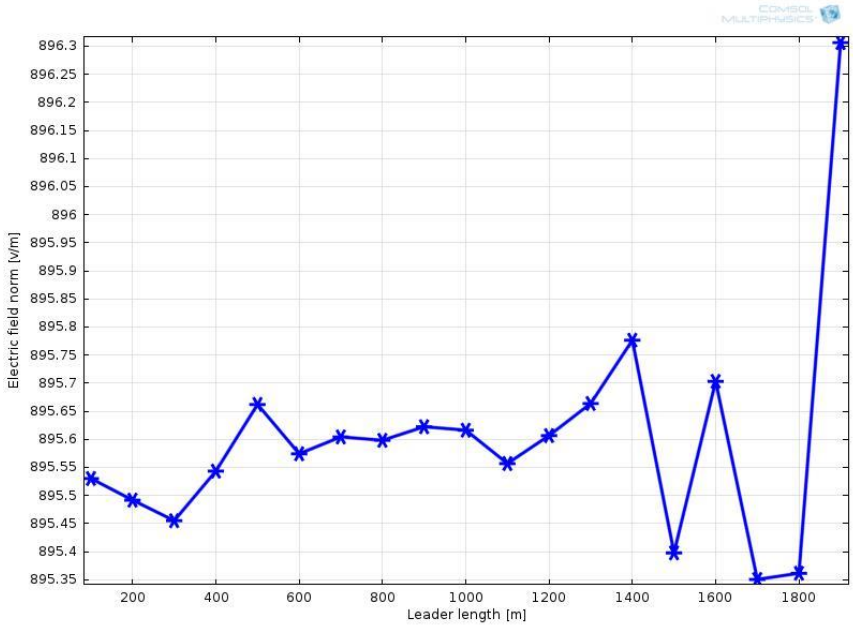

Figure 4.7: Stepped leader length with electric field on human level.

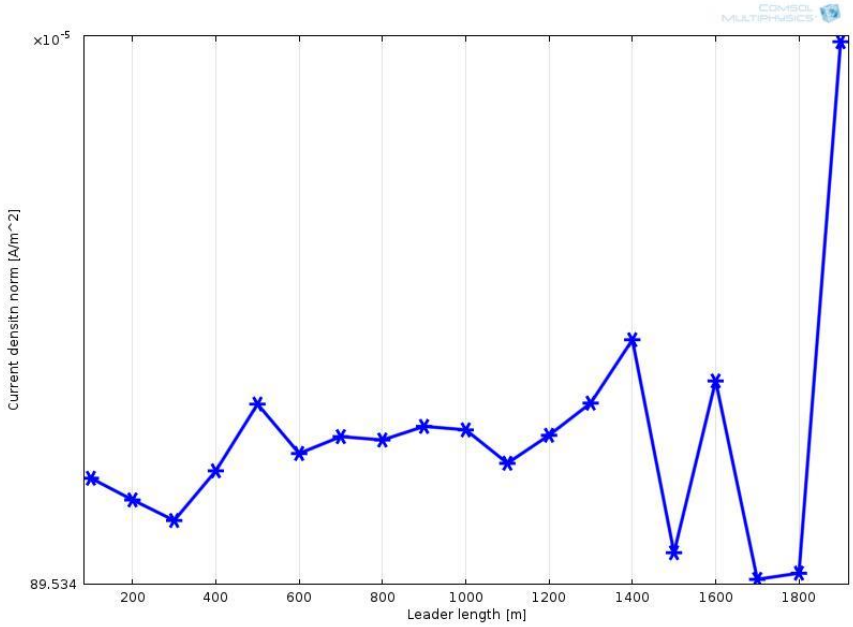

Figure 4.8: Stepped leader length with current density on human level.

The leader initiation position is changed by 500 m length step by step away from the first position to the right and left to analyse the field distribution in unsymmetrical cases. The electric field and current density distribution around the tower (at the top (green), left side (blue) and right side (red) of the tower) are shown in the Figures A.1 to A. 32 in Appendix A for a leader approaching to tower vertically.

As seen in the Figure 4.9, when the leader gets closer to the tower, electric field and current density increase.

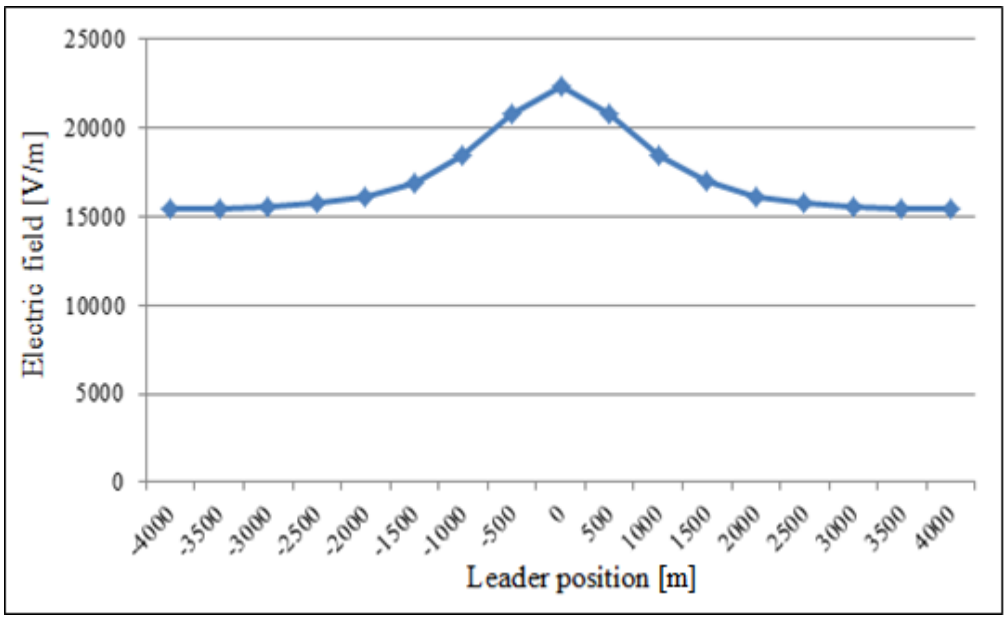

Figure 4.9: Electric field with respect to (x-coordinate).

In addition to that, it is observed that when the leader initiation point gets far from the tower, the electric field intensity and current density at right side and left side of the tower decrease. However, maximum electric field and current density at the top of the tower does not seem to change too much. Because the top of the tower forms a sharp point, which is also the highest point in the model, that is with the smallest curvature radius. All of those are compatible with lightning discharge theory and electrostatics.

In order to expand the model, a power line is added to the current model. The transmission line applied with 154 kV electrical potential and the leader with 100 A/m² boundary current source to analyse current density. The model has 114 domains, 225 boundaries, and 122 vertices. The complete mesh consists of 11821 domain elements and 1321 boundary elements. Figure 4.10 shows the geometric structure of the model.

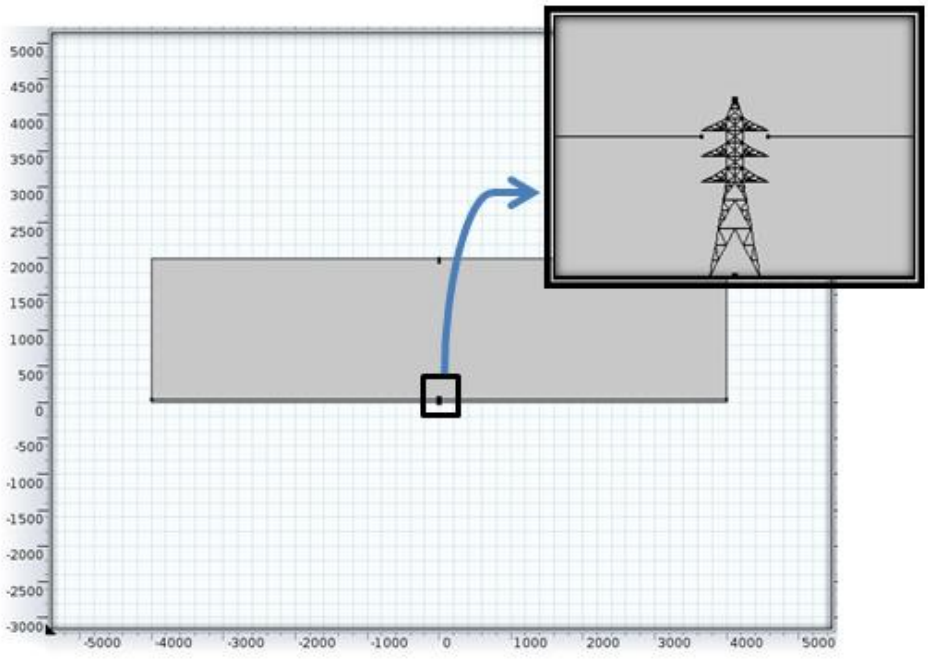

Figure 4.10: Geometric structure of tower and transmission line model.

Figure 4.11 show the generated mesh of the model.

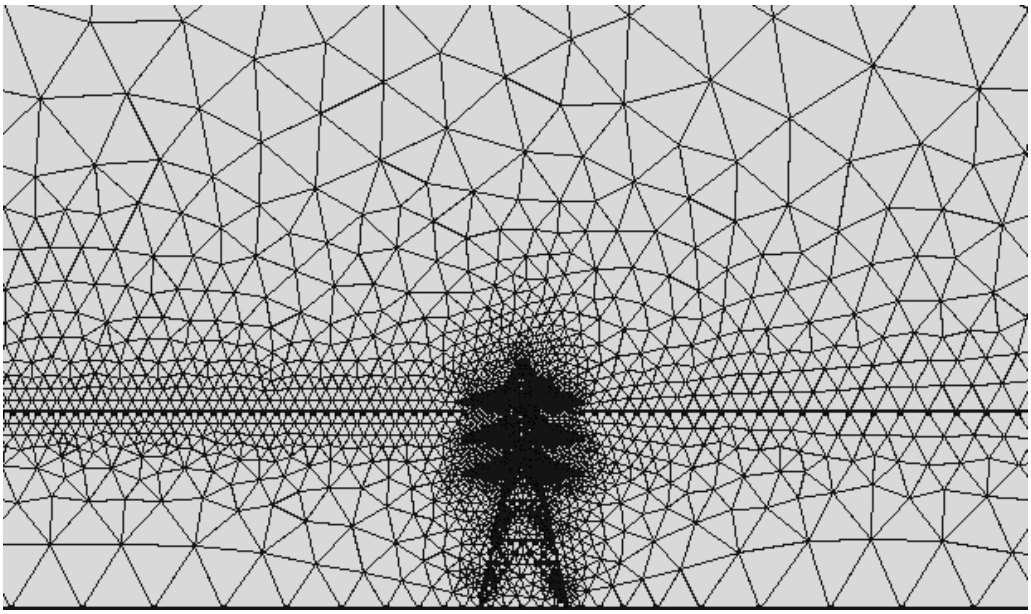

Figure 4.11: Finite element mesh for tower and transmission line.

After applying all the boundary conditions the mesh is generated and the problem is solved for electric potential, electric field and current density. The change in electric potential on the line with respect to lightning leader can be seen in the Figure 4.12. In this solution, lightning leader is assumed to be taking constant steps vertically. Since lightning travels with the speed of light, each step has a constant time. Therefore the graph in Figure 4.11 can be also considered as the change in time, which is compatible with the theory of travelling waves. It can safely assumed to be the change in time instead of arc length.

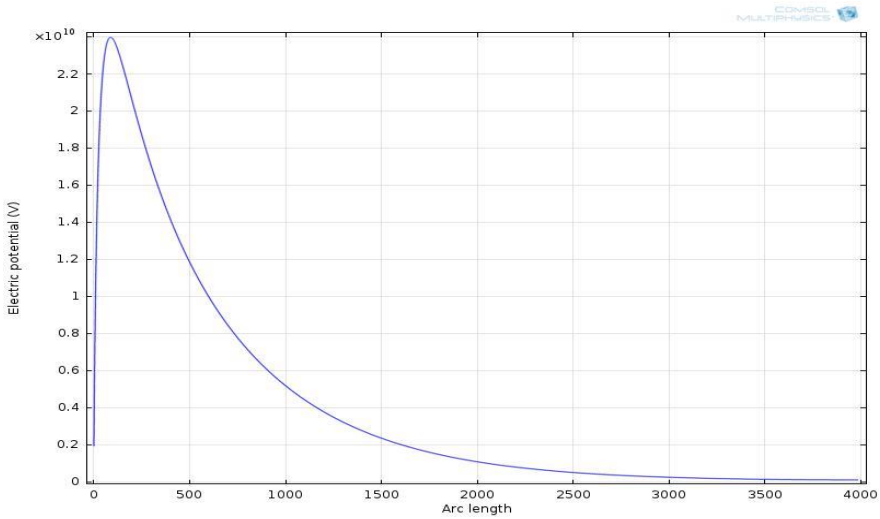

Figure 4.12: The electric potential on the line.

Figure 4.13 shows the electric field distribution on the line at the left side of the tower as the lightning leader (x- coordinate) travels from -4000 to 0, for the cases with different leader length. As shown in the Figure 4.13, if the lightning leader is closer to the tower, the intensity of electric field increases.

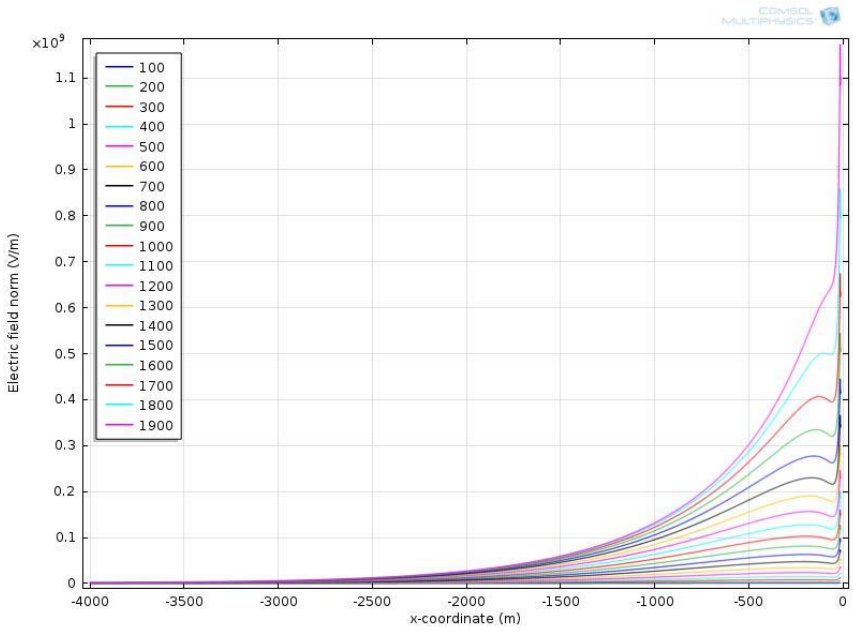

Figure 4.13: Electric field distribution on the left line.

The Figure 4.14 shows the electrical field distribution on the line at the right side of the tower (x-coordinate) from 0 to 4000, for all the cases with different leader length.

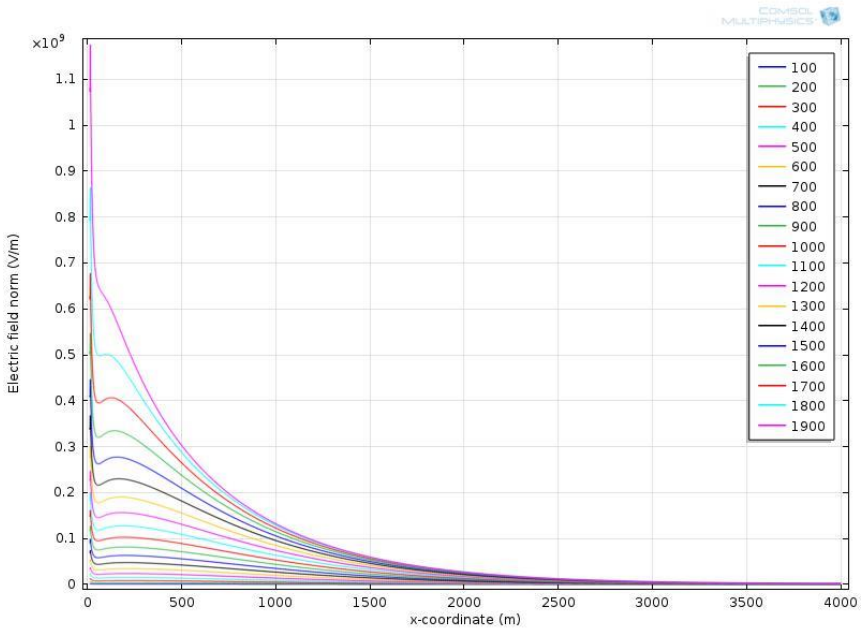

Figure 4.14: Electric field distribution on the right line.

The Figure 4.15 shows the current density distribution on the line at the left side of the tower (x-coordinate) from -4000 to 0, for all the steps of the leader.

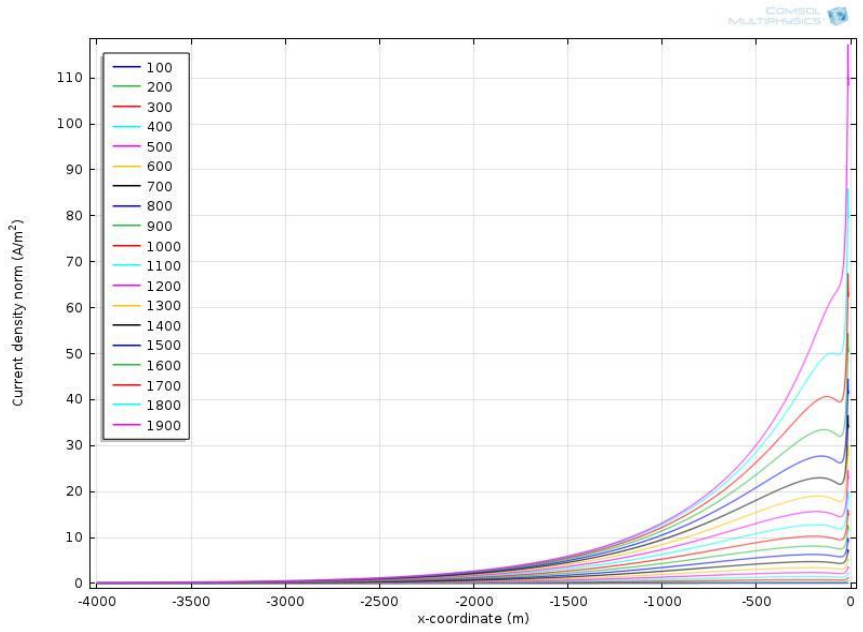

Figure 4.15: Current density distribution on the left line.

The Figure 4.16 shows the current density distribution on the line at the right side of the tower (x-coordinate) from 0 to 4000, for all the steps of the leader.

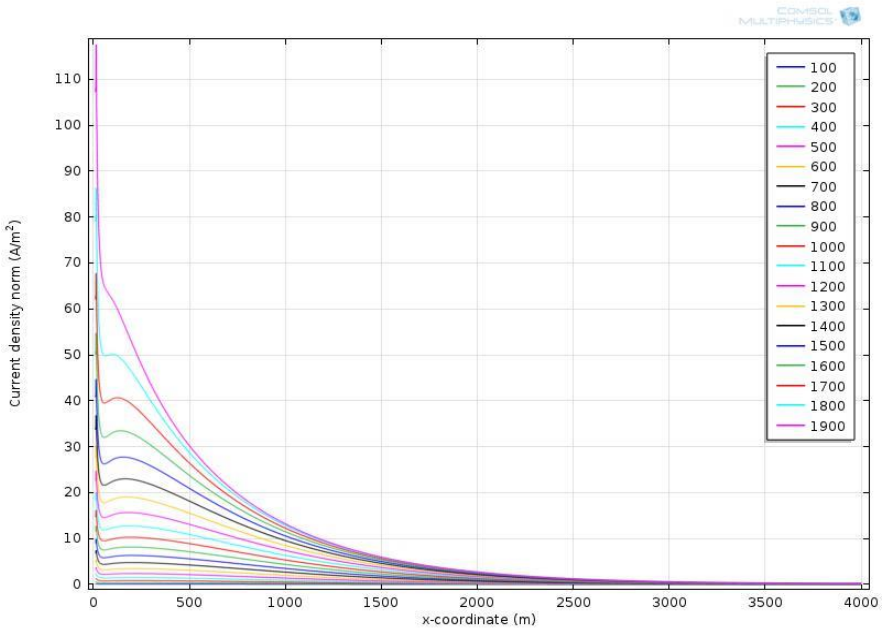

Figure 4.16: Current density distribution on the right line

As mentioned before, the Figures 4.12-16 can be considered as the change in time because lightning travels with constant speed (speed of light), and each step of the leader takes 300 ns to travel.

4.2.2 Random steps to the tower

To analysis the electric field and current density more realistically, the path of the lightning leader is changed from vertical constant steps to a random path. To create a random path for the lightning leader, Monte Carlo method is adapted to the FEM solution. The Monte Carlo technique is a statistical process [32], which operates generating casual variables and produces as result the probability function of the output variable. Monte Carlo model is a generally used computational method that depends on repeated random sampling to obtain numerical results.

In this study, the leader takes a step to the right or left or downward, the probability of a leader to go upward is considered to be zero. A step for the leader to take is determined randomly as seen in the Figure 4.17 the possibility for a lightning leader to take a step upward is 0, to left and right 25% and downward 50%.

```
xb=a;
yb=H;
xp=[a];
yp=[H];
for i=1:1000;
    n(i)=rand(1);
    if n(i)<0.25;
    xl=100;
    yl=0;
    elseif (n(i)>=0.25) && (n(i)<0.5)
    xl=-100;
    yl=0;
    else
    xl=0;
    yl=-100;
    end
xb=xb+xl;
yb=yb+yl;
if yb==0
    break
elseif xb >= 4000 || xb<=-4000
    break
end

xp=[xp xb];
yp=[yp yb];

end
```

Figure 4.17: Algorithm to creating random leader step.

A random number generator helps the model to take random steps as shown in the Figure 4.17. It is decided that when the random number which is in the range of 0 and 1 is between 0 and 0.25, the lightning should take a step to the right, when it is between 0.25 and 0.5 lightning takes a step to the left, otherwise lightning goes downward.

The model with a random path has a finalized geometry of 114 domains, 254 boundaries, and 145 vertices. The complete mesh consists of 4481 domain elements and 785 boundary elements. Figure 4.18 shows the model with its generated mesh.

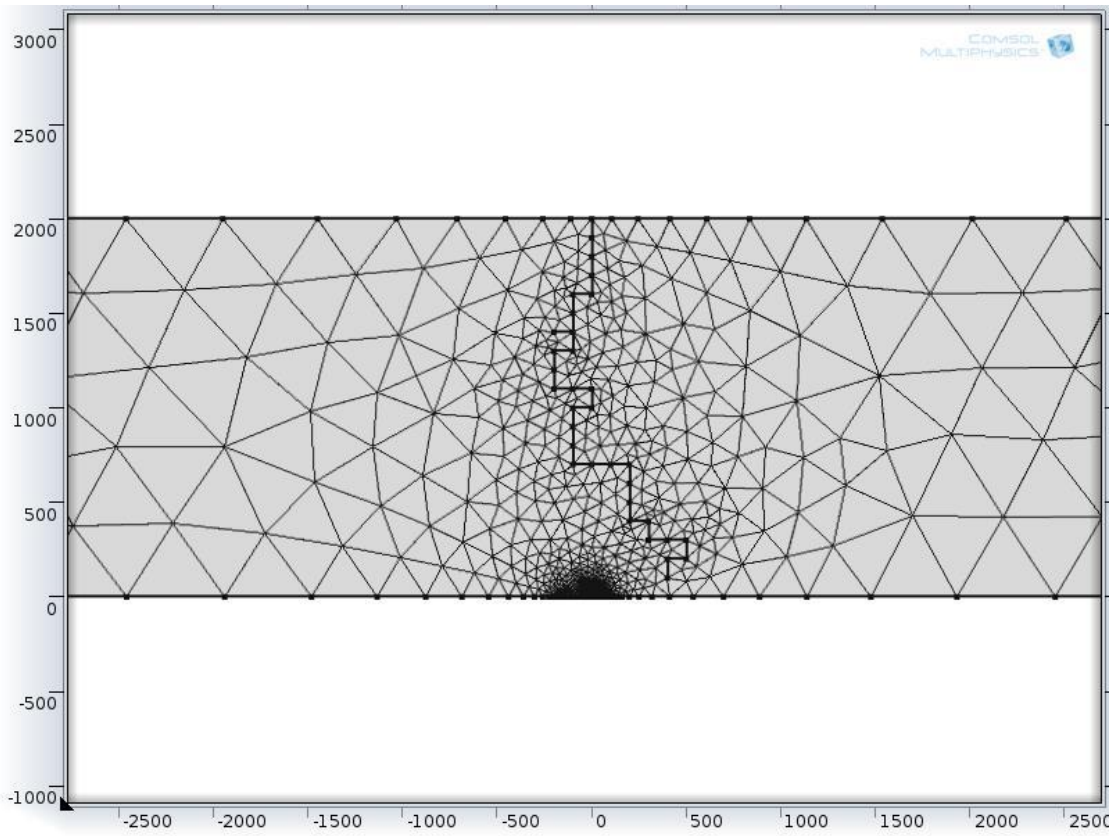

Figure 4.18: Mesh analysis for random steps to the tower

To analyse the electric field distribution, three random paths are generated for the leader. Each step has the length of 100 m. Figure 4.19 shows the evaluation of the electric field distribution at human level that is 2 m above the ground for three different random paths. As expected, the electric field intensity increases when the leader gets closer to the tower. The result shows that the calculated maximum electric field intensities for three different random paths are very close to each other.

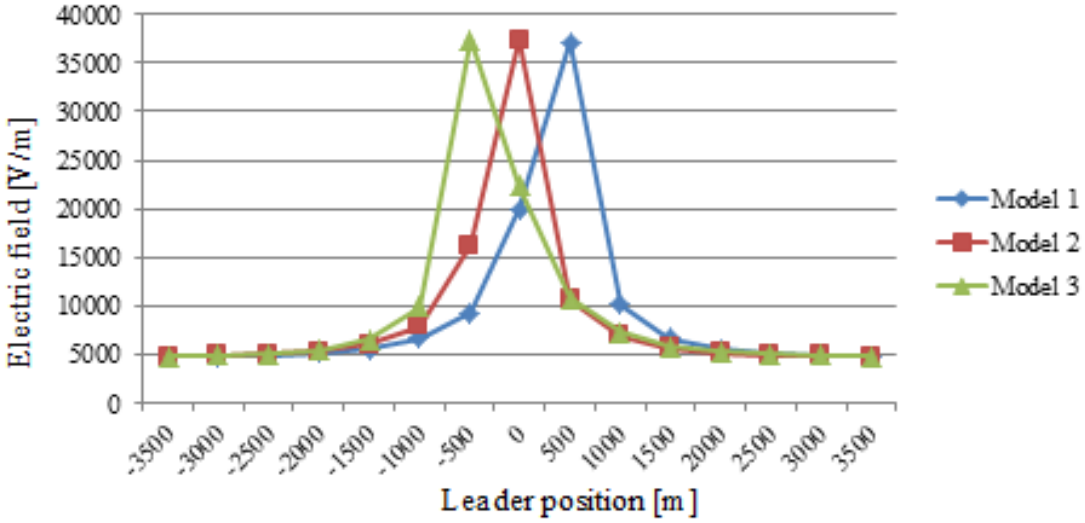

Figure 4.19: Three models of random stepped leader on human level.

The results show that, regardless of the path, the maximum electric field intensity does not change dramatically, proving the consistency of the model.

4.3 Discussions

The results show that, when a lightning leader gets closer to a structure on the ground, electric field intensity and current density increases. The highest level of both electric field and current density are observed at the top of the tower. During a symmetrical simulation, it is observed that, field and current density at the both sides of the tower are almost the same. All the calculations are given as graphs in the Chapter 4 and the numerical values can be seen in the Appendix. For example from Table B.1, the magnitude of electric field intensity is 15497.46143 [V/m] at the top of the tower while the value on the left and right sides of the tower are 12380.62462 [V/m] and 12940.44022 [V/m] respectively in the case of 100 m long leader. When the lightning leader reaches to 1900 m, the magnitude of electric field intensity at the top of the tower is 245654 [V/m], while on the left and right sides are 171328 [V/m], 175369 [V/m], respectively. Similar observation can be carried out for current density, as well. For the human level, the magnitude of electric field and current

density varies with the length of the leader; the highest field and current density are observed with a leader of 1900 m long. All those calculations are compatible with the lightning theory.

Random path for the lightning leader is more accurate and realistic than vertical path. It can be seen in the Figure 4.18 even though the leader path is completely random; the electric field intensity has almost the same magnitude.

Chapter 5

CONCLUSION AND FUTURE WORK

5.1 Conclusions

Lightning phenomenon is one of the most unpredictable weather hazards. It might be very destructive not only on the structures at the ground and power systems facilities but also on human. Therefore, it is very important to understand the effect of lightning.

In this study, an electrostatic model of a tower under thundercloud in the preliminary breakdown phase of lightning is presented. The analyses have been carried out numerically by means of electric field distribution as well as current density. The numerical solutions are obtained by using COMSOL software of Finite Element Method in this study. A multiphysics solutions including electrostatic, electromagnetic and/or heat distribution of a lightning is possible by finite element method. Furthermore, the numerical solution can be linked to the MATLAB to alter the solution if needed.

Electric field distribution and current density around a tower are observed in space and time. The relationship between electric field around the tower when a lightning leader approaches to it is given with figures and tables. As the results of this study of numerical analysis, it is noted that changes in electric field is informative about

lightning strike possibilities. Therefore, it is helpful to find a way to prevent the risks by analysing striking positions of lightning.

It is seen that, electric field strength reaches to very high intensities at the points those have small curvature radius on the tower such as the top and cross arms. Those points are very effective in case of a lightning strike. The results of simulations can use in risk assessment studies.

5.2 Future work

In the future studies, the model will be improved to have a more simulation. The lightning leader can be simulates by space charges. In order to model the return stroke, another beam from the structure on ground towards the lightning leader can be considered.

In this study, the model is created in two dimensions. The model can be solved in 3D to see the whether there is a change in the performance by comparing to 2D model. Heat analysis can be added to the model in order to observe the enhancement in terms of charge distribution of lightning phenomenon. According to the different analysis, the most suitable method of modelling a lightning channel can be selected.

REFERENCES

[1] Weather. Lightning Strikes “KSN.COM”, April 3, 2012.

[2] Sacurajima Volcano with lightning, “Wordless Tech”, March 12, 2013.

[3] AZ area of haboob and lightning, “Series of images from the San Simon”, Julay 12, 2013.

[4] C. Christopoulos, “Modelling of lightning and its interaction with structures,” Vol. 6 , no. 4, Engineering Science and Education Journal, Pages: 149 - 154 August, 1997.

[5] S. Kato, T. Narita, T.Yamada, and E. Zaima, “Simulation of Electromagnetic Field in Lightning to Tall Tower,” High voltage engineering, 1999. Eleventh International Symposium on (Conf. Publ. No. 467), vol. 2, Pages: 59 - 62, Publication Year, 1999.

[6] M.A. Uman, D.K. McLain, “Magnetic field of lightning return stroke”, Journal of Geophysical Research, Vol. 74, 1969.

[7] V.A. Rakov and A.A. Dulzon, “A modified transmission line model for lightning return stroke field calculations”, in Proc. 9th Int. Zurich Symp. Electromagnetic Compatibility, Zurich, Switzerland. Mar, 1991.

[8] C.A. Nucci, C. Mazzetti, F. Rachidi, and M. Ianoz, "On lightning return stroke models for LEMP calculations", in Proc.19th Int. Conf. Lightning Protection, Graz, Austria, Apr, 1988.

[9] V. Rakov, and M.A. Uman, "Review and evaluation of lightning return stroke models including some aspects of their application", IEEE Trans. Electromagn. Compat. 40 (4), 1998.

[10] D.M. Le Vine, and J.C. Willet, "The influence of channel geometry on the fine scale structure of radiation from lightning return strokes", J. Geophys. Res. 100, 1995.

[11] Wan Hao-jiang, Wei Guang-hui, and Chen Qiang, "Three-Dimensional Numerical Simulation of Lightning Discharge Based on DBM Model," Computer Science and Information Technology (ICCSIT), 2010 3rd IEEE International Conference, vol.3, Pages: 520 - 523, 2010

[12] M.S.I. Hossaini, and O. Goni, "Numerical Electromagnetic Analysis of GSM Tower under the Influence of Lightning Overvoltage using Method of Moments,". Power and Energy Conference, 2008. PECon 2008. IEEE 2nd International ,Digital Object Identifier: 10.1109/PECON.2008.4762554, Page(s): 695 – 700, 2008.

[13] F. Heidler, "Travelling current source model for LEMP calculation", Proc of the 6th Symposium and Technical Exhibition on Electromagnetic Compatibility,

Zurich, March 5-7, 1985.

[14] www.epa.org.kw, “beaatona”, journal of the envieronment - no. 115, , p. 20-28, julay, 2009.

[15] [Atmospheric electricity] From Wikipedia, the free encyclopedia Silvanus Phillips Thompson, “Elementary Lessons in Electricity and Magnetism,” 1915.

[16] Lukasz Staszewski, “Lightning Phenomenon – Introduction and Basic Information to Understand the Power of Nature”, University of Technology Wybrzeze Wyspianskiego 27.

[17] Assistant Professor Suna BOLAT, Lecture notes. “Advanced High Voltage Technique - Travelling Waves on Transmission Line”

[18] V. A. Rakov, and M. A. Uman, “Lightning: Physics and Effects”, Cambridge University Press, Cambridge, UK., via (KTH) Electrical Engineering, Experimental Observations and Theoretical Modeling of Lightning Interaction with Tall Objects, 2003.

[19] Evolution of a lightning stroke -the return stroke.htm, Internet.

[20] N. Theethayi, V. Cooray, “On the Representation of the Lightning Return Stroke Process as a Current Pulse Propagating Along a Transmission Line”. IEEE Journals & Magazines. Vol.20 , Issue: 2 , Part: 1. Pages: 823 - 837, 2005.

[21] N. Theethayi and V. Cooray, “Transmission Line Model - An Idealisation or Reality,” paper accepted for presentation, IEEE Bologna Power Tech

Conference, Bologn, Italy June 23th - 26 th, 2003.

[22] S. Andrew Podgorski, “Three-Dimentional Time Domain Model of Lightning Including Corona Effects,” Electromagnetic Protection Group, Institute for Information Technology. National Research Council of Canada, Ottawa, Canada K1A OR6.

[23] J. Dunkin - Wittenberg University Project Advisor – Dr. Daniel Fleisch “Digital Simulation of Thunder from Three-Dimensional Lightning,”

[24] Yazhou Chen, and Lin Wang, “Research on Channel-base Current of Lightning Return stroke ,” Mechanic Automation and Control Engineering (MACE), 2011 Second International Conference on, Digital Object Identifier: 10.1109/MACE.2011.5988804 , Page(s): 7579 - 7582, 2011.

[25] A. Haddad and D.Warne. “Advance in High Voltage Engineering”. IET Power and Energy Series 40.

[26] Klaus-JurgenBathe, “Finite Element Procedures,” Prentice Hall, 1996.

[27] Prof. Olivier de Weck, and Dr. Il Yong Kim, “Finite Element Method, ” Engineering Design and Rapid Prototyping. Januarry 12, 2004.

[28] Ozcan Kalenderli, and Suna Bolat, “Analysis of Lightning Strike to Airplane by Finite Element Method,” Istanbul Technical University, Istanbul, Turkey,

Eastern Mediterranean University, Famagusta, TRNC.

[29] Documentatoin of, “Comsol Multiphysics,”

[30] P. Franklin, “Methods of Advanced Calculus,”1st edn. McGraw-Hill Book Company Inc., New York and London, 1944.

[31] A.B.J. Reece, and T.W Preston, “Finite Element Methods in Electrical Power Engineering,”Oxford University Press, 2000.

[32] Fabio Mottola. “Methods and Techniques For The Evaluation of Lightning Induced Overvoltages on Power Lines”, November 2007.

APPENDICES

Appendix A: Electric field and current density distributions for a lightning leader that approaches vertically to the right and left sides of the tower.

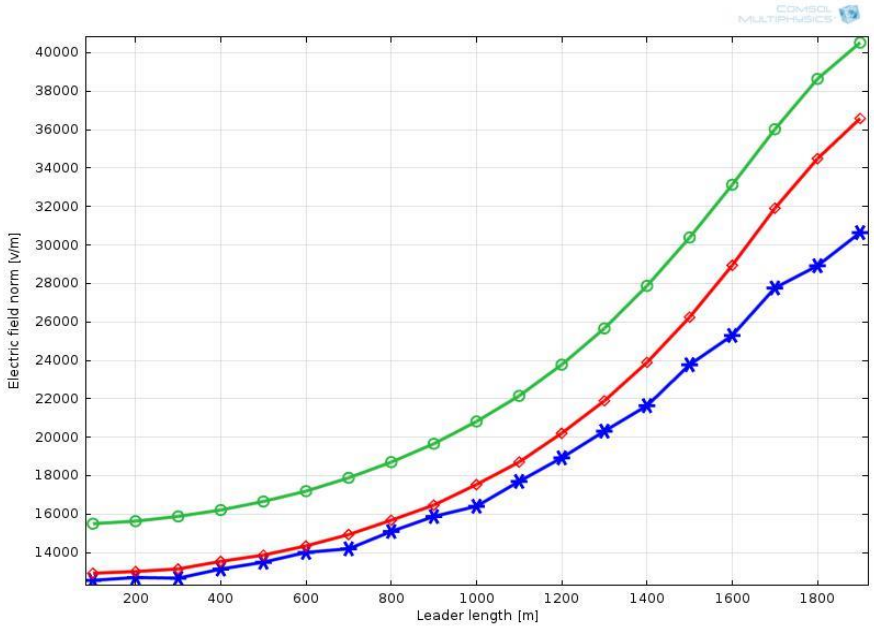

Figure A. 1: Electric field with respect to leader length that initiates at (500,2000).

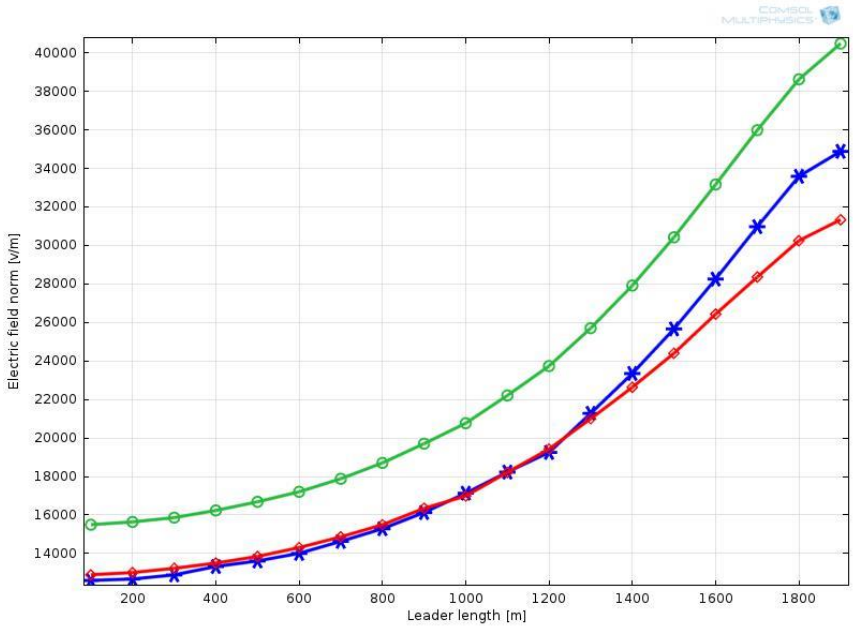

Figure A. 2: Electric field with respect to leader length that initiates at (-500,2000)

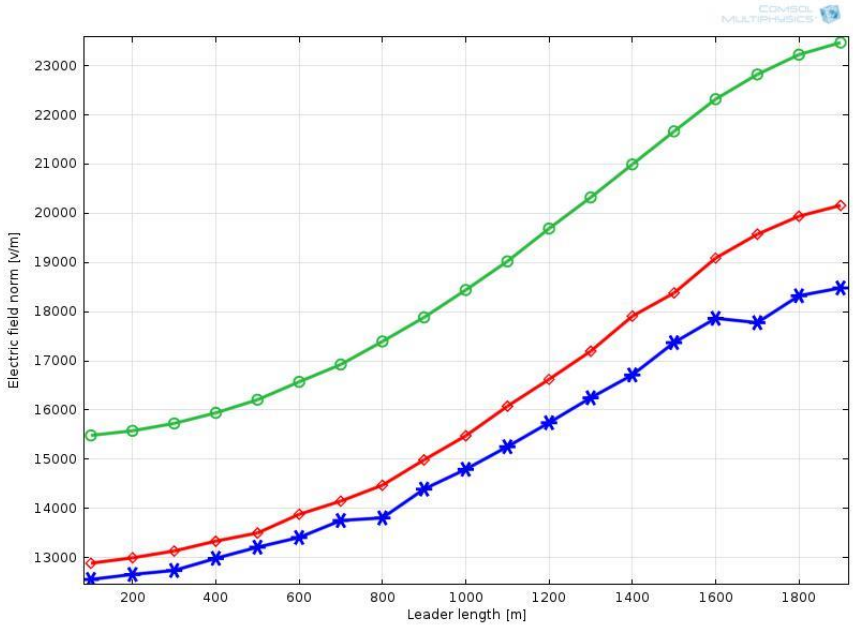

Figure A. 3: Electric field with respect to leader length that initiates at (1000,2000).

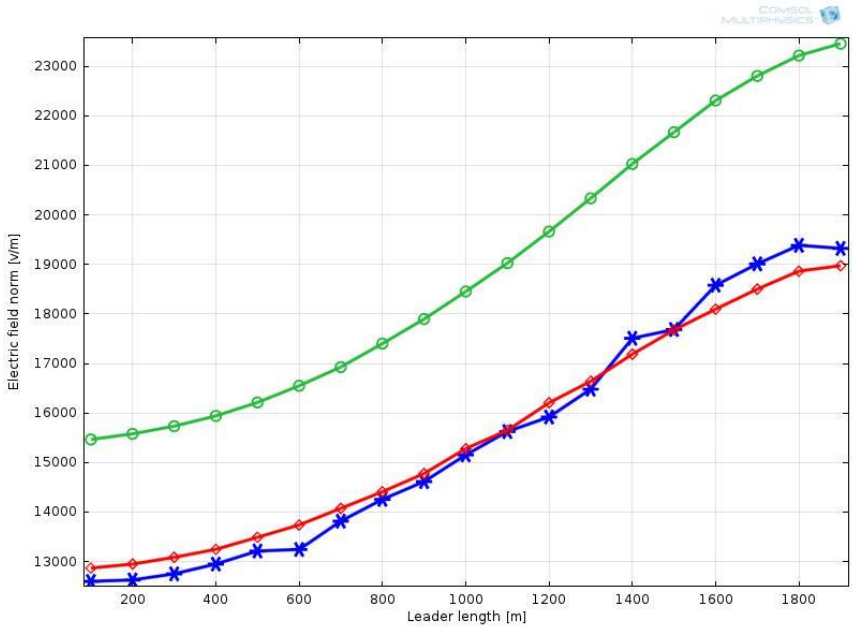

Figure A. 4: Electric field with respect to leader length that initiates at (-1000,2000)

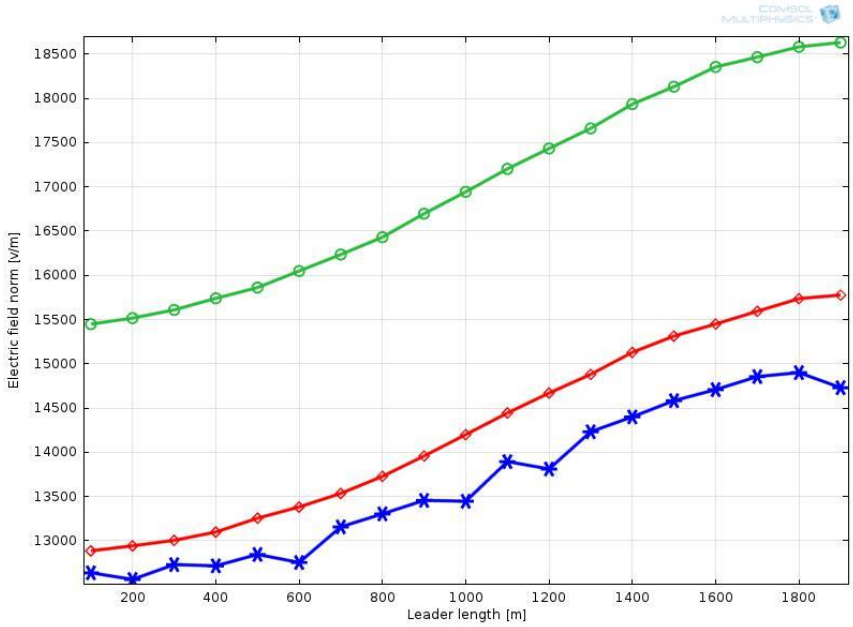

Figure A. 5: Electric field with respect to leader length that initiates at (1500,2000).

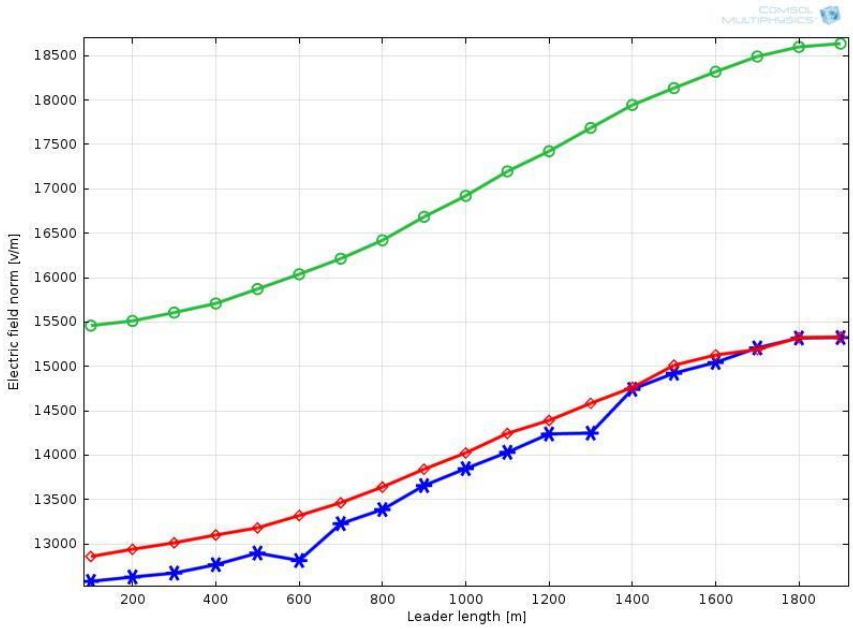

Figure A. 6: Electric field with respect to leader length that initiates at (-1500,2000)

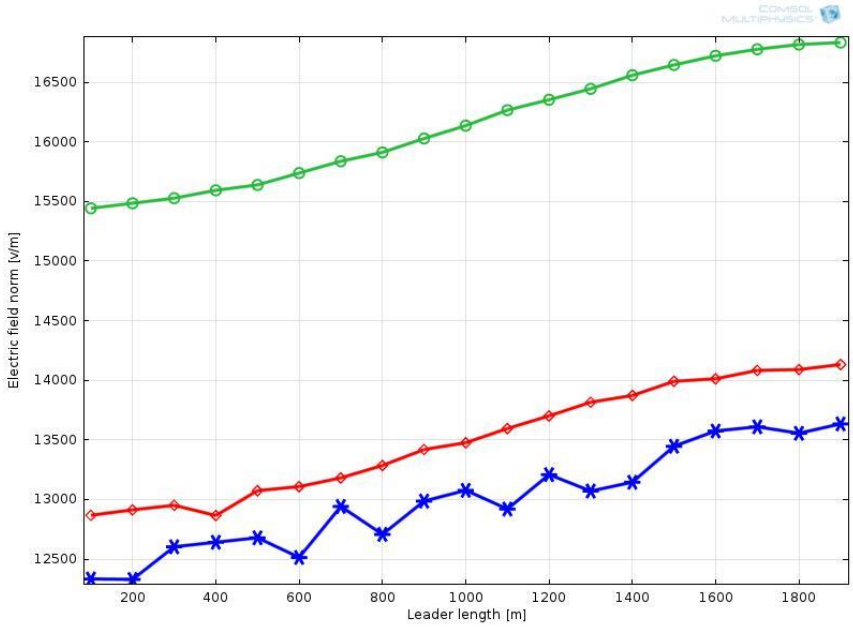

Figure A. 7: Electric field with respect to leader length that initiates at (2000,2000).

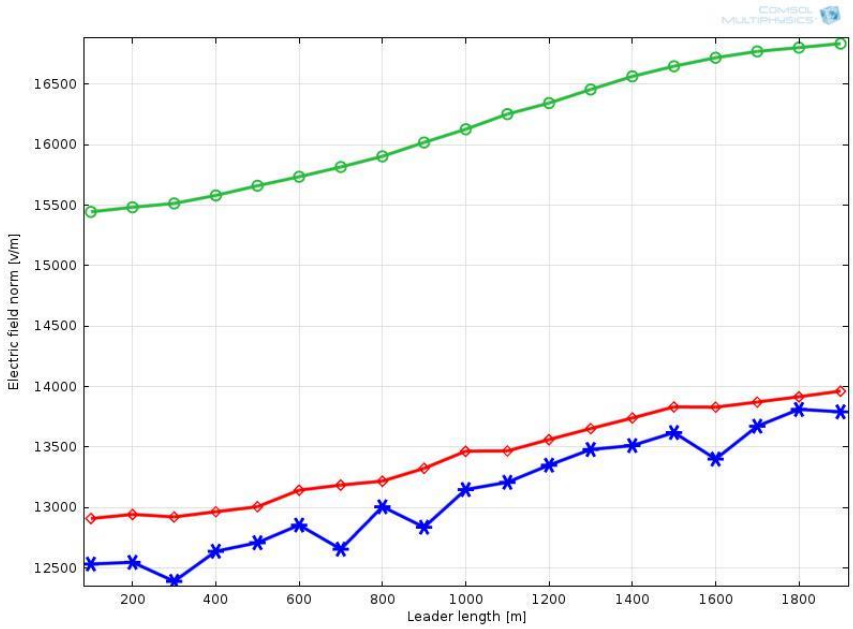

Figure A. 8: Electric field with respect to leader length that initiates at (-2000,2000)

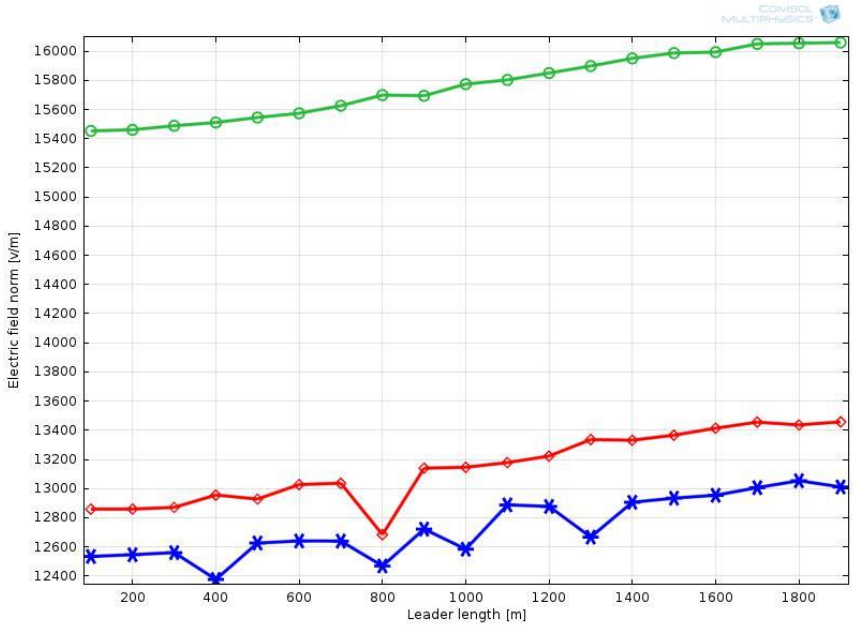

Figure A. 9: Electric field with respect to leader length that initiates at (2500,2000).

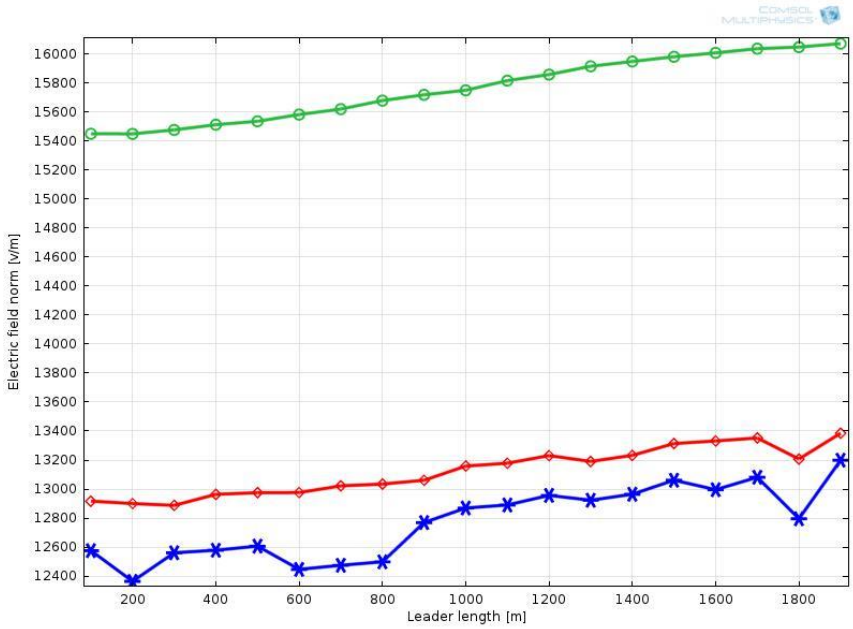

Figure A. 10: Electric field with respect to leader length that initiates at (-2500,2000)

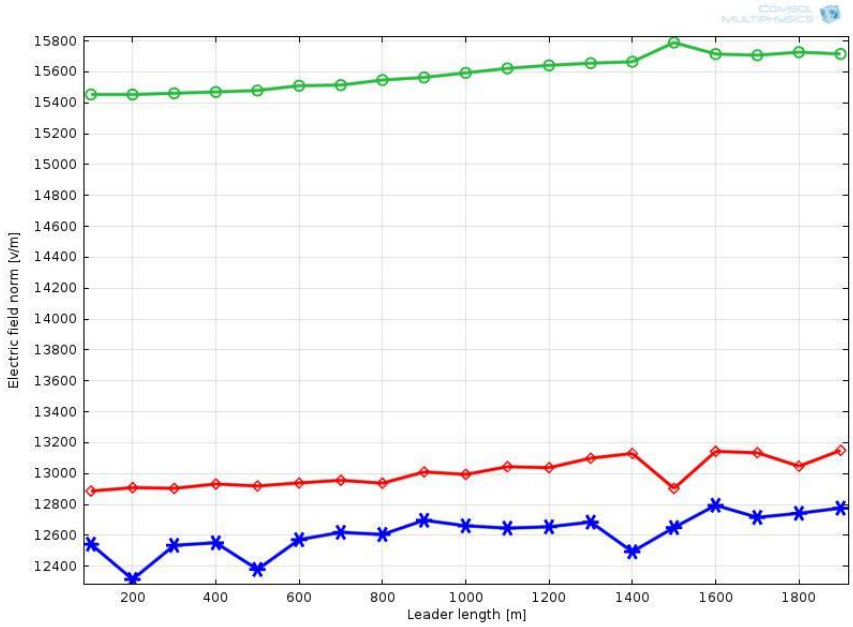

Figure A. 11: Electric field with respect to leader length that initiates at (3000,2000).

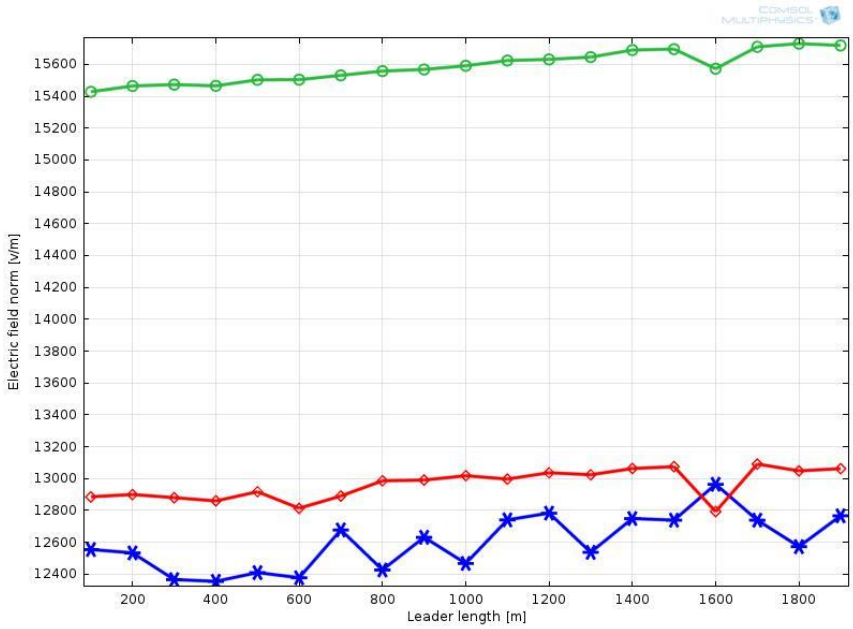

Figure A. 12: Electric field with respect to leader length that initiates at (-3000,2000)

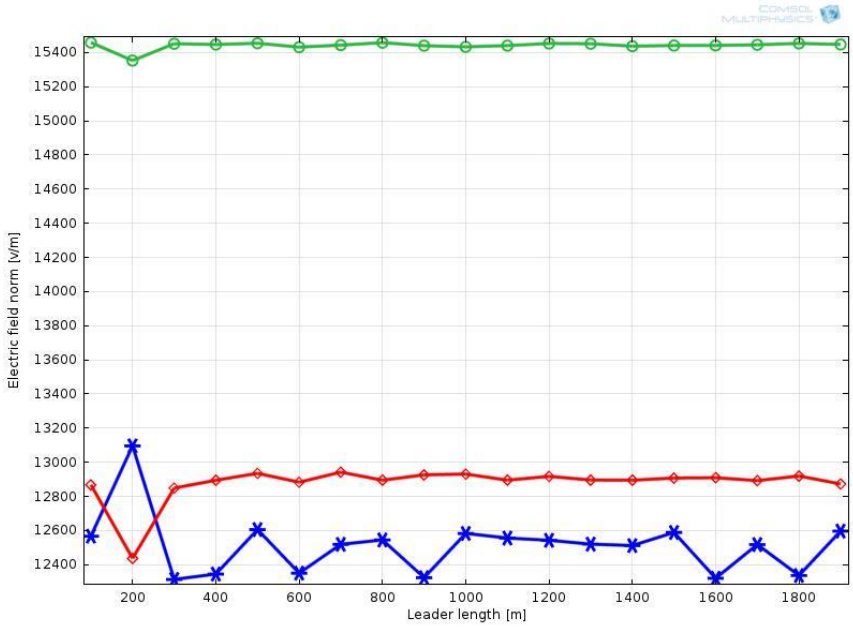

Figure A. 13: Electric field with respect to leader length that initiates at (3500,2000).

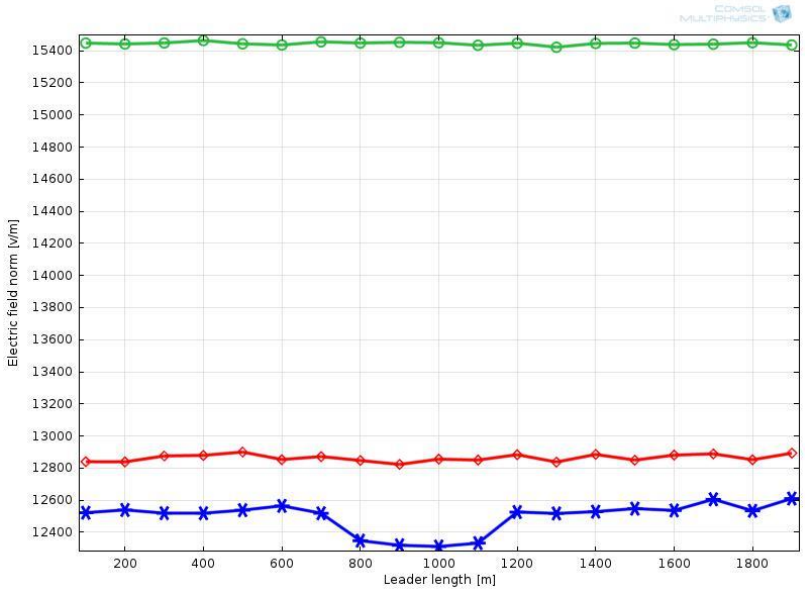

Figure A. 14: Electric field with respect to leader length that initiates at(-3500,2000)

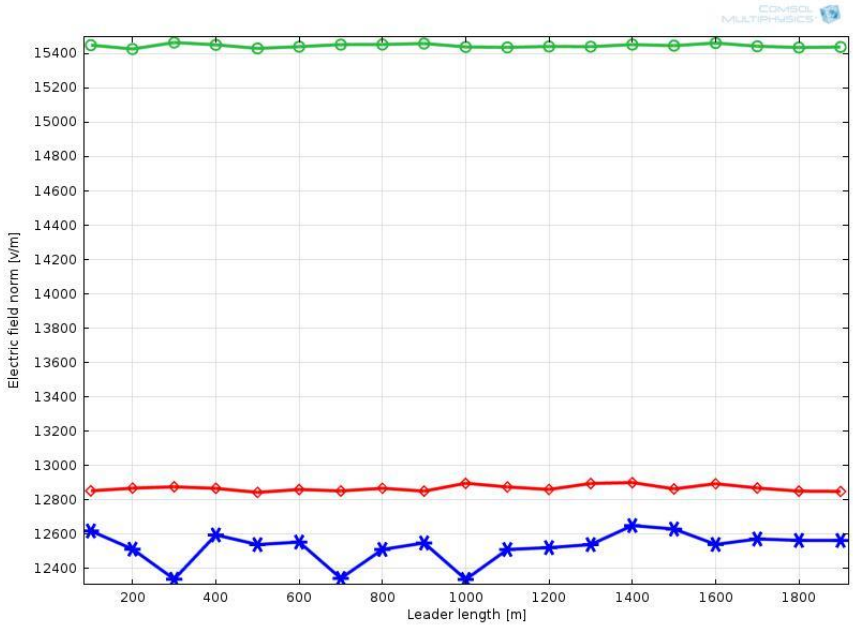

Figure A. 15: Electric field with respect to leader length that initiates at (4000,2000).

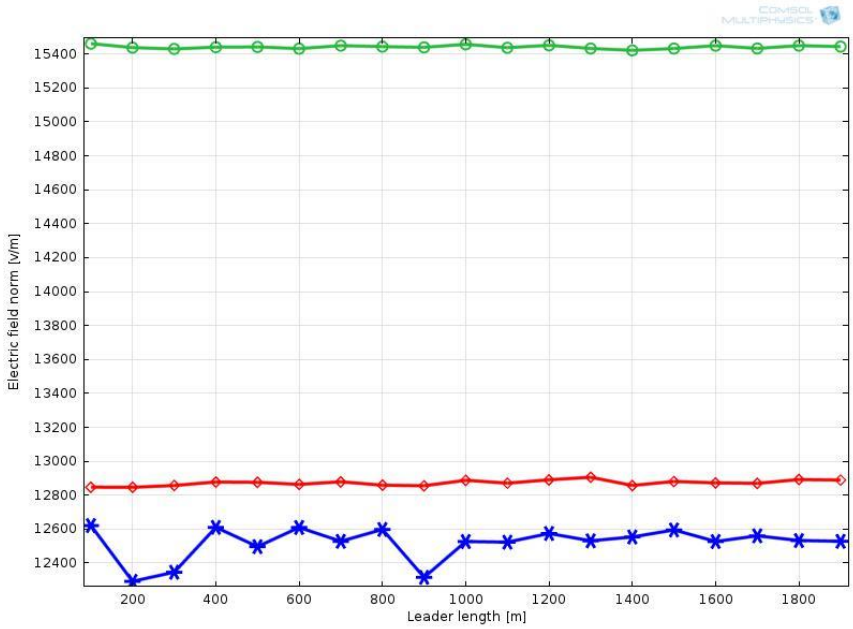

Figure A. 16: Electric field with respect to leader length that initiates at (-4000,2000)

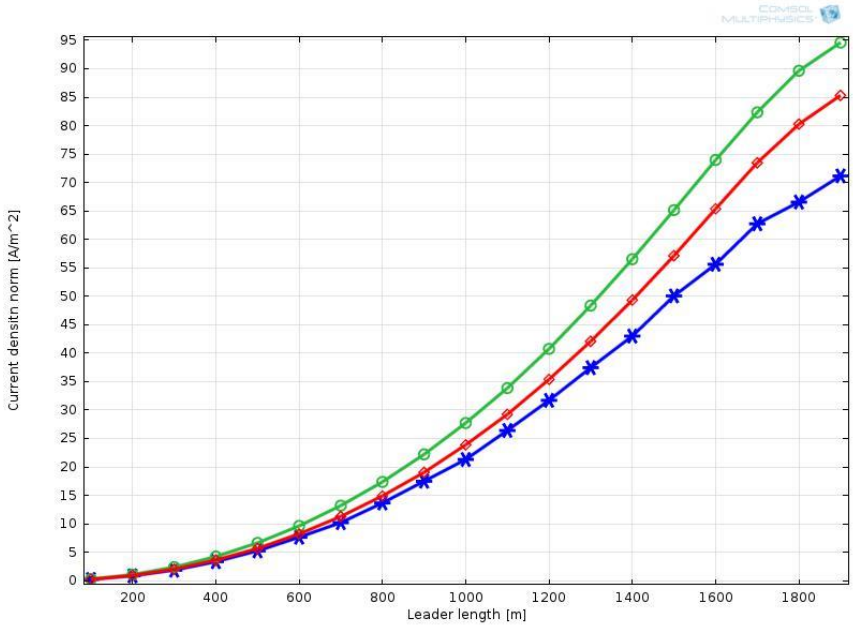

Figure A. 17: Current density with respect to leader length that initiates at (500,2000).

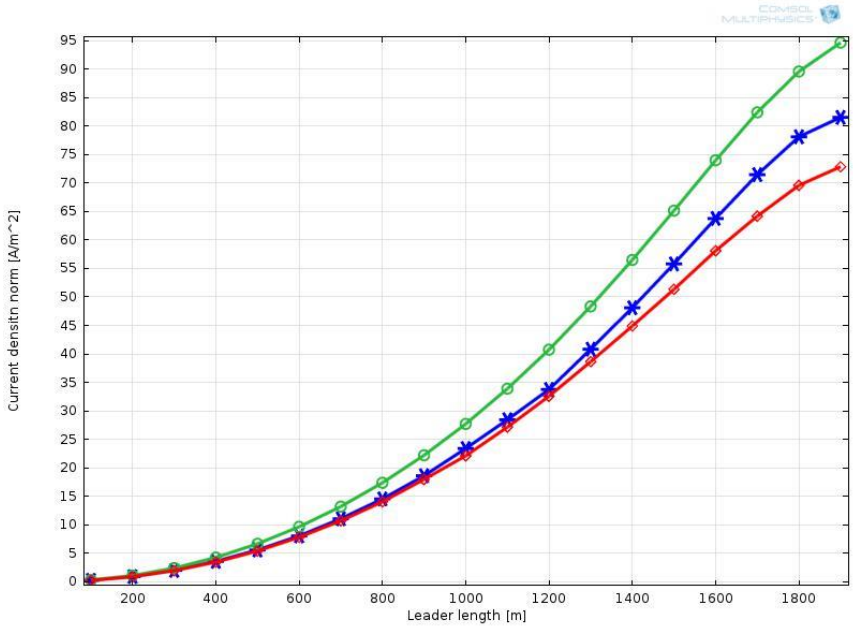

Figure A. 18: Current density with respect to leader length that initiates at (-500,2000)

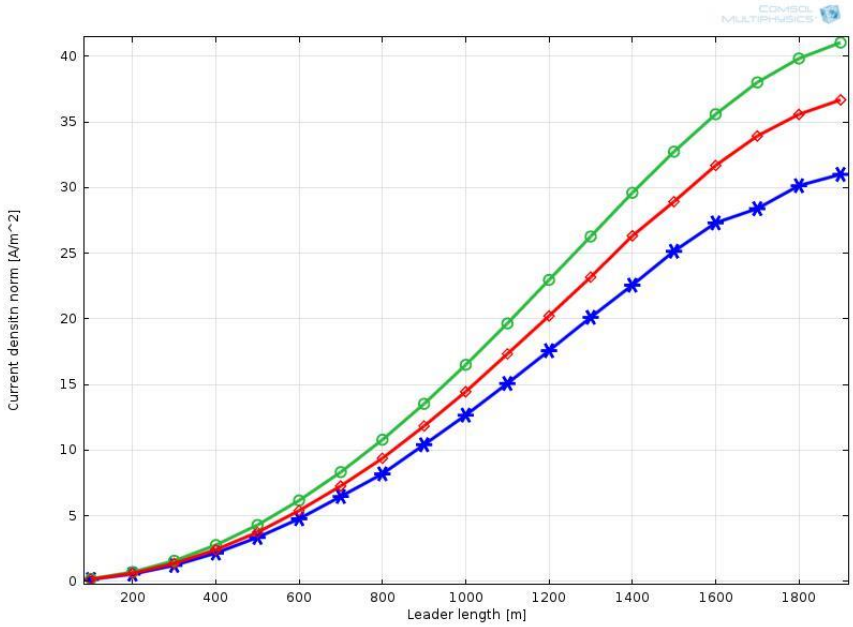

Figure A. 19: Current density with respect to leader length that initiates at (1000,2000).

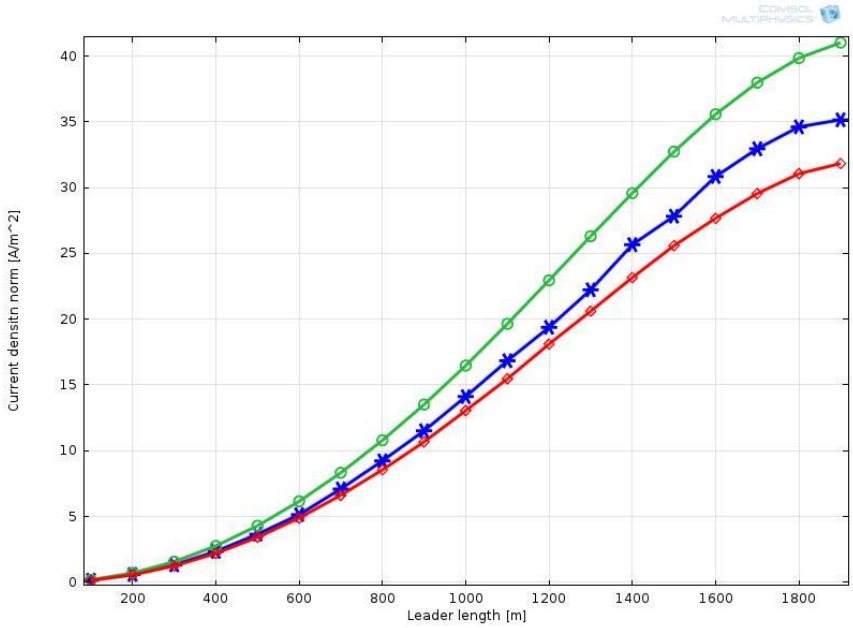

Figure A. 20: Current density with respect to leader length that initiates at (-1000,2000)

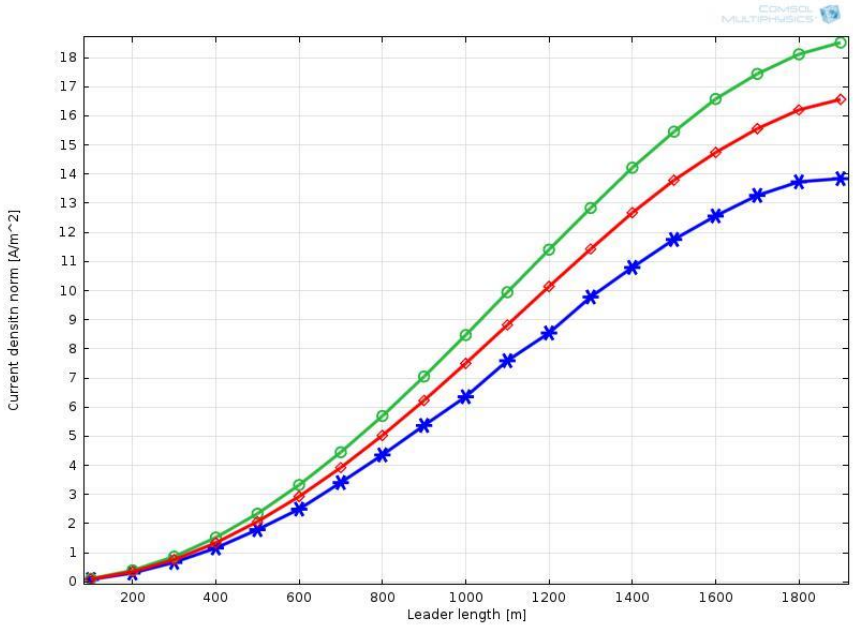

Figure A. 21: Current density with respect to leader length that initiates at (1500,2000).

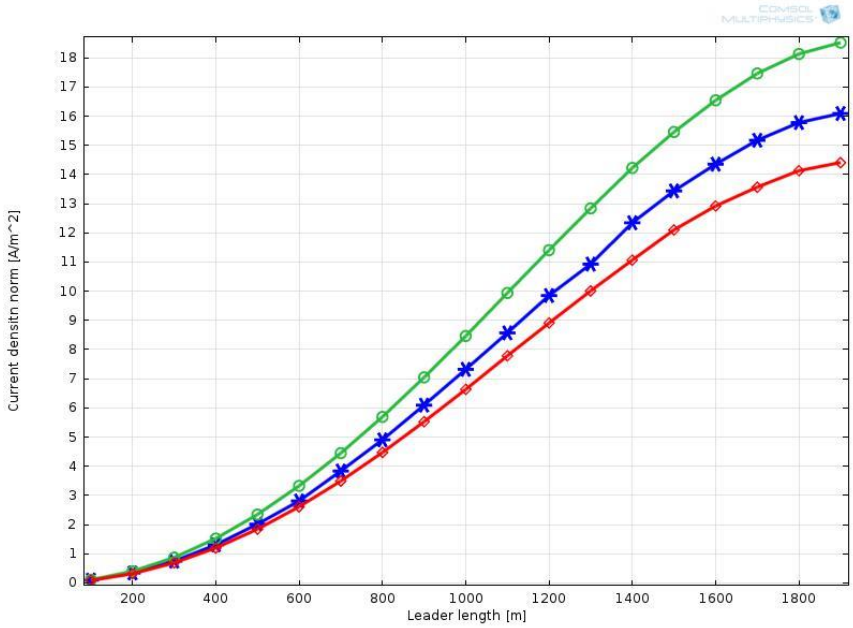

Figure A. 22: Current density with respect to leader length that initiates at (-1500,2000)

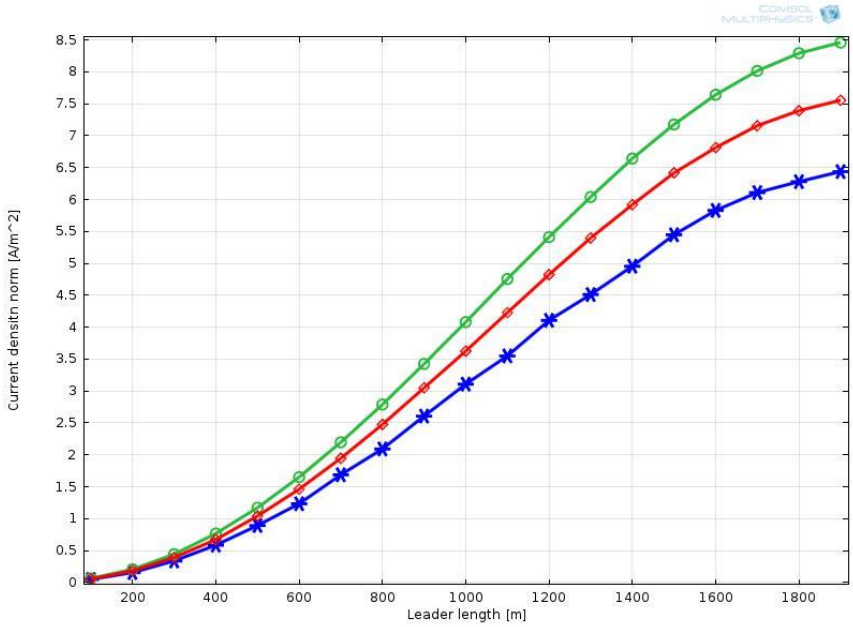

Figure A. 23: Current density with respect to leader length that initiates at (2000,2000).

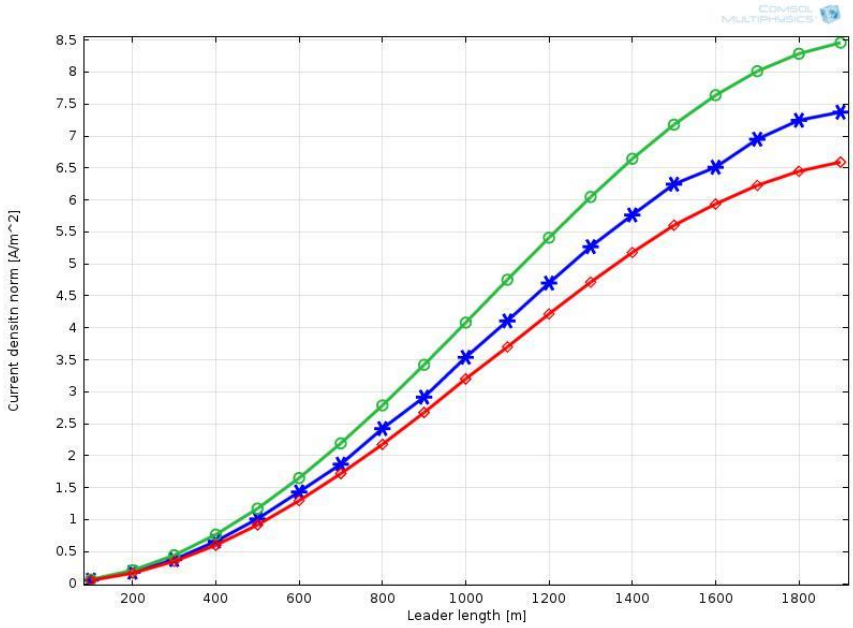

Figure A. 24: Current density with respect to leader length that initiates at

(-2000,2000)

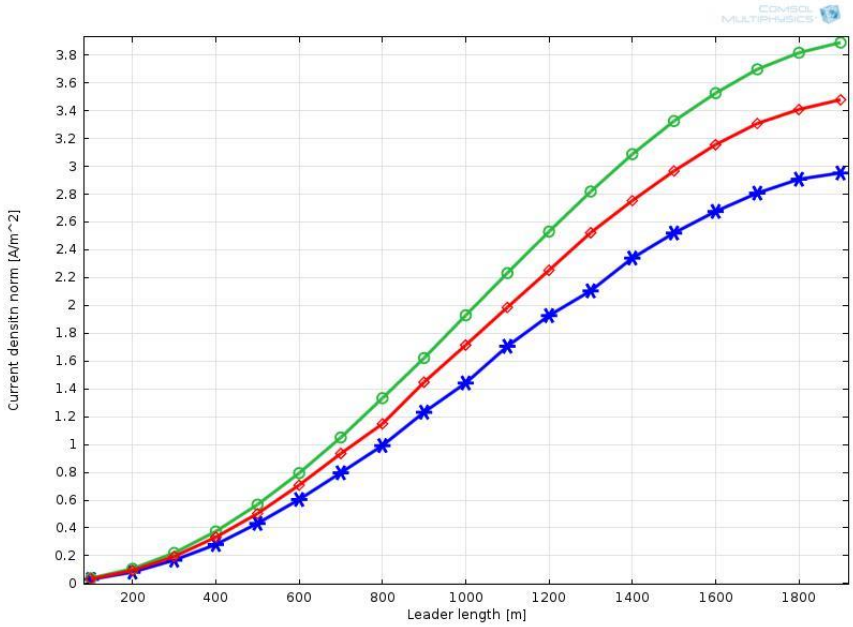

Figure A. 25: Current density with respect to leader length that initiates at (2500,2000).

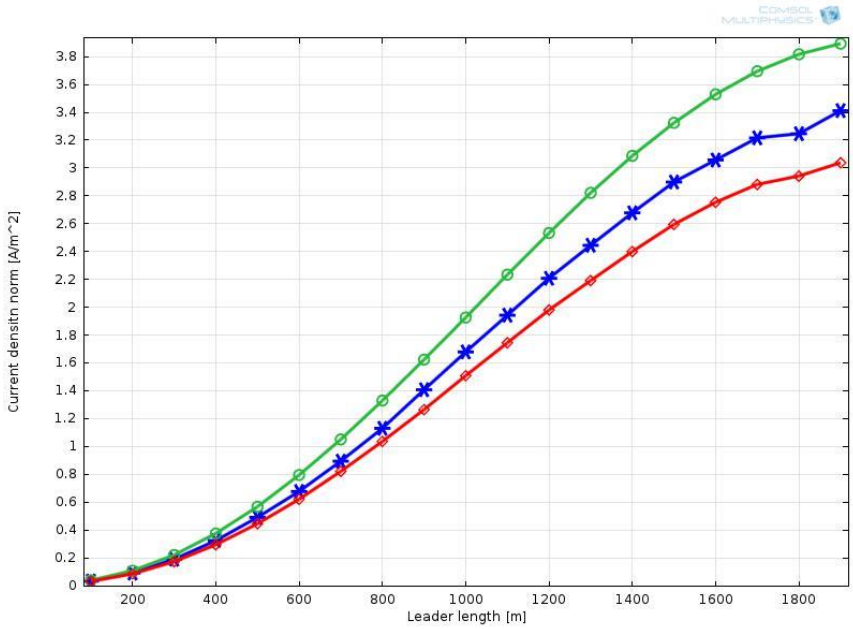

Figure A. 26: Current density with respect to leader length that initiates at (-2500,2000)

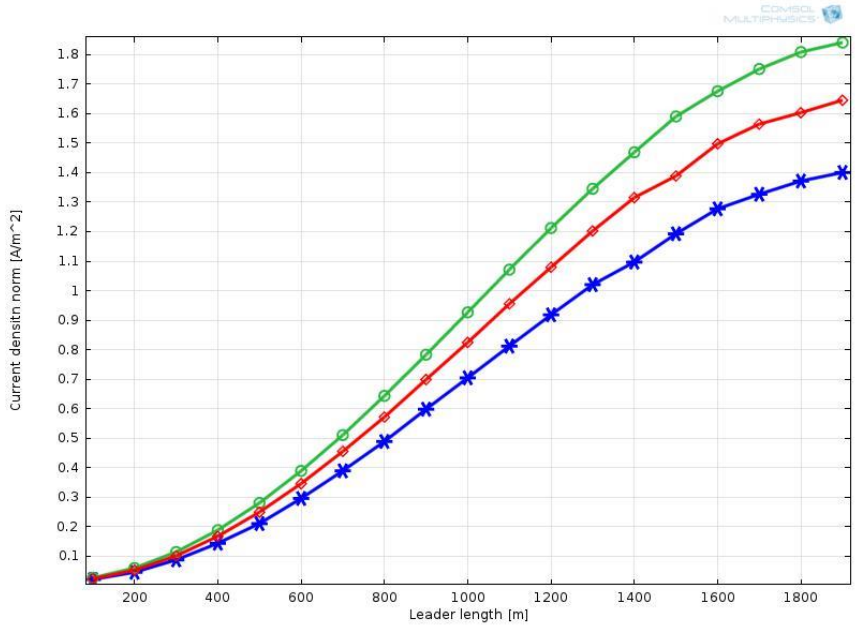

Figure A. 27: Current density with respect to leader length that initiates at (3000,2000).

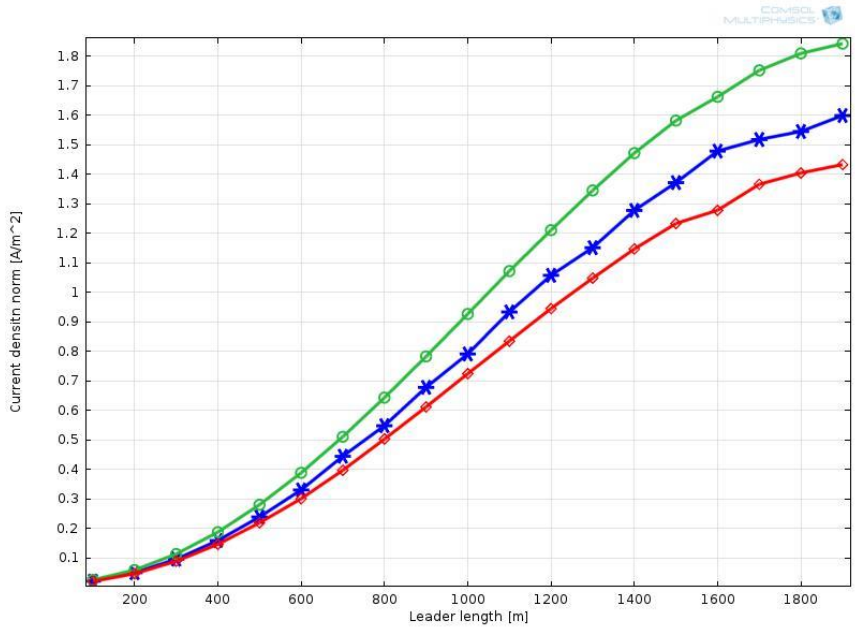

Figure A. 28: Current density with respect to leader length that initiates at (-3000,2000)

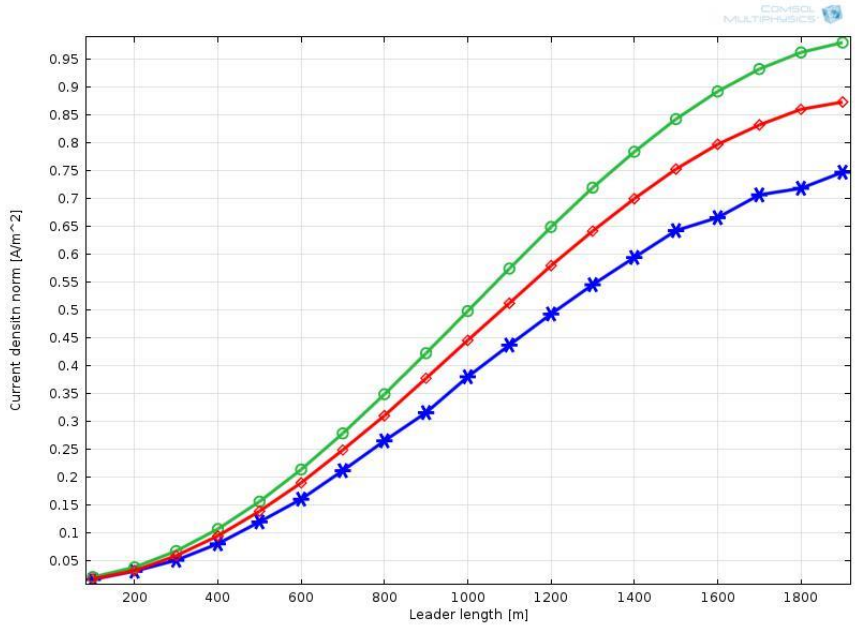

Figure A. 29: Current density with respect to leader length that initiates at (3500,2000).

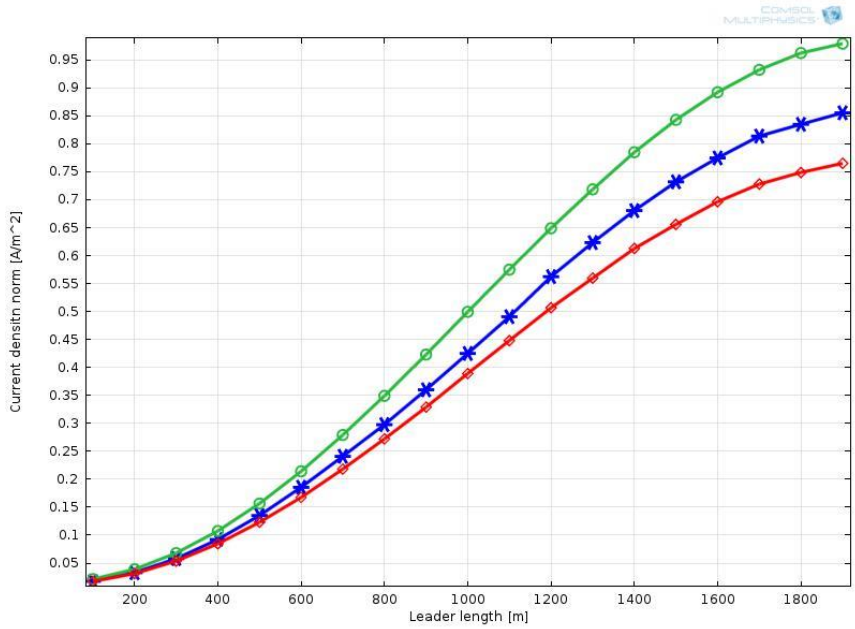

Figure A. 30: Current density with respect to leader length that initiates at (-3500,2000)

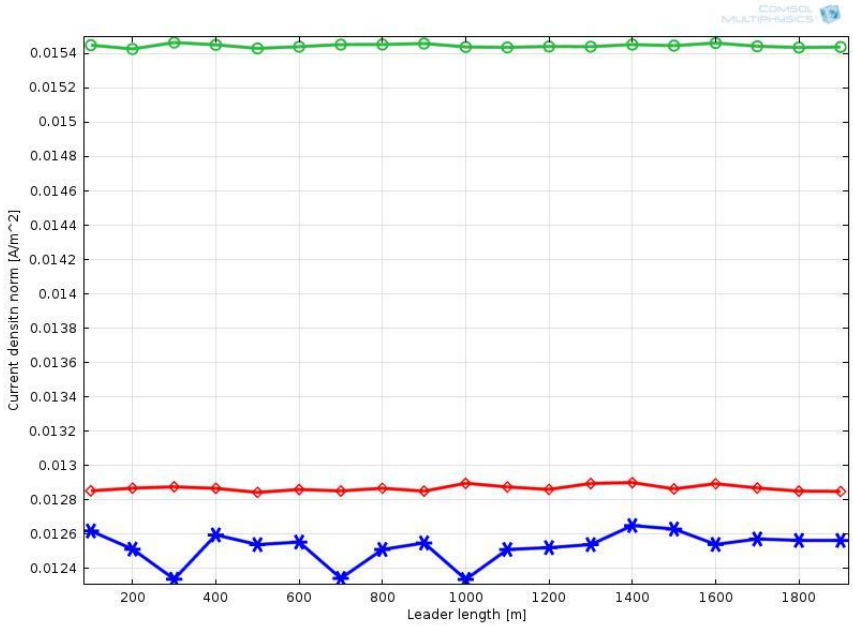

Figure A. 31: Current density with respect to leader length that initiates at (4000,2000).

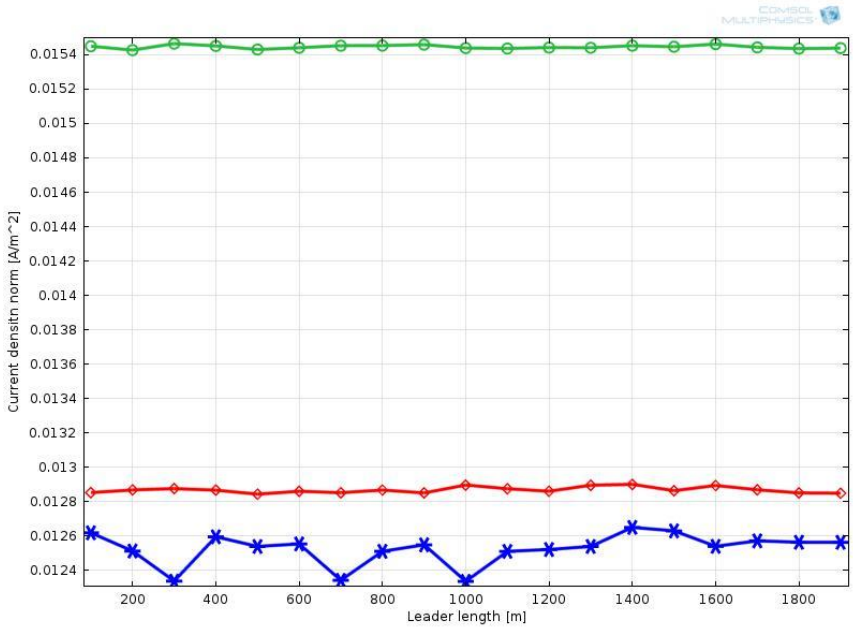

Figure A. 32: Current density with respect to leader length that initiates at (-4000,2000)

Appendix B: Electric field and current density magnitudes.

Table B. 1: Electric field distribution with respect to leader length (0,2000)

Stepped leader length [m]	Electric field [V/m] Left side of the tower	Electric field norm [V/m] Top of the tower	Electric field norm [V/m] Right side of the tower
100	12380.62462	15497.46143	12940.44022
200	12703.18982	15672.05998	13117.07062
300	13048.31022	15961.33997	13297.84422
400	13271.51663	16366.49176	13659.14555
500	13721.62665	16907.77066	14102.06987
600	14254.39872	17556.49164	14623.09074
700	14956.87416	18396.55878	15293.23483
800	15566.89543	19465.74436	16241.67109
900	16575.24238	20776.61646	17299.48831
1000	18097.8623	22292.15866	18560.59727
1100	19731.37155	24377.37875	20258.69781
1200	21842.822	26860.88395	22330.79898
1300	24596.02089	30392.95721	25246.37968
1400	28268.66536	34953.8935	29009.13033
1500	33124.89399	41688.13995	34559.12144
1600	41854.34654	51753.17738	42738.44455
1700	55596.24042	69193.2695	57059.34127
1800	83512.52076	1.05852e5	86012.72393
1900	1.71328e5	2.45654e5	1.75369e5

Table B. 2: Electric field with respect to stepped leader length (human level).

Stepped leader length [m]	Electric field norm (V/m) Human level
100	895.53029
200	895.49168
300	895.45518
400	895.54347
500	895.66219
600	895.57436
700	895.60434
800	895.59825
900	895.62242
1000	895.61632
1100	895.55696
1200	895.60671
1300	895.6639
1400	895.77658
1500	895.39785
1600	895.70332
1700	895.35048
1800	895.36149
1900	896.30665

Table B. 3: Current density with respect to leader length (0,2000)

Stepped leader length [m]	Current density (A/m^2) Left side of the tower	Current density (A/m^2) Top of the tower	Current density (A/m^2) Right side of the tower
100	0.25479	0.31929	0.26631
200	0.99997	1.23512	1.03256
300	2.26586	2.77493	2.30915
400	4.01611	4.95842	4.13331
500	6.3399	7.82118	6.51571
600	9.2376	11.39069	9.47645
700	12.76758	15.72184	13.05477
800	16.67442	20.87444	17.39792
900	21.49764	26.97653	22.43763
1000	27.69313	34.14785	28.4016
1100	34.41301	42.55877	35.33299
1200	42.51663	52.33189	43.46632
1300	51.74067	63.98205	53.10822
1400	62.98032	77.91048	64.62884
1500	75.32559	94.79008	78.58673
1600	93.89467	115.96092	95.87405
1700	116.11402	143.93459	119.16081
1800	147.62719	184.65734	152.03537
1900	197.66033	259.86713	202.28514

Table B. 4: Current density with respect to stepped leader length (human level).

Stepped leader length [m]	Current density norm (A/m^2) Human level
100	8.9553e-4
200	8.95492e-4
300	8.95455e-4
400	8.95543e-4
500	8.95662e-4
600	8.95574e-4
700	8.95604e-4
800	8.95598e-4
900	8.95622e-4
1000	8.95616e-4
1100	8.95557e-4
1200	8.95607e-4
1300	8.95664e-4
1400	8.95777e-4
1500	8.95398e-4
1600	8.95703e-4
1700	8.9535e-4
1800	8.95361e-4
1900	8.96307e-4

Table B. 5: Electric field distribution with respect to leader length (500,2000)

Stepped leader length [m]	Electric field [V/m] Left side of the tower	Electric field norm [V/m] Top of the tower	Electric field norm [V/m] Right side of the tower
100	12554.72012	15500.57731	12922.58297
200	12700.26738	15632.44591	13011.51448
300	12665.41588	15879.59279	13144.75426
400	13140.62698	16212.03965	13541.12505
500	13496.46168	16658.15402	13865.63247
600	14007.71212	17193.89956	14345.14734
700	14194.84555	17886.54682	14935.12858
800	15097.98691	18705.06602	15682.09916
900	15878.02492	19661.10184	16469.40516
1000	16407.87255	20817.62007	17538.23258
1100	17701.04949	22150.94069	18707.69448
1200	18927.50405	23774.37559	20210.48825
1300	20314.83008	25661.59875	21893.78623
1400	21639.71198	27875.1059	23890.17872
1500	23772.8975	30388.88692	26245.08249
1600	25295.5333	33134.88366	28944.73925
1700	27764.86638	36021.81866	31911.1831
1800	28919.00231	38642.38596	34491.19858
1900	30645.1924	40528.31238	36582.17858

Table B. 6: Electric field distribution with respect to leader length (-500,2000)

Stepped leader length [m]	Electric field [V/m] Left side of the tower	Electric field norm [V/m] Top of the tower	Electric field norm [V/m] Right side of the tower
100	12602.58829	15497.30422	12896.12027
200	12675.2627	15639.75454	13010.01322
300	12889.93238	15863.78813	13230.88833
400	13324.28466	16236.56846	13502.7303
500	13613.31345	16684.68508	13845.39817
600	14008.56692	17206.06498	14308.06652
700	14630.7834	17882.0488	14864.10851
800	15287.49436	18705.7054	15493.82277
900	16129.70852	19704.36281	16346.0824
1000	17134.03678	20768.05211	16988.77009
1100	18229.43395	22208.60647	18215.7698
1200	19251.55625	23737.10919	19427.44779
1300	21280.55541	25703.7031	20997.42939
1400	23353.04575	27920.08725	22635.17182
1500	25665.70042	30424.33046	24399.69194
1600	28254.51373	33165.73864	26435.45507
1700	30976.21355	35989.38411	28356.40144
1800	33589.82828	38630.59016	30250.87196
1900	34887.75907	40486.10947	31334.52183

Table B. 7: Electric field distribution with respect to leader length (1000,2000)

Stepped leader length [m]	Electric field [V/m] Left side of the tower	Electric field norm [V/m] Top of the tower	Electric field norm [V/m] Right side of the tower
100	12555.23214	15483.61099	12884.30714
200	12656.65714	15577.80053	12994.04575
300	12737.50683	15727.45879	13133.54114
400	12983.72038	15942.33784	13333.70343
500	13210.77858	16208.4645	13499.10884
600	13408.68076	16573.36641	13878.72566
700	13753.09265	16925.7759	14147.94639
800	13806.35541	17394.22568	14471.38122
900	14392.22493	17884.69406	14987.19348
1000	14794.63719	18441.05858	15475.99608
1100	15254.27701	19023.73777	16077.22196
1200	15742.12272	19690.67714	16624.47361
1300	16248.43162	20323.71431	17196.96911
1400	16713.56414	20995.56073	17908.5715
1500	17371.60353	21666.6488	18379.04018
1600	17864.58939	22322.12732	19089.80813
1700	17776.7151	22824.36975	19573.75358
1800	18323.69303	23226.74257	19940.98799
1900	18482.56193	23473.16974	20160.8499

Table B. 8: Electric field distribution with respect to leader length (-1000,2000)

Stepped leader length [m]	Electric field [V/m] Left side of the tower	Electric field norm [V/m] Top of the tower	Electric field norm [V/m] Right side of the tower
100	12600.80886	15465.2355	12868.2306
200	12628.33811	15579.1479	12949.14702
300	12752.34907	15734.3462	13085.24486
400	12950.15667	15941.21732	13246.80291
500	13213.0516	16213.39369	13490.25841
600	13244.11962	16549.60541	13738.8866
700	13816.1161	16928.43292	14073.89917
800	14255.69023	17402.42995	14410.50848
900	14615.42129	17897.68133	14777.5614
1000	15154.03773	18453.61507	15280.85342
1100	15625.32825	19027.2161	15650.76721
1200	15919.19718	19664.55195	16206.58065
1300	16481.57222	20336.41533	16640.99135
1400	17509.20395	21030.05234	17187.19543
1500	17685.44382	21670.58378	17677.06651
1600	18580.0476	22310.34551	18097.96598
1700	19011.55371	22807.27497	18502.4261
1800	19386.35832	23218.66206	18865.15077
1900	19324.22896	23459.49539	18974.8632

Table B. 9: Electric field distribution with respect to leader length (1500,2000)

Stepped leader length [m]	Electric field [V/m] Left side of the tower	Electric field norm [V/m] Top of the tower	Electric field norm [V/m] Right side of the tower
100	12637.30727	15448.39997	12885.53886
200	12562.63279	15516.39332	12942.22002
300	12729.89549	15609.15845	13004.09609
400	12716.03201	15740.09993	13097.91083
500	12844.97096	15861.18498	13254.61162
600	12753.94981	16049.10387	13381.52658
700	13156.63322	16235.05369	13534.67328
800	13303.25076	16431.20518	13727.60513
900	13455.83654	16696.94272	13957.69215
1000	13446.33634	16943.56682	14199.75232
1100	13894.42282	17203.30443	14443.39046
1200	13810.79212	17433.43759	14668.8502
1300	14231.92577	17660.95802	14880.38155
1400	14399.91828	17935.5416	15129.43937
1500	14583.29988	18132.19924	15313.37465
1600	14707.86824	18355.57484	15449.35634
1700	14855.15333	18466.3135	15593.73516
1800	14900.18522	18582.63801	15736.37706
1900	14729.90869	18631.43531	15776.99333

Table B.10: Electric field distribution with respect to leader length (-1500,2000)

Stepped leader length [m]	Electric field [V/m] Left side of the tower	Electric field norm [V/m] Top of the tower	Electric field norm [V/m] Right side of the tower
100	12578.38274	15459.42665	12858.14334
200	12626.89718	15512.55489	12940.08767
300	12671.10132	15606.05837	13012.35632
400	12766.34148	15708.93773	13100.19279
500	12896.60649	15871.69381	13180.55445
600	12813.09738	16038.01859	13318.93738
700	13228.12534	16213.67927	13464.38143
800	13387.11284	16420.42775	13640.91992
900	13657.25401	16684.98358	13842.13785
1000	13848.11546	16921.0522	14025.25817
1100	14032.13272	17196.99305	14244.90121
1200	14238.66141	17423.86286	14391.16712
1300	14248.38555	17686.16977	14583.79948
1400	14741.35007	17944.98662	14761.69319
1500	14923.02436	18135.32001	15012.57303
1600	15044.40192	18319.73158	15128.06757
1700	15208.18004	18491.41141	15190.03453
1800	15319.33368	18599.13232	15324.49355
1900	15324.44949	18636.20607	15330.94488

Table B. 11: Electric field distribution with respect to leader length (2000,2000)

Stepped leader length [m]	Electric field [V/m] Left side of the tower	Electric field norm [V/m] Top of the tower	Electric field norm [V/m] Right side of the tower
100	12333.57767	15442.16598	12867.39648
200	12329.73175	15484.52691	12913.12376
300	12603.55409	15526.95687	12951.27842
400	12641.41792	15592.96476	12865.44251
500	12678.95961	15638.37056	13074.36299
600	12513.86003	15737.60597	13107.88503
700	12941.54754	15837.00701	13181.32875
800	12707.5081	15910.95061	13285.14855
900	12986.43539	16027.7215	13419.17601
1000	13076.8488	16135.34063	13476.07193
1100	12920.12658	16265.49389	13594.90632
1200	13208.73243	16352.56402	13701.25412
1300	13070.77033	16444.1411	13815.70309
1400	13144.85506	16557.95637	13872.03952
1500	13446.69539	16644.52088	13990.86358
1600	13574.57765	16721.20292	14012.37132
1700	13609.72462	16776.07015	14082.46103
1800	13555.4656	16815.70537	14089.39538
1900	13633.96282	16832.48554	14131.7766

Table B. 12: Electric field distribution with respect to leader length (-2000,2000)

Stepped leader length [m]	Electric field [V/m] Left side of the tower	Electric field norm [V/m] Top of the tower	Electric field norm [V/m] Right side of the tower
100	12532.49786	15445.46877	12908.6902
200	12546.67976	15483.46469	12942.91044
300	12389.35754	15515.21099	12922.09439
400	12637.9995	15581.41479	12964.90579
500	12709.02247	15661.6653	13006.33819
600	12854.90818	15735.88723	13143.39344
700	12655.51107	15816.75911	13185.50797
800	13006.69477	15904.63503	13218.37295
900	12837.03139	16019.78422	13323.76351
1000	13148.75181	16128.85433	13465.76832
1100	13208.51476	16254.11769	13467.71081
1200	13350.21743	16345.38818	13562.197
1300	13479.96566	16457.90921	13652.78964
1400	13512.36449	16565.95819	13740.17174
1500	13620.03503	16650.2006	13832.24768
1600	13400.77508	16720.51545	13829.95562
1700	13672.79236	16772.92082	13872.22466
1800	13811.77057	16804.04165	13915.99268
1900	13791.49105	16837.21474	13962.96798

Table B. 13: Electric field distribution with respect to leader length (2500,2000)

Stepped leader length [m]	Electric field [V/m] Left side of the tower	Electric field norm [V/m] Top of the tower	Electric field norm [V/m] Right side of the tower
100	12534.73215	15453.29706	12859.17446
200	12546.49285	15460.88805	12859.60417
300	12561.01983	15488.53887	12871.17958
400	12377.10469	15510.88791	12955.8118
500	12626.67287	15545.25652	12928.0821
600	12640.67351	15573.87228	13027.40726
700	12640.08141	15626.0892	13036.90138
800	12469.4127	15699.02785	12684.23661
900	12722.14329	15694.30241	13139.88019
1000	12584.46169	15774.21385	13146.15327
1100	12888.23692	15802.90852	13178.3741
1200	12877.69161	15850.09985	13223.17828
1300	12667.53444	15898.15142	13335.95675
1400	12906.17684	15950.81364	13331.74792
1500	12934.47601	15987.34288	13366.48934
1600	12954.25373	15993.82465	13413.98922
1700	13006.68777	16050.31449	13455.77976
1800	13054.02896	16054.62979	13436.47997
1900	13011.36623	16059.41662	13457.95049

Table B. 14: Electric field distribution with respect to leader length (-2500,2000)

Stepped leader length [m]	Electric field [V/m] Left side of the tower	Electric field norm [V/m] Top of the tower	Electric field norm [V/m] Right side of the tower
100	12575.37433	15451.12373	12916.69593
200	12363.43513	15450.22556	12899.87836
300	12560.27524	15477.47438	12887.23408
400	12577.98035	15513.36915	12963.2773
500	12606.07703	15536.99108	12974.76109
600	12446.07932	15583.2283	12975.84084
700	12474.01484	15621.20083	13021.8466
800	12498.06149	15679.99018	13034.38697
900	12769.00343	15719.76669	13060.55955
1000	12869.12831	15750.95223	13158.49143
1100	12890.28901	15817.62836	13178.15994
1200	12956.22405	15859.3016	13230.88172
1300	12922.93786	15916.54889	13190.26174
1400	12964.30728	15949.57649	13232.5751
1500	13060.84768	15982.05991	13313.77912
1600	12995.59962	16008.96093	13331.7275
1700	13081.36141	16037.72161	13352.24142
1800	12795.31137	16048.82631	13207.31717
1900	13199.23889	16072.83645	13385.01331

Table B. 15: Electric field distribution with respect to leader length (3000,2000)

Stepped leader length [m]	Electric field [V/m] Left side of the tower	Electric field norm [V/m] Top of the tower	Electric field norm [V/m] Right side of the tower
100	12543.55128	15453.53897	12886.96975
200	12315.44609	15452.99343	12909.13027
300	12536.15391	15461.28514	12904.44983
400	12552.25849	15469.8425	12932.53461
500	12380.05631	15479.12343	12920.12182
600	12572.78445	15510.20053	12939.81757
700	12619.99284	15514.17885	12956.6918
800	12606.23702	15546.95135	12938.02812
900	12698.20616	15563.59204	13010.82346
1000	12662.16338	15593.06243	12994.72571
1100	12647.26474	15622.53219	13044.65979
1200	12655.74634	15641.75475	13038.26126
1300	12686.27673	15656.11503	13100.13991
1400	12494.63221	15665.02475	13130.34139
1500	12651.17954	15789.61255	12903.90779
1600	12795.07864	15714.94069	13143.84199
1700	12716.89624	15707.47312	13134.9961
1800	12743.19995	15727.10784	13047.88505
1900	12776.69191	15715.7951	13150.19492

Table B. 16: Electric field distribution with respect to leader length (-3000,2000)

Stepped leader length [m]	Electric field [V/m] Left side of the tower	Electric field norm [V/m] Top of the tower	Electric field norm [V/m] Right side of the tower
100	12554.28403	15428.0916	12885.26946
200	12532.99846	15464.68653	12899.65853
300	12365.52749	15473.44557	12879.79464
400	12354.5534	15465.56763	12859.32124
500	12409.3094	15503.22301	12916.82881
600	12377.16791	15504.3878	12813.41562
700	12677.29211	15531.4051	12890.09089
800	12426.38382	15558.18058	12985.86833
900	12631.09282	15568.64233	12990.28612
1000	12467.01021	15591.49823	13017.6305
1100	12740.43111	15624.46126	12996.49067
1200	12782.86999	15631.53832	13036.3622
1300	12536.81314	15646.19288	13023.60866
1400	12748.87569	15690.21181	13062.8037
1500	12738.60932	15696.23685	13074.33101
1600	12963.87118	15573.05725	12792.26913
1700	12738.71672	15710.64332	13091.07122
1800	12572.4384	15730.71569	13047.95394
1900	12766.11428	15719.08278	13061.93211

Table B. 17: Electric field distribution with respect to leader length (3500,2000)

Stepped leader length [m]	Electric field [V/m] Left side of the tower	Electric field norm [V/m] Top of the tower	Electric field norm [V/m] Right side of the tower
100	12567.65453	15458.55909	12868.19428
200	13096.29958	15352.90654	12436.9428
300	12313.97956	15451.65763	12848.92461
400	12345.43445	15446.82469	12894.75347
500	12606.03433	15454.27862	12935.03353
600	12350.78146	15431.48703	12883.32524
700	12519.44195	15443.40714	12942.1212
800	12545.1443	15457.75025	12894.87676
900	12324.40271	15440.20038	12926.40831
1000	12583.30301	15433.30609	12930.93266
1100	12556.20891	15440.51234	12895.23297
1200	12543.06607	15453.01259	12917.49491
1300	12520.60406	15451.53647	12896.06862
1400	12512.21668	15437.20314	12894.88078
1500	12589.02517	15441.00451	12907.84383
1600	12320.86096	15441.53219	12909.50547
1700	12518.25519	15445.14642	12892.47898
1800	12337.00157	15453.35141	12919.55979
1900	12597.22462	15447.23361	12873.03138

Table B. 18: Electric field distribution with respect to leader length (-3500,2000)

Stepped leader length [m]	Electric field [V/m] Left side of the tower	Electric field norm [V/m] Top of the tower	Electric field norm [V/m] Right side of the tower
100	12522.21297	15447.84668	12839.92843
200	12539.29905	15442.19881	12838.756
300	12519.30528	15448.38587	12875.56526
400	12518.87056	15463.8146	12879.34795
500	12537.99332	15443.22766	12899.94716
600	12564.80811	15435.71687	12853.3751
700	12518.80219	15455.66292	12871.8748
800	12347.97714	15448.286	12847.22068
900	12319.12841	15452.52674	12822.77256
1000	12311.58372	15450.16475	12855.66743
1100	12332.50215	15434.01303	12850.05928
1200	12526.47654	15447.20824	12883.51382
1300	12517.3192	15421.94457	12837.85662
1400	12528.78298	15445.63938	12884.97631
1500	12547.66977	15447.66848	12849.73766
1600	12536.32929	15438.40809	12880.86782
1700	12605.85945	15441.07628	12888.77013
1800	12534.0819	15450.25314	12852.1389
1900	12610.54189	15435.72691	12892.69274

Table B. 19: Electric field distribution with respect to leader length (4000,2000)

Stepped leader length [m]	Electric field [V/m] Left side of the tower	Electric field norm [V/m] Top of the tower	Electric field norm [V/m] Right side of the tower
100	12619.47573	15449.12287	12853.14266
200	12513.57595	15426.67705	12868.71738
300	12338.85554	15464.5003	12876.3799
400	12596.35901	15451.10036	12867.2408
500	12540.23131	15430.22676	12844.23179
600	12554.79585	15440.27807	12860.93424
700	12343.41394	15452.40491	12852.57733
800	12511.78686	15452.83869	12868.11919
900	12549.61611	15458.65147	12851.23156
1000	12337.32241	15438.75086	12897.4475
1100	12511.60736	15436.28597	12875.59967
1200	12522.42139	15441.45768	12861.3256
1300	12540.03294	15440.21557	12895.99113
1400	12650.89662	15452.58038	12901.35181
1500	12630.90796	15446.13442	12864.37938
1600	12540.89722	15461.6464	12894.65706
1700	12572.73717	15442.77558	12869.73851
1800	12564.65876	15435.47121	12851.47947
1900	12564.30516	15438.3319	12849.83294

Table B. 20: Electric field distribution with respect to leader length (-4000,2000)

Stepped leader length [m]	Electric field [V/m] Left side of the tower	Electric field norm [V/m] Top of the tower	Electric field norm [V/m] Right side of the tower
100	12621.08729	15461.00567	12847.26135
200	12292.49516	15437.26709	12846.38899
300	12346.2108	15429.69509	12857.03371
400	12610.60068	15439.92288	12877.79816
500	12497.00401	15441.38442	12875.89398
600	12610.0963	15431.34598	12863.53348
700	12528.31666	15449.06181	12879.07955
800	12598.19453	15443.18542	12858.80318
900	12315.94267	15438.87888	12855.49102
1000	12527.04834	15456.95185	12887.90028
1100	12523.39004	15436.81701	12870.75651
1200	12574.48592	15450.98139	12890.59658
1300	12531.25995	15432.33648	12905.58993
1400	12553.83009	15421.25132	12857.42358
1500	12595.31011	15431.91048	12880.99697
1600	12527.28631	15448.97548	12872.6339
1700	12560.58424	15432.50014	12869.69009
1800	12532.90611	15449.15003	12892.30784
1900	12528.49759	15443.29806	12889.07497

Table B. 21: Current density with respect to leader length (0,2000)

Stepped leader length [m]	Current density (A/m^2) Left side of the tower	Current density (A/m^2) Top of the tower	Current density (A/m^2) Right side of the tower
100	0.25479	0.31929	0.26631
200	0.99997	1.23512	1.03256
300	2.26586	2.77493	2.30915
400	4.01611	4.95842	4.13331
500	6.3399	7.82118	6.51571
600	9.2376	11.39069	9.47645
700	12.76758	15.72184	13.05477
800	16.67442	20.87444	17.39792
900	21.49764	26.97653	22.43763
1000	27.69313	34.14785	28.4016
1100	34.41301	42.55877	35.33299
1200	42.51663	52.33189	43.46632
1300	51.74067	63.98205	53.10822
1400	62.98032	77.91048	64.62884
1500	75.32559	94.79008	78.58673
1600	93.89467	115.96092	95.87405
1700	116.11402	143.93459	119.16081
1800	147.62719	184.65734	152.03537
1900	197.66033	259.86713	202.28514

Table B. 22: Current density with respect to leader length (500,2000)

Stepped leader length [m]	Current density (A/m^2) Left side of the tower	Current density (A/m^2) Top of the tower	Current density (A/m^2) Right side of the tower
100	0.25479	0.31929	0.26631
200	0.99997	1.23512	1.03256
300	2.26586	2.77493	2.30915
400	4.01611	4.95842	4.13331
500	6.3399	7.82118	6.51571
600	9.2376	11.39069	9.47645
700	12.76758	15.72184	13.05477
800	16.67442	20.87444	17.39792
900	21.49764	26.97653	22.43763
1000	27.69313	34.14785	28.4016
1100	34.41301	42.55877	35.33299
1200	42.51663	52.33189	43.46632
1300	51.74067	63.98205	53.10822
1400	62.98032	77.91048	64.62884
1500	75.32559	94.79008	78.58673
1600	93.89467	115.96092	95.87405
1700	116.11402	143.93459	119.16081
1800	147.62719	184.65734	152.03537
1900	197.66033	259.86713	202.28514

Table B. 23: Current density with respect to leader length (-500,2000)

Stepped leader length [m]	Current density (A/m^2) Left side of the tower	Current density (A/m^2) Top of the tower	Current density (A/m^2) Right side of the tower
100	0.2187	0.27685	0.23619
200	0.84068	1.06208	0.90549
300	1.84749	2.37774	2.01639
400	3.34036	4.23038	3.61967
500	5.2386	6.63722	5.65941
600	7.63585	9.6208	8.22216
700	10.20521	13.19562	11.2841
800	13.65997	17.36206	14.90289
900	17.48271	22.20346	19.03686
1000	21.31116	27.71823	23.89068
1100	26.41067	33.86001	29.23689
1200	31.69903	40.75514	35.38782
1300	37.44813	48.36089	42.08912
1400	43.0074	56.53297	49.32617
1500	50.06452	65.15473	57.13145
1600	55.62983	73.96795	65.37758
1700	62.75526	82.34783	73.48385
1800	66.56814	89.65992	80.26002
1900	71.16684	94.61311	85.33445

Table B. 24: Current density with respect to leader length (1000,2000)

Stepped leader length [m]	Current density (A/m^2) Left side of the tower	Current density (A/m^2) Top of the tower	Current density (A/m^2) Right side of the tower
100	0.23033	0.27677	0.22465
200	0.88213	1.06255	0.86119
300	1.97712	2.37509	1.92973
400	3.56086	4.23563	3.43156
500	5.55526	6.64628	5.37312
600	8.02918	9.62665	7.79898
700	11.04649	13.18378	10.67949
800	14.53001	17.36439	14.01976
900	18.5992	22.20056	17.95961
1000	23.38292	27.70076	22.10209
1100	28.44284	33.89368	27.13767
1200	33.75744	40.74677	32.57926
1300	40.83172	48.35132	38.64073
1400	48.11569	56.51132	44.90337
1500	55.81699	65.17048	51.3429
1600	63.79433	74.00806	58.11398
1700	71.49105	82.43335	64.20322
1800	78.14181	89.61162	69.61872
1900	81.55441	94.68096	72.87702

Table B. 25: Current density with respect to leader length (-1000,2000)

Stepped leader length [m]	Current density (A/m^2) Left side of the tower	Current density (A/m^2) Top of the tower	Current density (A/m^2) Right side of the tower
100	0.14647	0.1883	0.16315
200	0.54893	0.70622	0.61495
300	1.21252	1.56577	1.36552
400	2.15293	2.76498	2.41532
500	3.34561	4.29311	3.73453
600	4.7672	6.1628	5.38967
700	6.46765	8.32434	7.26654
800	8.19122	10.79016	9.37293
900	10.41061	13.52519	11.83201
1000	12.66286	16.49872	14.45087
1100	15.07682	19.64984	17.32831
1200	17.57507	22.96709	20.22643
1300	20.11485	26.27687	23.18329
1400	22.57068	29.60362	26.32053
1500	25.15232	32.73823	28.93186
1600	27.31029	35.59243	31.68732
1700	28.39788	38.01846	33.9337
1800	30.14814	39.83838	35.58208
1900	31.00791	41.0521	36.68101

Table B. 26: Current density with respect to leader length (1500,2000)

Stepped leader length [m]	Current density (A/m^2) Left side of the tower	Current density (A/m^2) Top of the tower	Current density (A/m^2) Right side of the tower
100	0.14647	0.1883	0.16315
200	0.54893	0.70622	0.61495
300	1.21252	1.56577	1.36552
400	2.15293	2.76498	2.41532
500	3.34561	4.29311	3.73453
600	4.7672	6.1628	5.38967
700	6.46765	8.32434	7.26654
800	8.19122	10.79016	9.37293
900	10.41061	13.52519	11.83201
1000	12.66286	16.49872	14.45087
1100	15.07682	19.64984	17.32831
1200	17.57507	22.96709	20.22643
1300	20.11485	26.27687	23.18329
1400	22.57068	29.60362	26.32053
1500	25.15232	32.73823	28.93186
1600	27.31029	35.59243	31.68732
1700	28.39788	38.01846	33.9337
1800	30.14814	39.83838	35.58208
1900	31.00791	41.0521	36.68101

Table B. 27: Current density with respect to leader length (-1500,2000)

Stepped leader length [m]	Current density (A/m^2) Left side of the tower	Current density (A/m^2) Top of the tower	Current density (A/m^2) Right side of the tower
100	0.15956	0.18807	0.15013
200	0.5976	0.70617	0.56157
300	1.32603	1.56648	1.24578
400	2.34653	2.76509	2.19695
500	3.65747	4.29682	3.41825
600	5.14479	6.15489	4.88533
700	7.09787	8.32676	6.6197
800	9.234	10.79602	8.55048
900	11.51902	13.51259	10.67293
1000	14.1194	16.47611	13.05468
1100	16.84012	19.65057	15.46776
1200	19.38472	22.95386	18.10867
1300	22.23246	26.30758	20.61146
1400	25.66735	29.57936	23.15996
1500	27.83105	32.73477	25.58821
1600	30.84806	35.57631	27.66929
1700	32.95471	37.9822	29.55135
1800	34.61773	39.8463	31.05773
1900	35.15487	41.0222	31.83217

Table B. 28: Current density with respect to leader length (2000,2000)

Stepped leader length [m]	Current density (A/m^2) Left side of the tower	Current density (A/m^2) Top of the tower	Current density (A/m^2) Right side of the tower
100	0.08659	0.11112	0.09727
200	0.30463	0.3973	0.34968
300	0.67126	0.87016	0.76574
400	1.16464	1.52466	1.3407
500	1.79533	2.34498	2.07115
600	2.50041	3.32809	2.93286
700	3.41236	4.45425	3.92507
800	4.36068	5.69747	5.03125
900	5.37268	7.0519	6.22986
1000	6.35919	8.47438	7.50491
1100	7.59593	9.9468	8.82326
1200	8.54647	11.40871	10.14292
1300	9.78215	12.83821	11.42951
1400	10.79737	14.22079	12.67382
1500	11.75719	15.45805	13.79209
1600	12.56422	16.58034	14.74307
1700	13.26907	17.44175	15.55844
1800	13.73652	18.11579	16.20611
1900	13.84531	18.51737	16.56561

Table B. 29: Current density with respect to leader length (-2000,2000)

Stepped leader length [m]	Current density (A/m^2) Left side of the tower	Current density (A/m^2) Top of the tower	Current density (A/m^2) Right side of the tower
100	0.09495	0.11118	0.08809
200	0.34113	0.39711	0.31377
300	0.74606	0.86988	0.68609
400	1.30664	1.5213	1.19962
500	2.01522	2.3464	1.84237
600	2.80985	3.32777	2.61288
700	3.83702	4.44902	3.49277
800	4.90594	5.69303	4.47107
900	6.09546	7.04606	5.52673
1000	7.32196	8.46523	6.63436
1100	8.57177	9.94047	7.78653
1200	9.8535	11.40891	8.91003
1300	10.93062	12.84186	10.01393
1400	12.34814	14.22802	11.06876
1500	13.44125	15.45959	12.10382
1600	14.35511	16.54521	12.92218
1700	15.17648	17.46548	13.56963
1800	15.78145	18.1347	14.13174
1900	16.09314	18.52321	14.41096

Table B. 30: Current density with respect to leader length (2500,2000)

Stepped leader length [m]	Current density (A/m^2) Left side of the tower	Current density (A/m^2) Top of the tower	Current density (A/m^2) Right side of the tower
100	0.0484	0.06351	0.05549
200	0.15561	0.20704	0.18291
300	0.33856	0.44303	0.39242
400	0.58534	0.76762	0.67314
500	0.89291	1.17144	1.04123
600	1.23424	1.65114	1.46252
700	1.68766	2.19746	1.94531
800	2.09303	2.7884	2.47643
900	2.6074	3.42467	3.04961
1000	3.10788	4.08092	3.62523
1100	3.54989	4.75531	4.22785
1200	4.10761	5.41203	4.82361
1300	4.51193	6.0403	5.39855
1400	4.95523	6.64215	5.91942
1500	5.44776	7.17656	6.41686
1600	5.82944	7.64199	6.8123
1700	6.10968	8.0157	7.15755
1800	6.28028	8.29256	7.39158
1900	6.43773	8.45966	7.55568

Table B. 31: Current density with respect to leader length (-2500,2000)

Stepped leader length [m]	Current density (A/m^2) Left side of the tower	Current density (A/m^2) Top of the tower	Current density (A/m^2) Right side of the tower
100	0.05405	0.06352	0.05065
200	0.17769	0.20697	0.1633
300	0.37539	0.44272	0.34714
400	0.66113	0.76683	0.60019
500	1.01233	1.17322	0.91603
600	1.43468	1.65131	1.2966
700	1.86712	2.19404	1.71906
800	2.42432	2.78678	2.17666
900	2.91663	3.42201	2.67485
1000	3.53953	4.0817	3.20246
1100	4.10899	4.75338	3.70098
1200	4.70009	5.40969	4.21792
1300	5.26974	6.04795	4.7148
1400	5.76593	6.64486	5.17881
1500	6.24723	7.17862	5.60431
1600	6.51233	7.63868	5.9374
1700	6.95092	8.01448	6.22862
1800	7.24704	8.28746	6.44925
1900	7.37412	8.4614	6.59338

Table B. 32: Current density with respect to leader length (3000,2000)

Stepped leader length [m]	Current density (A/m^2) Left side of the tower	Current density (A/m^2) Top of the tower	Current density (A/m^2) Right side of the tower
100	0.03009	0.03857	0.03339
200	0.08239	0.10736	0.09445
300	0.1683	0.22054	0.19478
400	0.28115	0.3751	0.33357
500	0.43296	0.5681	0.50347
600	0.6047	0.79439	0.70846
700	0.7968	1.05068	0.93486
800	0.99259	1.33317	1.14861
900	1.23229	1.62216	1.4487
1000	1.44251	1.92925	1.71524
1100	1.70671	2.23291	1.98664
1200	1.9273	2.53164	2.25342
1300	2.10489	2.81928	2.52328
1400	2.34072	3.0878	2.75378
1500	2.52095	3.32588	2.96685
1600	2.67622	3.52684	3.15647
1700	2.80787	3.69813	3.30836
1800	2.90774	3.81706	3.40919
1900	2.95293	3.89044	3.47927

Table B. 33: Current density with respect to leader length (-3000,2000)

Stepped leader length [m]	Current density (A/m^2) Left side of the tower	Current density (A/m^2) Top of the tower	Current density (A/m^2) Right side of the tower
100	0.03266	0.03856	0.03101
200	0.0908	0.10728	0.08471
300	0.19009	0.22038	0.17269
400	0.3238	0.37507	0.29436
500	0.49064	0.56742	0.44466
600	0.67699	0.79506	0.62091
700	0.89439	1.05032	0.82091
800	1.13054	1.32978	1.03629
900	1.40759	1.62421	1.2648
1000	1.67924	1.92643	1.50834
1100	1.94287	2.23464	1.74471
1200	2.20819	2.5334	1.98052
1300	2.4453	2.82221	2.19155
1400	2.67816	3.08757	2.40022
1500	2.89958	3.32467	2.59537
1600	3.05779	3.52962	2.75408
1700	3.2167	3.69543	2.88255
1800	3.24664	3.81715	2.94244
1900	3.4124	3.89367	3.03796

Table B. 34: Current density with respect to leader length (3500,2000)

Stepped leader length [m]	Current density (A/m^2) Left side of the tower	Current density (A/m^2) Top of the tower	Current density (A/m^2) Right side of the tower
100	0.02099	0.02658	0.02281
200	0.04529	0.05969	0.05242
300	0.08725	0.11399	0.10082
400	0.14358	0.18811	0.16724
500	0.2105	0.28032	0.24925
600	0.29565	0.38893	0.34595
700	0.38924	0.51049	0.45489
800	0.48872	0.64337	0.57148
900	0.59826	0.78294	0.69881
1000	0.70451	0.92657	0.82458
1100	0.81203	1.07141	0.9554
1200	0.91817	1.21232	1.07936
1300	1.02045	1.34548	1.20251
1400	1.09702	1.46935	1.31556
1500	1.19288	1.59052	1.38892
1600	1.27747	1.67632	1.49781
1700	1.32694	1.75132	1.56474
1800	1.37165	1.809	1.60353
1900	1.40077	1.84124	1.64597

Table B. 35: Current density with respect to leader length (-3500,2000)

Stepped leader length [m]	Current density (A/m^2) Left side of the tower	Current density (A/m^2) Top of the tower	Current density (A/m^2) Right side of the tower
100	0.02222	0.02654	0.02156
200	0.05088	0.05972	0.04743
300	0.09661	0.11409	0.08965
400	0.15981	0.18813	0.14714
500	0.23947	0.28088	0.21972
600	0.33113	0.389	0.30152
700	0.44518	0.51114	0.39761
800	0.54866	0.64358	0.50331
900	0.67846	0.78315	0.61205
1000	0.79143	0.92687	0.72468
1100	0.93391	1.07228	0.83512
1200	1.05764	1.21072	0.94531
1300	1.15137	1.34518	1.04815
1400	1.27759	1.47165	1.14696
1500	1.37168	1.58179	1.23328
1600	1.47842	1.66217	1.27812
1700	1.51765	1.75173	1.36607
1800	1.5448	1.80907	1.40438
1900	1.59884	1.84228	1.43272

Table B. 36: Current density with respect to leader length (4000,2000)

Stepped leader length [m]	Current density (A/m^2) Left side of the tower	Current density (A/m^2) Top of the tower	Current density (A/m^2) Right side of the tower
100	0.01708	0.02139	0.01815
200	0.03181	0.03882	0.03278
300	0.05146	0.06801	0.05961
400	0.08104	0.1074	0.09503
500	0.12026	0.15668	0.1394
600	0.161	0.21415	0.1904
700	0.21226	0.2791	0.24935
800	0.26568	0.34926	0.31084
900	0.31627	0.42293	0.37796
1000	0.38056	0.49845	0.446
1100	0.43746	0.57471	0.51273
1200	0.4932	0.64927	0.57993
1300	0.54578	0.71988	0.64203
1400	0.59462	0.78421	0.70013
1500	0.64286	0.84286	0.75314
1600	0.66606	0.89241	0.79755
1700	0.70688	0.93256	0.83225
1800	0.71864	0.96239	0.86032
1900	0.7475	0.98015	0.87338

Table B. 37: Current density with respect to leader length (-4000,2000)

Stepped leader length [m]	Current density (A/m^2) Left side of the tower	Current density (A/m^2) Top of the tower	Current density (A/m^2) Right side of the tower
100	0.01767	0.02138	0.01745
200	0.03302	0.03901	0.03116
300	0.05807	0.06798	0.0538
400	0.09227	0.10752	0.08455
500	0.13519	0.15661	0.12312
600	0.18574	0.21424	0.16757
700	0.24111	0.27922	0.21818
800	0.29778	0.34919	0.27221
900	0.36008	0.4231	0.32892
1000	0.42506	0.4995	0.38921
1100	0.49077	0.57496	0.44817
1200	0.56248	0.64906	0.50667
1300	0.62338	0.71857	0.55973
1400	0.68063	0.78495	0.61269
1500	0.732	0.84296	0.65593
1600	0.77482	0.89237	0.69646
1700	0.81382	0.93237	0.72794
1800	0.83491	0.96239	0.74881
1900	0.85541	0.97923	0.76497

Table B. 38: Electric field with respect to leader length (human level).

Stepped leader length [m]	Electric field norm (V/m), Human level
100	895.53029
200	895.49168
300	895.45518
400	895.54347
500	895.66219
600	895.57436
700	895.60434
800	895.59825
900	895.62242
1000	895.61632
1100	895.55696
1200	895.60671
1300	895.6639
1400	895.77658
1500	895.39785
1600	895.70332
1700	895.35048
1800	895.36149
1900	896.30665

Table B. 39: Current density with respect to leader length (human level).

Stepped leader length [m]	Current density norm (A/m^2), Human level
100	8.9553e-4
200	8.95492e-4
300	8.95455e-4
400	8.95543e-4
500	8.95662e-4
600	8.95574e-4
700	8.95604e-4
800	8.95598e-4
900	8.95622e-4
1000	8.95616e-4
1100	8.95557e-4
1200	8.95607e-4
1300	8.95664e-4
1400	8.95777e-4
1500	8.95398e-4
1600	8.95703e-4
1700	8.9535e-4
1800	8.95361e-4
1900	8.96307e-4

Table B. 40: Electric field intensities for 3 cases when the leader path is random

Random leader position [m]	Model 1	Model 2	Model 3
-3500	4847.65951	4858.78161	4871.16186
-3000	4885.01208	4917.9299	4945.66334
-2500	4979.25935	5044.52434	5108.76740
-2000	5170.47445	5332.65864	5498.78521
-1500	5607.36894	6028.00883	6510.97416
-1000	6640.69912	7992.22543	9985.52810
-500	9318.71476	16293.61165	37342.45497
0	20037.58436	37385.03741	22297.92775
500	37107.92992	10690.66516	10756.56871
1000	10165.68591	6950.70083	7259.37808
1500	6652.69378	5712.56491	5876.99536
2000	5567.32186	5210.70973	5282.09147
2500	5139.89383	4991.29548	5022.81461
3000	4962.25724	4897.17749	4913.22183
3500	4883.67121	4850.4365	4860.39310

Appendix C: Algorithm for the random leader path:

```
function out = s100sss
% s100.m
% Model exported on Aug 28 2014, 13:23 by COMSOL 4.3.2.152.
import com.comsol.model.*
import com.comsol.model.util.*
model = ModelUtil.create('Model');
model.modelPath('/E:\Thesis\comsol tests');
model.name('s100.mph');
model.modelNode.create('mod1');
model.geom.create('geom1', 2);
H = 2000;
a = 0;
model.param.set('H','2000[m]','Height of the cloud');
model.param.set('a','-3500[m]','Starting point of the leader');
model.geom('geom1').feature.create('r1', 'Rectangle');
model.geom('geom1').feature.create('imp1', 'Import');
model.geom('geom1').feature.create('pt1', 'Point');
model.geom('geom1').feature.create('mov1', 'Move');
model.geom('geom1').feature.create('sca1', 'Scale');
model.geom('geom1').feature.create('pol1', 'Polygon');
model.geom('geom1').feature('r1').set('pos', {'-4000' '0'});
model.geom('geom1').feature('r1').set('size', {'8000' '2000'});
model.geom('geom1').feature('imp1').set('type', 'dxf');
model.geom('geom1').feature('imp1').set('filename',
'E:\Thesis\comsol
tests\a24.dxf');model.geom('geom1').feature('mov1').setIndex('displx
', '-592.11212158203', 0);
model.geom('geom1').feature('mov1').setIndex('disply', '-
486.08889770508', 0);
model.geom('geom1').feature('mov1').selection('input').set({'imp1'})
;
model.geom('geom1').feature('sca1').set('type', 'anisotropic');
model.geom('geom1').feature('sca1').set('pos', {'-8.2795020969896'
'53.52948'});
model.geom('geom1').feature('sca1').set('anisotropic',
{'1.2499999719361' '0.97326326370239'});
model.geom('geom1').feature('sca1').set('factor', {'1.2499999719361'
'0.97326326370239'});
model.geom('geom1').feature('sca1').selection('input').set({'mov1'})
;
%%about the polygons%%
xb=a;
yb=H;
xp=[a];
yp=[H];
for i=1:1000;
    n(i)=rand(1);
    if n(i)<0.25;
    xl=100;
    yl=0;
    elseif (n(i)>=0.25) && (n(i)<0.5)
    xl=-100;
    yl=0;
    else
    xl=0;
    yl=-100;
    end
xb=xb+xl;
```

```
yb=yb+yl;

if yb==0
    break
elseif xb >= 4000 || xb<=-4000
    break
end
xp=[xp xb];
yp=[yp yb];
end
fid=fopen('polydata.txt','w');
fprintf(fid, '%f %f \n', [xp(:) yp(:)]');
fclose(fid);
model.geom('geom1').feature('pol1').set('type', 'open');
model.geom('geom1').feature('pol1').set('filename',
'E:\Thesis\comsol tests\polydata.txt');
model.geom('geom1').feature('pol1').set('source', 'file');
model.geom('geom1').run;
 model.physics.create('es', 'Electrostatics', 'geom1');
 model.physics('es').feature.create('gnd1', 'Ground', 1);
% model.physics('es').feature('gnd1').selection.set([2 4 5 6 7 8 9
10 11 12 13 14 15 16 17 18 19 20 21 22 23 24 25 26 27 28 29 30 31 32
33 34 35 36 37 38 39 40 41 42 43 44 45 46 47 48 49 50 51 52 53 54 55
56 57 58 59 60 61 62 63 64 65 66 67 68 69 70 71 72 73 74 75 76 77 78
79 80 81 82 83 84 85 86 87 88 89 90 91 92 93 94 95 96 97 98 99 100
101 102 103 104 105 106 107 108 109 110 111 112 113 114 115 116 117
118 119 120 121 122 123 124 125 126 127 128 129 130 131 132 133 134
135 136 137 138 139 140 141 142 143 144 145 146 147 150 151 152 153
154 155 156 157 158 159 160 161 162 163 164 165 166 167 168 169 170
171 172 173 174 175 176 177 178 179 180 181 182 183 184 185 186 187
188 189 190 191 192 193 194 195 196 197 198 199 200 201 202 203 204
205 206 207 208 209 210 211 212 213 214 215 216 217 218 219 220 221
222 223 224 225 226 227 228 229 230]);
 model.physics('es').feature.create('pot1', 'ElectricPotential', 1);
% model.physics('es').feature('pot1').selection.set([3 148 149]);
 model.mesh.create('mesh1', 'geom1');
 model.mesh('mesh1').feature.create('ftri1', 'FreeTri');
 model.result.table.create('evl2', 'Table');
 model.view('view1').axis.set('xmin', '-4275.458984375');
 model.view('view1').axis.set('ymin', '-4272.19140625');
 model.view('view1').axis.set('xmax', '4275.458984375');
 model.view('view1').axis.set('ymax', '6272.19140625');
 model.physics('es').feature('ccn1').set('epsilonr_mat', 'userdef');
 model.physics('es').feature('pot1').set('V0', '100000000');
 model.mesh('mesh1').run;
 model.result.table('evl2').name('Evaluation 2D');
 model.result.table('evl2').comments('Interactive 2D values');
 model.study.create('std1');
 model.study('std1').feature.create('stat', 'Stationary');
 model.sol.create('sol1');
 model.sol('sol1').study('std1');
 model.sol('sol1').attach('std1');
 model.sol('sol1').feature.create('st1', 'StudyStep');
 model.sol('sol1').feature.create('v1', 'Variables');
 model.sol('sol1').feature.create('s1', 'Stationary');
 model.sol('sol1').feature('s1').feature.create('fc1',
'FullyCoupled');
 model.sol('sol1').feature('s1').feature.remove('fcDef');
 model.study('std1').feature('stat').set('initstudyhide', 'on');
 model.study('std1').feature('stat').set('initsolhide', 'on');
 model.study('std1').feature('stat').set('notstudyhide', 'on');
```

```
 model.study('std1').feature('stat').set('notsolhide', 'on');

 model.result.create('pg1', 'PlotGroup2D');
 model.result('pg1').feature.create('surf1', 'Surface');
 model.sol('sol1').attach('std1');
 model.sol('sol1').feature('st1').name('Compile Equations:
Stationary');
 model.sol('sol1').feature('st1').set('studystep', 'stat');
 model.sol('sol1').feature('v1').set('control', 'stat');
 model.sol('sol1').feature('s1').set('control', 'stat');
 model.sol('sol1').runAll;
 model.result('pg1').name('Electric Potential (es)');
 model.result('pg1').set('showhiddenobjects', true);
 model.result('pg1').feature('surf1').name('Surface');
 model.result('pg1').feature('surf1').set('descr', 'Electric
field');
 model.result('pg1').feature('surf1').set('descractive', true);
 model.result('pg1').feature('surf1').set('expr', 'es.normE');
 model.result('pg1').feature('surf1').set('unit', 'V/m');
out = model;

mphgeom(s100sss)
```